TABLE OF CONTENTS

ROLE OF QUATERNARY ADDITIONS ON DISLOCATED MARTENSITE, RETAIN AUSTENITE AND MECHANICAL PROPERTIES OF Fe/Cr/C STRUCTURAL STEELS

Bangaru Venkata Narasimha Rao

Materials and Molecular Research Division
Lawrence Berkeley Laboratory

and

Materials Science and Mineral Engineering
University of California
Berkeley, California 94720

ABSTRACT

The influence of quaternary alloy additions of Mn and Ni to Fe/Cr/C steels which have been designed to provide superior mechanical properties has been investigated. Transmission electron microscopy and x-ray analysis revealed increasing amounts of retained austenite with Mn up to 2w/o and with 5 w/o Ni additions after quenching from 1100°C. This is accompanied by a corresponding improvement in toughness properties of the quaternary alloys. In addition, the generally attractive combinations of strength and toughness in these quaternary alloys is attributed to the production of dislocated lath martensite from a homogeneous austenite phase free from undissolved alloy carbides. Grain-refining resulted in a further increase in the amount of retained austenite.

The phenomenon of Tempered Martensite Embrittlement (TME) has been studied in detail in the quaternary alloys using a combination of TEM, fractography and mechanical property testing involving both slow as well as high strain rate toughness parameters and it is shown that TME is a fairly general phenomenon in steels containing appreciable amounts of retained austenite. TME is coincident with the decomposition of retained austenite into interlath coarse carbides and the fracture path is transgranular with respect to prior austenite grains but intergranular with respect to individual martensite crystals. Addition of Mn did not show any shift in the TME temperature of the base alloy (300°C) although 5 Ni addition postponed the onset of TME to 400°C. It is concluded that graphitizing elements such as Ni, Al, Si are beneficial in postponing TME.

Fundamental studies of lath martensite formation revealed that the so called "laths" are indeed "small platelets" and that the orientation of adjacent laths in a packet is the result of minimization of the overall shape deformation. This is not normally achieved by a single-step twin mechanism but most commonly through a multistep orientation process involving rotation of adjacent laths along a common axis such that the shear vector completes a 2Π rotation in a group of adjacent laths. The austenite retention in these alloys is studied in detail and it is shown that carbon is essential in the stabilization of austenite and that both Kurdjumov-Sachs (K-S) and Nishiyama-Wasserman (N-W) orientation relations between retained austenite and martensite can occur within a single martensite packet.

GENERAL INTRODUCTION

The martensitic transformation in ferrous materials is perhaps the most widely exploited transformation for producing a variety of strength-toughness combinations in structural alloys. Yet, it is the most complex transformation defying the attempts by various investigators to synthesize a clear understanding of the structure-property relations in alloys transformed to produce martensite. Metallurgically, this transformation is of considerable significance as it is the simplest and yet most economical known means of producing a homogeneous distribution of a high density of dislocations in the product phase simply via the solid state shear transformation in the parent phase of suitable composition. In spite of numerous investigations of this important class of transformation, several questions regarding the mechanism of transformation, crystallography, morphology and substructure in interstitial free ferrous alloys, plain carbon as well as alloy steels, remain incompletely answered.(1-6) The mechanism of hardenability and the reasons for the observed variations in martensite formation temperatures as well as substructure as a function of alloying are not well understood.(2,4,7-11) So also, questions regarding martensite nucleation remain quite elusive(2,3,12,13). The shear transformation is characterized by innumerable slip barriers such as boundaries and interfaces, for e.g., lath, packet, grain boundaries and several interfaces: carbide/matrix, twin, austenite/martensite. These various interfaces and boundaries either by themselves(14) or due to secondary processes such as segregation(15) and/or precipitation of second phase particles at these interfaces(16,17) can control in a signifcant way the deformation and fracture behavior of steel and it is only recently that a systematic correlation of structure-property relations in these alloys has been carried out.(18-20)

It is clear from the brief summary above that both a fundamental understanding of the martensitic transformation as well as the influence of microstructure developed on the subsequent mechanical preoperties are vital for further exploitation of this transformation in ferrous materials. The present investigation is concerned with these two important aspects and is divided into two parts. The first part deals with the structure-property relations and the control of microstructure by means of alloying and heat-treatment to achieve desirable combinations of mechanical properties. The second part is concerned with a fundamental understanding of the formation of dislocated (lath) martensite as it is by far the least understood but most widely utilized transformation in metallurgical applications.

PART 1.

DESIGN OF Fe-4Cr-0.3C-X QUATERNARY ALLOYS FOR IMPROVED TOUGHNESS-STRENGTH PROPERTIES

I. INTRODUCTION

As part of a continuing program(18,21,22) on the systematic investigation of the influence of alloying on the microstructure and mechanical properties of experimental steels, the present work is concerned with the influence of quaternary alloy additions to the experimental Fe|Cr|C ternary system. From the previous work on the influence of ternary substitutional solute additions to simple Fe-C steels, important conclusions regarding the effects of Cr(18), Mo(21), Mn(22), Co(10) etc. on the substructure and morphology of Fe-C martensites have emerged which eventually led to the control and design of alloys to obtain desirable microstructures for optimum combination of properties(18,21,23). However, the commercial steels existing today have normally a very complex chemistry based on one or several of the following reasons: (i) elements added in combination give better hardenability than if added individually(8,24), (ii) several elements are added in combination to exploit the benefits of secondary hardening(8,25) and/or strengthening from intermetallics such as in very low carbon maraging steels(26,27), (iii) some elements are added to produce grain refinement(8,28) and (iv) a few elements are added in order to eliminate/defer the onset of various kinds of embrittlement during tempering of steel(29,30) while others are added to suppress

H_2 susceptibility.(31) Often, however, the influence of the individual alloying elements in a complex commercial steel on its microstructure and properties is unknown and thus, in designing commercial steels, empiricism has taken the place of a systematic approach. The need for an understanding of the individual influence of various alloying elements on the structure and properties of much simpler, impurity free experimental alloys clearly exists. It is not always easy to isolate the individual effects of two alloying elements present in a steel due mainly to the uncertainty of their mutual interaction behavior. Nevertheless, an attempt is made here to study the effects of quaternary additions on the structure and properties of the experimental Fe|Cr|C steel. The ternary Fe|Cr|C steel was chosen mainly because a large volume of information about this steel is already available and because it can possess superior combinations of properties to existing complex commercial alloys(10,18,32,33).

A significant observation made recently(18,34) using the sophisticated methods of high resolution transmission electron microscopy is the identification of thin interlath films of retained austenite in alloys apparently having their M_s and M_f temperatures much above room temperature. Since its discovery several investigators attributed improved fracture toughness properties to the presence of retained austenite(18,23,30,35-38). Although in several instances the improvement in toughness properties could not be singly attributed to the retained austenite,(30,35,37) best properties were often associated with microstructures containing large quantities of stable retained austenite.(23,35,37) Kohn observed(36) that excessive enrichment of austenite during isothermal holding above M_s temperature may make the retained γ an undesirable constituent for plane strain fracture toughness. Almost all the previous work on the influence of austenite on toughness was carried out on commercial steels wherein the complex chemistry and impurities complicate the interpretation. The chemical and mechanical stabilizations of austenite as well as its morphology (whether continuous interlath films or discrete islands) could have important repercussions on its influence on the toughness of steel. It is thus, one of the important objectives of the current investigation to try to assess unambiguously the role of retained austenite on the mechanical behavior by varying its amount and stability by either heat-treatment or alloying (or both) of the simple experimental Fe-Cr-C alloys. Secondly, in order to improve the toughness to strength ratio (which in turn increases the critical flaw size) steels are usually tempered following quenching and the thermal instability of austenite ensuing tempering could significantly affect the toughness properties. It is thus another objective of the research to study the thermal stability of austenite as a function of type and amount of qua-ternary alloying.

In addition, design of quaternary alloys of optimum composition to further develop the stength and toughness of the base steel from the above understanding constitutes an inherent part of the research. For this purpose some selection guidelines discussed in the following section are used to select the quaternary alloy additions.

II. APPROACH FOR IMPROVING TOUGHNESS-STRENGTH PROPERTIES

The approach adopted to obtaining good combinations of strength and toughness is primarily microstructural control by alloying, heat-treatment or combinations of both. In what follows, the design guidelines for improved mechanical properties are outlined and in the subsequent section, the choice of quaternary alloying based on these principles is discussed.

A. Design Guidelines

i) Carbon Content:

Increasing the carbon content of the steel is by far the most effective and economical way of raising the strength of steel. However, depending on the total alloy content of the steel, it has been shown(32), above 0.4%C, the steel is susceptible to intergranular cracking. Besides, while significant gains in strength could be obtained through C addition, the toughness deteriorates monotonically. From a fracture mechanics viewpoint, increasing strength without a corresponding increase in toughness would only result in poor utilization of the available strength of steel in engineering applications where resistance to the propagation of existing cracks is important (See Appendix 1). At 200,000 psi yield strength level, a minimum of 80 KSI-in$^{1/2}$ plane strain fracture toughness is needed for a critical flaw size of 0.1" if 60-80% of available strength is to be utilized (Appendix 1). Above about 0.35%C, martensitic steel attains significant contribution to strengthening from substructural twinning. However, as will be discussed shortly, this kind of strengthening is undesirable from a toughness viewpoint. Thus, with a view to designing tough structural steels at an yield strength level of 200,000 psi, the carbon content of all the alloys investigated is maintained at a maximum of 0.3%.

ii) <u>Martensite Substructure</u>:

The invariant plane strain condition for the martensitic transformation requires an inhomogenous shear in the product phase on a fine scale which will not alter the crystal structure of the product(1). This requirement contributes to the substructures observed in martensitic steels and there are only two known types of shear which would not alter the original crystal structure, viz., slip and twinning. The former produces dislocated substructures while the latter twinned. Several investigations in the past(18,39) (recently summarized in ref. 4) revealed that twinned martensites possessed much inferior toughness properties to dislocated martensites when compared at the same strength level. Upon tempering the twinned martensite, extensive twin boundary carbide precipitation occurs and this twin boundary carbide may be even more detrimental than twinning itself. Twinning reduces the available number of active slip systems(40) and is detrimental to the toughness of carbon containing steels(41) both in as-quenched and tempered conditons and therefore, should be avoided.

iii) <u>Retained Austenite</u>:

Although the exact mechanisms by which interlath films of retained austenite promote toughness of a steel are not clearly understood, several recent investigations(18,23,35) suggest that small quantities of interlath austenite are beneficial to toughness properties. By increasing the stability of retained austenite to transformation under mechanical stress/strain or under thermal energy, its potential for improved properties can be vastly increased. One of the simplest ways of increasing the stability of austenite would be to add an austenite (fcc) stabilizer. The most economical way of doing this is to increase carbon content. However, the detrimental effects of retained γ in high carbon steels wherein it transforms to twinned martensite have been recognized for a long time. Therefore, fcc stabilizers which do not increase the propensity for twinning should be selected for stabilizing austenite and preventing premature transformation during stressing/straining or tempering. The present study aims to successfully exploit the austenite for improved properties by

(1) avoiding excessive carbon enrichment

(2) improving stability with fcc stabilizers which do not markedly further increase its tendency for twinning

(3) maintaining continuous interlath film morphology wherein the individual martensite crystals are entrapped by austenite

(4) maintaining good coherence at the martensite/austenite interfaces

(5) increasing the amount of austenite if found beneficial

iv) Coarse Undissolved Carbides:

Coarse undissolved alloy carbides can act as slip barriers resulting in a stress concentration at the carbide/matrix interface(42). This could result in either (i) carbide cracking(43) or (ii) interface cracking or (iii) crack nucleation in the matrix due to piled up dislocations. In addition, the carbide/matrix interfaces can provide an easy crack path if the interfacial cohesion is poor. Cox and Low(44) demonstrated that during plastic fracture, the resistance to fracture decreases with increasing inclusion size which is attributed to the ease of void nucleation and growth at coarser particles. Therefore, coarse undissolved carbides can promote brittle fracture and also reduce fracture resistance during plastic fracture and should be eliminated by proper heat treatment. The problem of undissolved coarse carbides becomes particularly acute in alloy steels containing alloying elements which have a stronger carbide forming tendency than iron.

v) <u>Lowering of Ductile to Brittle Transition Temp (DBTT)</u>:

Phenomenologically DBTT represents a change in mode of fracture–from low energy brittle (often cleavage) fracture below DBTT to high energy ductile fracture (dimpled rupture) above DBTT. While the Fe/4Cr/0.35C base steels exhibited excellent plane strain fracture toughness properties(18), their impact properties remained rather low(10,33). Relatively high DBTT in these steels was thought to be the reason and in fact, it was shown(33) that in Fe|4Cr|0.4C bainitic steel, the DBTT lies above room temperature. In order to further develop these steels for technological applications, it is necessary to lower the DBTT through suitable alloying. Again, the underlying principle in the selection of suitable alloying elements for this purpose is the achievement of lower DBTT without increasing transformation twinning. Toughening of alloys by second phases has been known for a long time. The impact toughness at -196° C of cryogenic 9 Pct Ni steel was shown to be enhanced by austerite of volume fraction (f) ≈ 0.1 and size (r) 0.1 to 0.15 μm dispersed in ferrite, formed by intercritical heat-treatment(43,45,46). In the case of brittle matrices insertion of a ductile metallic phase renders a startling improvement in strength-toughness combinations(43). A suitable dispersion of a ductile metallic phase of suitable volume fraction, size and morphology to form microduplex structure does seem to impart good impact toughness to an otherwise brittle matrix.

vi) Grain Refining:

For a given alloy composition, the DBTT can be altered by suitable micro-as well as macro-structural modifications and one of the most potent ways of lowering DBTT is by grain refining (Cottrell(47) and Petch(48)). Grain refining in addition imparts the added benefits to the structure in decreasing the severity of segregation of embrittling constitutents(49), increasing the yield strength(50) and improving fatigue properties(51).

Thus, in order to improve the mechanical properties microstructural control is the basic approach adopted to achieve the following features:

(i) Maintain dislocated lath martensite.

(ii) Promote a fine dispersion of carbides in martensite either through auto-tempering or tempering following quenching.

(iii) Promote stability and occurrence of retained austenite as thin interlath films. This is also necessary to avoid interlath brittle films of carbide.

(iv) Eliminate coarse undissolved alloy carbides.

(v) Lower DBTT and increase upper shelf energy.

The above design criteria are achieved through a combination of non-conventional heat-treatments and quaternary alloying. The choice of non-conventional heat-treatments will be discussed in a later section but for the present the next section deals with the choice of quaternary alloying.

B. Choice of Quaternary Alloying

Although no systematic structure-property correlation exists, it is generally accepted(52) that of all the common alloying elements that are often added to medium and low carbon steels, only Mn and Ni improve both toughness and strength as measured by impact and room temperature tension tests. Additions of up to 2% Mn to a steel is known(9) to increase its hardenability substantially. Nevertheless, excessive additions of Mn are to be avoided for it was shown(22) that in medium carbon steels, Mn in excess of 3 w/o leads to large fractions of twinned substructures and secondly, since Mn lowers M_s significantly(4), higher Mn contents result in the suppression of auto-tempering. There are also reports that Mn addition lowers DBTT(52,53). The influence of Ni is in several respects identical to that of Mn although higher percentages of Ni can be added to a steel without promoting substructural twinning(54) especially in the presence of carbon(39). Importantly, both Mn and Ni are fcc austenite stabilizers and one of the design goals, viz., increased stability of austenite, would be accomplished through the addition of Mn and Ni. Mn and Ni are in fact reported$^{(8)}$ to promote retention of γ in the as-quenched structures of some medium and high carbon steels. Besides achieving the design criteria with Mn and Ni there are further academic interests in studying the effects of Mn and Ni since these two elements are invariably present in most commercial alloys. Mn is added in commercial alloys primarily to combine with residual sulphur in preference to Fe to produce less damaging Mn S.

Quaternary alloys containing Mn up to 2 w/o and Ni of 5 w/o are thus designed to meet the specific microstructural criteria.

III. EXPERIMENTAL PROCEDURE

A. Materials Preparation

The quaternary alloys and ternary base alloy were supplied by Daido Steel Company in Japan in the form of 2.5" wide by 1" thick bars and 1/2" dia. rods. Round tensile specimens were obtained from the 1/2" dia. rods and the K_{IC} plane strain fracture toughness specimens and the Charpy-V-notch impact toughness specimens were obtained from the 1" thick bars. The chemical compositions of the vacuum melted alloys after homogenization at 1200°C for 24 hrs furnace cooled) are given in Table I.

B. Heat-Treatment

All austenitizing treatments were carried out in vertical tube furnaces under argon atmosphere. Oversized tensile, Charpy and K_{IC} specimens were cut from their respective stock and final machining was done under flood cooling after heat-treatment. All isothermal transformations were carried out by quenching into a salt pot located directly underneath the furnace containing agitated salt maintained at the required temperature. Tempering treatments were carried out by immersing the specimens for one hour in salt pots maintained at the required temperature. At the end of tempering treatments all the specimens were quickly quenched into water. Some of the heat-treatments employed in this investigation are schematically illustrated in Fig. 1.

C. X-Ray Analysis

X-ray analysis was used to monitor the per cent retained austenite after various heat-treatments. For this purpose when available, specimens were cut from fractured K_{IC} specimens, otherwise broken Charpy specimens were used. After repeated mechanical polishing and etching in a solution containing 96 ml. H_2O_2 + 4 ml. HF to obtain a shiny surface, the specimens were scanned in a Picker X-ray diffractometer with a fixed horizontal stage using CuK_α radiation. The scan angle (2θ) covered was from 40^0 to 100^0 which includes the prominent $(111)_\gamma$, $(311)_\gamma$, $(220)_\gamma$, and $(222)_\gamma$ reflections. Careful analysis of the diffraction data obtained failed to reveal any retained austenite in any of the samples. There was considerable background noise in the diffractogram which might have obscured any peaks from retained austenite. A modified method consisting of a more sophisticated instrument and technique to suppress the background noise to accentuate the retained austenite peaks was used by Dr. R. L. Miller(55,56) at U.S. Steel

Corporation to detect the austenite levels in these specimens.

D. Dilatometry

A commercial dilatometer (Theta Dilatronic III R dilatometer) was used to establish the phase transformation temperatures, viz., M_s, M_f, austenite start temperature A_s and austenite finish temperature A_f of the alloy steels.

E. Mechanical Testing

1. Tensile Testing

The dimensions of the 1.25" gauge round tensile specimen are shown in Fig. 2(A). Tensile testing was done at room temperature in a 300 Kip capacity MTS testing machine at a cross head speed of 0.04"/min.

2. Fracture Toughness Testing

Plane strain fracture toughness values were obtained by testing standard compact tension crack-line loaded toughness specimens shown in Fig. 2(B). Following heat-treatment at least 0.01 in. was removed from either flat-surface of the K_{IC} blanks. The thickness for most of the specimens conformed to the ASTM specification$^{(57)}$ for plane strain condition, viz., thickness $2.5\left(\frac{K_{IC}}{\sigma_y}\right)^2$. However, for some heat treatments of the Mn modified specimens the thickness was less than that required to satisfy plane strain condition. In this case, a method based on Chells criteria and dealt with in detail in Appendix 2 was used to convert the K_Q values into calculated K_{IC}. The 300 Kip MTS machine was again used for fatigue pre-cracking the specimens to a minimum crack length of 0.05 in. which were subsequently tested in the same machine to obtain the fracture toughness data. The orientation of crack propagation with respect to the long dimension of the bar stock is L-T.(57)

3. Charpy Impact Testing

Standard Charpy-V-Notch specimens shown in Fig. 2(C) were obtained from oversized heat-treated blanks. A minimum of 2, and in most cases, 3 Charpy-V-Notch specimens were tested for each treatment and the tabulated results correspond to the average of these tests. In some plots the scatterband is also shown. Some below and above room temperature impact tests were also conducted in order to determine the ductile-brittle transition temperature. For this purpose, a mixture of methanol and dry ice were used to obtain subzero temperatures. Charpy specimens were immersed in these mixtures for sufficiently long times to attain the temperature of the bath before breaking them. For above room temperature tests a water bath with thermostat was used.

F. Metallography

1. Optical Metallography

Specimens for optical metallography were cut from broken Charpy bars, mounted in boldmount, abraded on silicon carbide papers down to 600 grit, and polished on 1 μ diamond abrasive wheel. For revealing the martensite microstructure the specimens were etched in 2% and 5% nital solutions. For revealing prior austenite grain boundaries in fine grained specimens, etching was carried out in an etchant of 5 gm. of picric acid in 100 cc of water saturated with dodecylbenzene sulfonate.

2. Electron Metallography

Where available, thin foils for transmission electron microscopy were obtained from bulk, heat-treated fractured K_{IC} test specimens and in other situations broken Charpy specimens were used. About 25 mil. thick slices were cut from these specimens and following cleaning to remove any oxide scale, these were chemically thinned to less than 5 mils. at room temperature in a solution of 4-5% HF in H_2O_2. Both 2.3 mm and 3.00 mm discs were spark cut from the chemically thinned slices which were then sanded down to about 2 mils thick. These thin foils were finally electropolished in a twin jet electro-polishing apparatus at room temperature using a chromic-acetic acid solution made of 7 gm. CrO_3, 400 ml. CH_3COOH and 21 ml. distilled water. The polishing voltage varied from 25 to 35 volts for 2.3 mm discs and from 35-45 volts for 3 mm discs. Thin foils so obtained were stored in alcohol and were subsequently examined in Siemens Elmiskop IA (2.3 mm discs) and Philips EM 301 (3 mm discs) microscopes at an operating voltage of 100 KV.

3. Scanning Electron Microscopy and Energy Dispersive Analysis of X-rays

Fractography was conducted on both tensile as well as Charpy specimens, using an AMR-1000 scanning electron microscope at 20 KV. The fracture surfaces were preserved by masking with a tape during cutting and specimen preparation. This tape was later dissolved in acetone. An energy dispersive analysis of x-rays (EDAX) unit, attached to the microscope permitted semi-quantitative analysis of inclusions and precipitates.

IV. RESULTS

A. Transformation Temperatures and Heat-Treatment

The martensite transformation temperatures M_s and M_f and the austenite formation temperatures obtained by dilatometry are tabulated in Table I. The somewhat lower M_s and M_f temperatures in the base Fe|Cr|C steel are attributed to the somewhat higher carbon content of the base alloy over the quaternary alloys. In general, both the M_s and M_f temperatures decreased with the quaternary alloy additions although their difference remained approximately constant around 100°C. Mn and Ni both being strong fcc stabilizers, from Table I one could notice a general trend of lowered A_s and A_f temperatures as well as narrower austenite formation region with additions of Mn and Ni. It will be clear from the discussion presented in subsequent sections that while M_s temperatures measured by dilatometry are fairly precise, the M_f temperatures represent only approximate martensite finish temperatures and they are not true indication of 100% martensite formation.

It was proposed to characterize initially the influence of various alloy additions on the morphology and substructure of singly treated Fe|4Cr|0.3C base steel. For this an austenitizing temperature of 1100°C and ice water quench were chosen (Fig. 1). This temperature is in the single phase austenite region(58), Fig 3 and 4 high enough to dissolve all the alloy carbides.(18,58) For the alloy modified with 5 Ni (alloy E), a conventional high temperature austenization followed by rapid quench resulted in quench cracking(32). Thus, it was necessary to modify the heat-treatment for this alloy and based on earlier research on the phenomenon of intergranular quench cracking(32), the modification consisted of isothermal holding below M_s at 200°C for 1-5 min before finally quenching into water at room temperature (Fig. 1).

Grain refining double treatments designed with a view to combine the benefits of high temperature austenitization and fine grain size consisted of intermediate low temperature (200°C-1 hr) tempering between the initial high temperature austenitization and final low temperature grain refining austenitizing treatment (Fig. 1) at 870°C. In the case of base and Mn modified alloys, the intermediate tempering treatment was used to promote a fine dispersion of tempered carbides. This dispersion was hoped to augment the preferential nucleation of austenite at carbide/matrix interfaces(59,60) and thus, serve to bring about a more uniform, fine distribution of austenite crystals during subsequent austenitization. In the case of Ni modified alloys, the need for an intermediate tempering cycle is obviated by the interrupted quench during the initial high temperature austenitization.

B. Microstructural Characterization

(i) Optical Metallography:

Optical metallography was carried out with the intention of recording any variations in the gross features of microstructure, for e.g., prior austenite grain size, coarse undissolved carbides etc. with composition and heat-treatment. Fig. 4 shows representative optical micrographs for steels D and E. There were no observable differences in the optical microstructure between the base and modified alloys. The structure represents typical lath martensite occurring in packets (Fig. 4a) although in the 5 Ni modified alloy some indication of transition from lath to plate morphology is discernible (Fig. 4c). However, as will be shown in a later section, transmission electron microscopy revealed predominately lath martensitic structure even in the 5 Ni modified alloy. There were no undissolved coarse alloy carbides present in any of the single high temperature treated alloys [see for eg. Fig. 4(a) and (c)] nor could optical metallography resolve any undissolved second phase particles in any of the grain refined steels [Figs. 4(b) and (d)]. These structures also did not reveal any proeutectoid or isothermal decomposition products.

Fig. 5 shows the plot of measured average prior austenite grain sizes(61) as a function of alloying for the single and grain refining double treatments. The grain sizes of 5 Ni modified alloy closely resembled those of base alloy, viz., 170 μm for the single high temperature treated specimens and 20 μm for the grain refined specimens. In every case, double treatments caused an approximate ten fold refinement in the grain size compared to single treatments. For the same length of holding at 1100°C, there appears to be a significant austenite grain coarsening with increasing Mn content particularly above about 0.5 w/o Mn. The 2 wt% Mn alloy had about 60-70% larger prior austenite grain size compared to the base ternary Fe|Cr|C alloy. In contrast, the Ni modified alloy did not show any such grain coarsening. Both Mn and Ni act similarly in stabilizing austenite and since both of them lower A_3 temperature, from Fig. 3, 1100°C is certainly expected to fall within the single austenite phase field. However, Mn can form MnS with the residual sulphur in the alloy steels (<0.01 w/o in all steels) in preference to CrS(62) as the stabilities of sulphides on the basis of free energies of formation can be represented in decreasing order as MnS>CrS>FeS>NiS.(63) However, this can not explain the observed austenite grain growth as the solution temperature for MnS is higher than that for CrS.(63,64) Allen et al(65) and Jolley(52) reported that Mn refined grain boundary carbides whereas Ni did not have any such refining ability. However, it was pointed out earlier that no undissolved carbides could be resolved in any of the quaternary alloys after 1100°C austenitization. Thus, the exact reason for the observed grain coarsening with Mn remains unclear.

(ii) Transmission Electron Microscopy:

Structural characterization by transmission electron microscopy was performed on all the single treated quenched as well as quenched and 200°C tempered conditions of all the alloys but a detailed characterization of evolution of the microstructure during tempering was limited to the 0.5% Mn and 2% Mn modified alloys in the single treated condition and for the 5% Ni modified alloy in the double treated condition as it was considered that conclusions from these representative compositions and heat-treatments can be utilized to predict the behavior of other alloys. In this section only the martensite substructure and the carbide precipitation are covered and a detailed treatment of retained austenite is postponed to a latter section.

a. Structure of as-quenched alloys

The parallel lath morphology of martensite in all the alloys is evident (from Figs. 8, 9, 19-21, 55). Two points of significant variation in structure, viz., substructure of martensite and precipitation of carbides due to auto-tempering are worth noting. The substructure of Mn modified alloys (up to 2 w/o Mn) remained essentially dislocated (Figs. 6, 7 and 19). However, a small percentage (~ 10% of the laths examined) of twinning was observed in the 5 Ni modified alloy as shown in Fig. 8 (c) through (f). These are the well known $\{112\}_\alpha$ microtwins(66) and the SAD* pattern. Fig. 8 (e) obtained from the BF figure 8(d) is analysed in Fig. 8 (f). The amount of auto-tempering decreased with increasing Mn content consistent with decreasing M_s temperature(4) (Table I). In alloys modified with Mn up to 1 w/o

---

* The abbreviations BF = Bright Field, DF = Dark Field and SAD = Selected Area Diffraction will be used throughout the text.

both cementite and ε-carbide can be found but in 2 Mn modified alloy little of any auto-tempered carbides can be found (Fig. 7). Characteristic "cross-hatched"(66) appearance of ε-carbide was observed in the 0.5% Mn modified alloy. $<110>_{\alpha}$ widmanstâtten cementite precipitation was observed in some areas of the 1% Mn modified alloy. In other areas of the specimen, as Fig. 6 shows, extensive ε-carbide precipitation was observed. Comparison of the micrograph and the diffraction pattern which is a $[101]_{\alpha}$ zone, Figs. 6 (a) and (c), indicates that the needles are growing in $<211>_{\alpha}$ directions. The diffraction pattern from the carbides is weak due to the small size of the carbide particles but it is consistent with two $[134]_{\epsilon}$ zones with the ε-carbide reflections streaked perpendicular to the $[01\bar{1}0]_{\epsilon}$ directions. In spite of the isothermal hold between M_s and M_f in the case of Ni modified alloy, only ε-carbide precipitation was noted in these alloys as shown in Fig. 9. These carbide particles are about 300 A^o wide and about 0.5 μ long. The characteristic "wavy" interface(67) of these particles can be clearly seen in Fig. 9 (b) and the "cross-hatched" appearance of ε-carbide is also evident in the BF micrograph, Fig. 8 (a).

b. Structure of tempered alloys

200°C Tempering: Tempering at 200°C resulted in well established $<110>_{\alpha}$ widmanstatten cementite platelets in all the Mn modified alloys. Fine, wavy ε-carbide precipitates continued to coexist with cementite at this temperature. In the case of Ni modified alloys, the dominant carbide is ε carbide. Fig. 10 shows the widmanstatten carbides in the 2 Mn modified alloy. These cementite platelets are about 200 A^o wide and 0.5 μ long. The influence of Mn in promoting cementite coarsening can be discerned from a comparison of 200°C tempered structures in the 0.5 Mn and 2 Mn modified alloys shown in Fig. 48.

<u>300°C Tempering</u>: In this section changes occurring within the martensitic laths will be considered. Structural changes occurring at the lath boundaries will be dealt with in the next section in connection with retained austenite. Figs. 11, 12, and 13 illustrate the intralath carbide precipitation in 0.5 Mn, 2.0 Mn and 5 Ni modified alloys. The beginning of spheroidization of intralath cementite platelets is evident in Figs. 11 and 12 (c) and (d) of the Mn modified alloys. In other areas $(110)_\alpha$ widmanstatten platelets of cementite still exist as in Fig. 12 (a) and (b). Fig. 12 (d) clearly shows the ongoing process of spheroidization wherein one or more spheroids form on each cementite platelet. In the case of grain refined 5 Ni modified alloy, the intralath precipitation consisted of a fine distribution of cementite platelets wherein spheroidization can be considered as in very early stages (Fig. 13). As will be shown in the next section, the large stringers marked by arrows are retained austenite (Fig. 13 (b)) and not carbides. However, a

very fine distribution of spheroidal particles, presumably M_7C_3, nucleated at dislocations seems to be taking place, Fig. 13 (b). It was not possible to identify this fine carbide due to insufficient diffraction information.

One significant crystallographic observation made with cementite preciptitation in these quaternary alloys is that the majority of diffraction patterns analyzed (including Figs. 11 (c) and 13 (c)) did not indicate the well established Bagaryatskii orientation relationship between ferrite and carbide(66,68).

<u>500°C Tempering</u>: Figs. 14 through 18 illustrate the structural changes accompanying 500°C tempering in the quaternary alloys. Coarse spheroidized cementite in 0.5 Mn modified alloy is shown in Fig. 14 (a) and (b) and Fig. 14 (c) and (d) show the interlath precipitation of cementite. The diffraction patterns for this alloy also showed indication of M_7C_3 carbides although precipitation of M_7C_3 carbides is more intense in the 2 Mn alloy as shown in 15 (a) and (b). The bright field picture Fig. 15 (a) shows a very fine, uniform distribution of M_7C_3 carbides. Interestingly enough, some $(110)_\alpha$ cementite platelets still exist at this temperature and the DF picture Fig. 15 (b) obtained from a superposed cementite and M_7C_3 reflection shows both these carbides in bright contrast. Fig. 16 also shows the continued presence of fine $(110)_\alpha$ widmanstatten cementite platelets in the 2 Mn modified alloy while Fig. 17 reveals the twin boundary cementite precipi-

tation in the 5 Ni alloy. The intralath cementite precipitation in this alloy is shown in Fig. 18 revealing a ragged appearance for the carbides indicating that they may be dissolving. The occurrence of the carbide M_7C_3 = $(Cr, Fe)_7C_3$ in alloy steels has been the subject of a number of studies(25,33,69). Particular interest attaches to the question whether this carbide forms in a ferrite matrix already containing cementite by in-situ nucleation or from completely separate nuclei. The present results especially the evidence presented in Fig. 15 suggest that a separate nucleation of M_7C_3 is the favored reaction in these alloys in agreement with the observations made by Dyson and Andrews(69). Also, the SAD patterns obtained from the alloys showing appreciable amounts of M_7C_3 precipitation show considerable streaking (Figs. 15 (c), 18 (c)). Precipitate shape can not be held responsible for producing this diffraction effect as the morphology of precipitate as judged from the BF and DF micrographs (Fig. 15) is spherical. Dyson and Andrews(69) also observed streaky diffraction patterns associated with M_7C_3 precipitation and they attributed this to the faulting of crystal structure rather than to the precipitate shape.

C. Behavior of Retained Austenite

One of the significant structural observations made recently(18) with the use of transmission electron microscopy is the identification of small amounts of high temperature austenite phase retained at room temperature in alloy steels that were supposed to undergo 100% transformation to martensite at this temperature. Since this retained austenite is a metastable phase at this temperature its transformation characteristics following the supply of thermal or mechanical energy and a detailed characterization of structural changes occurring at the austenite/martensite interfaces become important. This section therefore deals with the identification, morphological characterization, transformation behavior and analysis of volume fraction of this austenite phase. A more fundamental study of the orientation relationships, habit plane and interface coherency etc. are dealt with in the section on formation of lath martensite.

(i) Electron Metallographic Observations:

Rao et al(34) and Thomas(23,76) have recently dealt in considerable detail with the problems encountered and the care and sophistication necessary in the unequivocal identification of retained austenite, particularly when it is present in small quantities. Furthermore, interference with the carbide reflections occurs in the selected area diffraction patterns. The discussion here will be limited to the presentation of actual results.

Figs. 19 through 21 and Fig. 55 presented in connection with the analysis of the crystallography of retained austenite illustrate the typical interlath film morphology of the high temperature phase. The advantages of utilizing $(200)_\gamma$ reflection for DF imaging of retained austenite have been emphasized in the past(34,23) and whenever possible the foil is tilted such that $(200)_\gamma$ reflections are strongly excited (Fig. 21 (f)). Of most significance from this study of the amount and morphology of retained austenite is the conclusion that there is a monotonic increase in the amount of retained austenite with Mn addition (Figs. 19 and 21) and highest amounts of retained austenite were found in the 5 Ni modified alloy interrupted quenched to room temperature following single high temperature austenitization, Fig. 20. Fig. 21 shows this monotonic increase in the volume fraction of retained austenite with quaternary alloying in the DF imaging mode. It is important to emphasize here that the above conclusion is based on examination of not just one or two micrographs but several micrographs from several thin foils.

The grain refined structures showed a similar behavior in the occurrence of retained austenite with quaternary alloying. Moreover, in every alloy there is an increase in the volume fraction of retained austenite in the grain refined structures compared to single treated coarse grained structures. Although the electron metallographic estimation of the volume fraction of retained austenite has its limitations, an attempt was made here and it was estimated that the 2 Mn modified alloy had about 4 to 5% retained austenite while the 5 Ni modified alloy showed about 6 to 8% in the single treated condition.

Thermal Stability The stability of retained austenite was followed as a function of tempering temperature. At 200°C tempering, the retained austenite was stable in all the alloys. Fig. 22 shows this in 1.0 Mn modified alloy and evidently there was no decrease in the amount of austenite following this tempering. Most interesting behavior occurred following 300°C tempering. While the base alloy and the Mn modified quaternary alloys showed no indication of any retained austenite (Figs. 23, 24), the 5 Ni alloy showed substantial amounts of this phase stable following this tempering treatment, Fig. 25. As is clear from Figs. 23 and 24, the decomposition of austenite resulted in the precipitation of coarse interlath stringers of cementite and the thickness of the interlath carbide stringers is a function of initial retained austenite content, viz., the 2 Mn alloy showed coarser interlath carbides compared to the 0.5 Mn alloy.

In the Ni modified alloy, the retained austenite present after this treatment is somewhat discontinuous compared to as-quenched morphology and attendant with this, there is some lateral thickening of the austenite films, as revealed in Fig. 25 which may be a result of an attempt to decrease the total $\alpha|\gamma$ surface area.

The continued presence of interlath cementite particles following 500°C tempering in the 2 Mn and 0.5 Mn modified alloys is shown in Figs. 26 and 14, respectively, although these carbides appear to be somewhat finer than those present following 300°C tempering (Figs. 23 and 24). In contrast, in the 5 Ni alloy most significant structural changes seem to be taking place within the martensite laths as already referred to in the earlier section (Figs. 17 and 18) and neither coarse boundary carbides nor evidence for significant amounts of retained austenite was obtained in these alloys following 500°C tempering.

(ii) x-Ray Analysis

Within the prior austenite grain obviously a single variant of retained austenite crystal orientation exists and therefore, depending on the prior austenite grain size, a monovariant austenite may be contributing to the x-ray diffraction, a situation similar to the cases wherein preferred orientation exists. This and the fact that only small volume fractions of highly deformed austenite phase are present in these alloy steels complicate the detection and accurate analysis of the volume fraction of this phase(34,70). Conventional x-ray analysis failed to resolve the austenite peaks in all the qua-ternary alloys. However, sophisticated methods of x-ray analysis wherein special precautions are taken to suppress the background to accentuate the austenite peaks(55,56) did reveal retained austenite in these alloys. Figs. 27 through 29 show the volume fraction of this phase as a function of composition and heat-treatment. While much confidence can not be laid on the absolute numbers, the trend and relative variations in the volume fraction of austenite are quite important. The following important conclusions can be drawn from these plots: the % retained austenite increases with amount of Mn addition (Figs. 27 and 28). Highest amounts of retained austenite were found in the 5 Ni modified alloys (Fig. 28) particularly when held in the M_s-M_f region, during the quench from austenite phase field when a 3.4% retained austenite was found. Grain-refining increases the amount of retained austenite in the as-quenched structures of all the alloys (compare Figs. 27 and 28). Fig. 29 shows the thermal stability of this austenite from which it is clear that in the 2 Mn modified alloy, the retained austenite undergoes more or less complete transformation at 300°C tempering whereas in the 5 Ni modified alloy, a major fraction of the original austenite remains stable even after 400°C tempering. Significantly, these x-ray analysis results are in total agreement with those of electron metallographic observations and thus, each one confirms the other.

D. Mechanical Properties

The mechanical properties of the base and quaternary alloy steels are summarized in Tables II through IV.

(i) Tensile Properties:

Fig. 30 shows the variation of Rockwell hardness Rc, as a function of tempering temperature. The remarkable temper resistance of all the alloys in the tempering range 300-500°C is evident which is also reflected in the strength vs. tempering temperature plots of Figs. 31 and 32. The 2 Mn alloy in the single treated condition exhibits rapid loss of hardness and strength between as-quenched and 300°C tempered conditions. Fig. 33 shows the strength of quaternary alloys as function of Mn content. The high strength levels for the base alloy are presumably due to somewhat higher carbon content in this alloy. The variation of tensile ductility with tempering temperature of the single treated and grain refined structures is shown in Figs. 34 (a) and (b) respectively. The initial retained γ volume % from x-ray analysis is also indicated on the plots of Fig. 34 (a).

(ii) Fracture Properties:

Plane strain fracture toughness tests were conducted only for the as-quenched and 200°C tempered treatments due to material limitations as well as lack of practical interest for tempering treatments at higher than 200°C. However, Charpy impact toughness tests were conducted for tempering temperatures up to 600°C. The data from the plane strain fracture toughness testing as well as impact testing is tabulated in Tables II through IV and plotted in Figs. 35 through 42.

Significant improvement in the plane strain fracture toughness at a given yield strength is obtained with quaternary alloying of either Ni or Mn, although 2 Mn modified alloy showed better toughness values than the 5 Ni modified alloy, especially when compared in the quenched and tempered condition, Fig. 35. The higher Mn alloys are somewhat brittle in the as-quenched condition (ice water quenching) due to the absence of any auto-tempering but following 200°C tempering, these alloys exhibit excellent toughness properties (Tables II & III and Fig. 35). The substantial improvements in plane strain fracture toughness achieved with quaternary alloying is also reflected in the plot of K_{IC} vs % Mn or Ni of the grain refined structures, Fig. 36. The improvement in this property shown by the quaternary alloys is particularly significant following the 200°C tempering. Again, the toughness properties of 5.0 Ni modified alloys are somewhat inferior although it should be noted that the 5 Ni alloys have higher strengths, (Table IV and Fig. 32).

The Charpy-V-Notch impact toughness properties of the modified alloys are depicted in Figs. 37 through 42. Fig. 37 shows the superior impact toughness of the quaternary alloys at a given strength level and Fig. 38 illustrates the improvement in impact toughness with wt % Mn or Ni added to the grain refined structures. The behavior of impact toughness is similar to the behavior of plane strain fracture toughness and the improvement in the impact toughness is particularly significant following 200°C tempering (Fig. 38). The behavior of the impact toughness for the entire tempering temperature range, viz., up to 600°C is illustrated in Figs. 39, 40 and 41 as a function of composition and heat-treatments. The points of significant importance that emerge from these plots are: (i) while the base ternary alloy, the 0.5 Mn modified alloy and the 5 Ni modified alloy show only tempered martensite embrittlement, the 2 Mn modified alloy shows two kinds of embrittlement, viz., tempered martensite embrittlement as well as temper embrittlement (Figs. 39, 41). (ii) The embrittlement phenomenon (in impact toughness) occurring in these modified alloys can not be avoided by grain refining. However, the impact toughness values at all temperatures can be improved by grain refinement (Figs. 40 and 41). (iii) The temperature of occurrence of tempered martensite embrittlement is a function of composition, Fig. 41. In the 2 Mn modified alloy, it seems to occur around 300°C (Fig. 34 (a)) whereas in the 5 Ni alloy, this temperature is around 400°C.

In order to study the influence of quaternary alloying on the ductile brittle transition temperature (DBTT), the plot of impact energy vs. testing temperature is obtained for various alloys shown in Fig. 42. It is clear that there is no significant variation in the ductile-brittle transition temperature as a result of Mn addition of up to 2 w/o although the 5 Ni addition showed a substantial lowering of the DBTT (50% Energy Criterion) from about -40°C for the ternary alloy to -70°C for the 5 Ni quaternary alloy. More significantly, however, all the ternary alloying resulted in a considerable upward shift in the upper shelf energies. Since there is no sharp drop off in impact energy at a particular temperature for any of these alloys, the DBTT will depend strongly on the criterion used to determine it.

F Fractography and Particle Characterization

Since the Charpy-V-Notch impact energy values showed the most interesting variations with alloying and heat-treatment particularly following various tempering treatments, fractography was concentrated on the broken Charpy bars to study the operative failure modes in these alloys and to try and correlate the failure modes with the microstructural changes.

Fig. 43 shows brittle, quasi-cleavage fracture in as-quenched Mn modified alloys subjected to single high temperature treatment. The 2 Mn alloy does reveal a highly brittle fracture with numerous secondary cracks on the fracture surface (Fig. 43 (b)). The extremely fast quench employed together with a high alloy content which suppressed the M_s temperature to very low values resulted in little auto-tempering in these alloys and thus, the residual stresses resulting from high transformation strains can make the martensite packet boundaries extremely weak(32). As a result, decohesion and consequently secondary cracks can be generated at these boundaries during fast fracture in order to relieve mounting stress concentrations. The origin of secondary cracks in high strength steels has been well studied and documented in the literature. In contrast, following a low temperature tempering which results in interlath precipitation of carbides, both the Mn modified alloys regain ductility and Figs. 44 (a) and (c) show the fracture mode at this tempering temperature which is mainly highly ductile dimpled rupture. Also evident from these fractographs is that the average size of dimples in the 2 Mn alloy is smaller than that of the 0.5 Mn alloy and that most of these dimples in the former are associated with spherical precipitates the identifcation of which will be presented later. The most interesting changes in fracture mode took place following 300°C tempering as shown in Figs. 44 (b) and (d). The ductile dimpled rupture at 200°C tempering is replaced by brittle quasi-cleavage fracture with parallel ridges on the fracture surface. These are indicative of severe interlath tearing or fracture which is particularly prominent in the 2 Mn alloy, Fig. 44 (d). The average distance between these parallel ridges measured on the fractograph is of the same order as the average lath width (Table VII).

Following 500°C tempering, brittle intergranular fracture dominated the failure mode in 2 Mn alloy (Fig. 45 (b)) whereas transgranular quasi-cleavage fracture persisted in the 0.5 Mn alloy (Fig. 45 (a)). The kind of intergranular embrittlement shown in Fig. 45 (b) is commonly associated with segregation of certain species to the prior austenite grain boundaries which lower the intergranular cohesion(15) rather than with any grain boundary precipitation. In contrast, Fig. 46 shows the fractographs of grain refined 5 Ni modified alloy as a function of tempering temperature and the failure mode throughout the tempering process remains clearly ductile dimpled rupture. Regions similar in appearance to the intergranular microvoid colaescence(64) on the fractograph of the as-quenched 5 Ni alloy, Fig. 46 (a), are replaced by 100% ductile dimpled rupture following 200°C tempering, Fig. 46 (b) and the gain in impact toughness is apparent from Fig. 41.

An x-ray energy dispersive analysis unit attached to the scanning electron microscope was used to qualitatively characterize any inclusions in the experimental alloys and Fig. 47 presents some of the results in the 2 Mn alloys. The fractographs of this alloy revealed most inclusions situated at the dimples (Fig. 44 (c) and the analysis of nearly spherical, about 2μ in dia. inclusions in the 200°C tempered alloy (Figs. 47 (a) and (b)) revealed that these are indeed (Mn, Fe) S particles. These inclusions were also observed near the grain boundaries as revealed by the 500°C tempered specimen fractograph, Fig. 47 (c). The corresponding EDAX analysis again confirmed that these are indeed (Mn, Fe) S particles. Fig. 47 (c) also clearly shows the decohesion at the particle/matrix interface. However, at this tempering temperature, as discussed earlier, the prior austenite grain boundaries are the weakest and the preferred fracture mode is intergranular. In contrast, the Ni modified alloys revealed primarily [illegible] particles. The 2 Mn alloy showed the highest amount of inclusions but this alloy is also characterized by a very high impact energy. Thus the influence of Mn in promoting matrix toughness due to favorable microstructural changes appears to more than compensate the loss in toughness due to the increased amount of inclusions which promote easy void nucleation and growth as well as decohesion at the interface.

V. DISCUSSION

A. Influence of Composition and Heat-Treatment on Microstructure

(i) As-Quenched Steels

Martensite structure: The morphology and substructure of ferrous martensites have been subjects of a number of investigations(3-6,10,14,18,21,22,39,40,54) and therefore, a detailed discussion of the factors affecting these two important structural parameters will not be attempted here. In the present investigation all the quaternary alloys revealed predominantly "lath" martensitic structure (Figs. 4, 6-9) irrespective of their composition. This is to be expected since predominantly plate martensitic structure is found only in high-carbon, high nickel and high nitrogen alloys(54,71,72). What is of more significance in these structural steels is their substructure, as it is now well established(4,18) that substructure plays a paramount role in controlling the toughness of steel. The substructure of martensite is a consequence of the invariant plane strain condition for the shear transformation(1) as alluded to before.

The lattice invariant shear can be either slip (dislocated martensite) or twinning (twinned martensite) and the factors affecting the transition from slip to twinning are points of considerable debate and controversy(3,10,54). Kelly and Nutting proposed that low stacking fault energy in austenite favors the formation of lath martensite.(40) A problem with this hypothesis is that manganese lowers the stacking fault energy of austenite whereas nickel has the opposite effect and yet both of them favor twinned plate martensite formation when present in sufficient quantities. Owen, et. al.(73) advanced a hypothesis according to which dislocated martensite in iron alloys is always associated with a cubic phase whereas twinned martensite is tetragonal. However, this again fails to explain cubic twinned martensite that forms in Fe-Ni, Fe-Pt and Fe-Mn alloys(54). Other investigators(3,4,54) pointed out the importance of temperature of formation of martensite in dictating the substructure of martensite, viz., as the M_s temperature goes down, at a critical temperature the transition from dislocated substructures to twinned structures occurs. A purely temperature explanation is also not satisfactory as Co is shown to raise M_s temperature but without having any significant effect on the amount of substructural twinning(10,21). Secondly, dislocated martensite continued to exist in binary Fe-Ni alloys with M_s temeratures much lower than the critical M_s temperature in alloys containing C(14,74) (for example, compare 5 Ni modified alloy with binary Fe-20Ni alloy studied in this investigation, Table VI). In order to get around this difficutly, it was first suggested by Johari and Thomas(75) that not only temperature but also alloy composition may significantly influence the extent of twinning in the martensite and the important factor is the relative magnitudes of the critical resolved shear stresses for twinning and slip at a given temperature for a particular alloy composition(3,4).

Das and Thomas(39) reported that additions of up to 12.5 w/o Ni to a 0.24C steel did not result in any significant twinning. In the present study the base alloy contains 4 w/o Cr and ~ 0.3 w/o C and both Cr and C are shown(18) to be potential promoters of twinning. Since Ni itself is not a strong promoter of twinning, it is concluded that the observed small amount of twinning in 5 Ni modified alloys (Fig. 8) can be considered as a result of the indirect effect of Ni through lowering of M_s (Table I) which, in the presence of potential twin promoters, results in twinning. In contrast to the behavior of Ni steels, Huang and Thomas(22) found that an upper limit to the addition of Mn to a 0.25 w/o C steel in order to avoid excessive amounts of twinning was a mere 3 w/o. This implies that in the presence of C, Mn is just as much a promoter of twinning as Cr.(18,22) In the present investigation by limiting the maximum Mn addition to 2 w/o, twinning is avoided. This is probably due to the overriding influence of the somewhat higher M_s temperature (Table I) in these alloys compared to Ni modified alloys in maintaining the critical resolved shear stress for slip lower than that for twinning. There were no significant variations in lath widths with either composition or heat-treatments designed to change the prior austenite grain size and the martensite packet size (see Table VII and the discussion in a later section). Roberts(76) also found a similar behavior of lath width variation with martensite packet size and Mn content and an explanation for this is proposed in a latter section.

Retained Austenite: High temperature fcc austenite phase can be stabilized at room temperature by a variety of mechanisms, some of which are not fully understood. In general, one would expect that elements which are fcc stabilizers should promote retained austenite. However, as would be clear from the evidence presented in Part 2 in connection with lath martensite formation, in alloys whose bulk M_s and M_f temperatures are above room temperature austenite can be stabilized at room temperature only in the presence of interstitial C (perhaps also N). This is in agreement with the observation made years ago by Yeo(77) who reported that carbon is vital for the stabilization of the austenite to martensite transformation. Furthermore, Rao et al.(34) were able to resolve small quantities of retained austenite even in very low C unalloyed steels. The fact that presence of C alone is not a sufficient condition for stabilizing austenite in the as-quenched structures is shown by the work of Clark and Thomas(21) who reported that no resolvable quantities of retained austenite could be found in a medium C steel modified with Mo additions up to 4 w/o. Clearly, the substittional alloying-interstitial C interactions must also be playing an important role in stabilizing austenite. However, it was suggested(23) that the observation of retained austenite in Fe|Cr|C steels and the absence of this phase in Fe|Mo|C steels can be partly reconciled with the fact that Mo is a more potent alloying element(8) compared to Cr in limiting the austenite phase field. Interstitial C can stabilize austenite in several ways: (i) it can physically segregate from the lath martensite to the surrounding austenite and this partitioning can lower the local M_s sufficiently below room temperature whereby austenite is stabilized at room temperature - i.e., "chemical stabilization".(74) This kind of stabilization should therefore be particularly effective during slow cooling from austenitizing temperature, for e.g., air cooling.(37)

(ii) The second stabilization, known as thermal stabilization.(78-80) is caused again by diffusion of interstitials C & N but this time not to achieve partition but to form dislocation atmospheres to inhibit their motion. These pinned dislocations can be in the martensite/austenite interface in which case they would directly inhibit interface motion or they can be in either phase, thus, inhibiting stress relaxation in the martensite or austenite; (iii) The third stabilization, known as mechanical stabilization, is concerned with the plastic deformation in austenite accompanying the shear transformation. Edmondson and Ko(81) and Kelly and Knutting(40) studied this phenomenon. Rao and Thomas(32) have considered in detail the question of accommodation of strain resulting from lath martensite formation and concluded that increasing C content increases the dilatation in the martensite lattice and the consequent accommodation in austenite.

The direct influence of substitutional alloying elements alone is not sufficient in stabilizing austenite in the directly quenched structures although strong fcc stabilizers such as Ni and Mn are primarily responsible in reverted austenite formation for e.g. in quenched and reheated specimens of maraging steels.(82,26) This is particularly true in the light of the observations made in Part 2 with binary Fe-Ni alloys where no retained austenite could be resolved.

Thus, it seems that in the structural steels of interest C is necessary for stabilizing austenite and the other substitutional alloying elements may affect the amount of retained austenite through their interaction with C. In the present investigation not one but several of the above factors might have been responsible for the observed increase in volume fraction with % Mn or Ni addition (Figs. 27 and 28). Increasing Mn addition results in a drop in M_s temperature which therefore discourages large scale migration of C during and after the *martensitic transformation. Therefore, excessive partitioning* of C and the consequent chemical stabilization may not be the major factor. Similarly, thermal stabilization can also be discounted as the primary reason for the presence of the high temperature phase particularly in the fast quenched (ice water quench) single treated specimens consistent with the observation that liquid N_2 refrigeration does not reduce much the volume fraction of austenite.(83) However, the fact that most of the C in Mn modified alloys stayed in solution (as exemplified by the lack of auto-tempering discussed earlier) results in an increased accommodation of strain which could mechanically stabilize the austenite. The addition of 7 w/o Ni in various respects results in the same kind of behavior with respect to retained austenite as the Mn modified alloys and due to the lowest M_s temperatures the Ni modified alloys showed the highest amounts of retained austenite. In the single treated interrupted quenched structures of Ni modified alloys highest amount of retained austenite was found due to the promotion of C partitioning and migration to dislocations during the M_s-M_f hold (i.e., chemical and thermal stabilization) in addition to the mechanical stabilization. In this connection, an important factor arising from the alloying element-C interaction which could significantly affect the mobility of

C has to be considered. Alloying elements such as Si, Al and Ni promote graphitization and have carbide forming tendencies either less than iron (Ni, Al) or negative (Si).(8) In addition Ni and Si also raise the activity of C in martensite(84) and similar behavior is expected of Al(30) whereas exactly the reverse behavior is expected with some of the carbide forming elements such as Mn, Cr, Mo, Ti, etc. which due to the attractive interaction with C (in the increasing order) lower the activity coefficient for C. The result is that Ni, Si and Al favor C partitioning to austenite and thereby increase its volume fraction(24,36) whereas Mn,Cr, Mo, Ti etc. disfavor C partitioning and this sort of austenite stabilization. The situation with the present alloys is complicated due to the quaternary alloying but it appears that in the 5 Ni modified alloys increased amounts of stabilized austenite can also be expected due to the promotion of C partitioning. It is clear that a technique capable of analysing C concentrations in regions which are typically 300-500 Å wide is invaluable in pinning down the exact γ stabilization mechanism. It is being attempted to solve this problem by the use of high resolution lattice imaging at the $\gamma|\alpha$ boundary. In general, the carbide-forming elements, while powerful in deep hardening influence, are not so effective in retaining austenite as are nickel and manganese(8). Apart from composition, one of the important microstructural features that affects the stability of austenite is the prior austenite grain size. In the present investigation the amount of retained austenite in grain refined alloys was always higher than the corresponding coarse grained structures (compare Figs. 32 and 33). These results are in agreement with earlier work by Brobst and Krauss(85) and Leslie and Miller(86) who studied the stabilization of austenite by closely spaced boundaries.

Finally, it is important to distinguish between the terms "mechanical stabilization" and "mechanical stability". The former is already discussed and the latter refers to the stability of retained austenite to transformation under applied stress or strain. Thus, factors which promote the former need not do so for the latter and vice versa. The former refers to the mechanism of retained austenite existence whereas the latter refers to its subsequent transformation characteristics.(87) Both Mn and Ni [illegible] promote mechanical stability of retained austenite.(88) A similar distinction exists between "thermal stabilization" and "thermal stability".

(ii) Tempered Steel

Structural Changes and Precipitation in Martensite: There are three primary variations within the martensitic phase of the tempered structures that need discussion, viz., coarsening of cementite with increasing Mn additions (Figs. 10-12), stabilization of ε-carbide in Ni containing steels (Figs. 8,9) and the observation of M_7C_3 carbides in high Mn (2 w/o) and high Ni (5 w/o) alloys even at low tempering temperatures (Figs. 12, 13, 15). Tempering of alloy steel martensite has been the subject of numerous investigators(74,69,25,2). It is now fairly well documented that it involves several stages, viz., clustering and preprecipitation of interstitial elements, precipitation of ε-carbide (Stage I tempering), decomposition of retained austenite (Stage II tempering), precipitation of cementite (Stage III tempering) and precipitation of alloy carbides (Stage IV tempering). The complex role of alloying elements in controlling the kinetics of tempering reactions, stability and occurrence of alloy carbides has been the subject of several papers in the literature(25,30,74,88,89) but unfortunately, most of them are concerned with either plain C steels or C steels modified primarily with one alloying element. The introduction of a quaternary alloying element in the present study introduces a further degree of complexity which is absent in the several studies made using a ternary system.

The kinetics of coarsening and spheroidization of cementite in the martensite matrix are variously related to the diffusivity of substitutional solute(2,25), alloy content, the disribution coefficient for the alloying element between cementite and ferrite(2), the interstitial C activity as influenced by the substitutional solute(84), variations in the interfacial energy between the cementite and ferrite matrix as a result of alloying(25) and in this regard, the degree of lattice coherency(8), etc.

Mn and Ni have important differences as regards their influence on cementite stability. Both Cr and Mn stabilize cementite by overcoming the metastability of Fe_3C existing in the plain carbon steels whereas graphitizing elements such as Si, Al and Ni destabilize the already metastable cementite although the former is more potent than the latter two in doing so.(90) While Cr can replace Fe up to 15 w/o in cementite, Mn can totally substitute for Fe(90) in the same phase. Jack and Nutting(2[illegible]) considered the local-equilibrium model developed by Hillert(91) to explain the rate of coarsening of cementite in quenched and tempered alloy steels and showed a rate constant dependent on $1/(1-K)^2$ where K is the distribution coefficient for the alloying element between cementite and ferrite. The present results suggest that because large amounts of Mn can dissolve in cementite(7[illegible]), the increased distribution coefficient may be the reason for the observed coarsening. Similarly, large scale replacement of Fe in cementite by Mn could result in changes in lattice constants of the carbide which could affect the lattice coherency and, consequently, the interfacial energy. The increased tendency for spheroidization even at low tempering temperatures (300°C) with increasing Mn in the present study (Fig. 12) points to the increased interfacial energy of the carbide/matrix interface.

In the case of Ni modified qua-ternary alloys, the behavior appears to be the result of a compromise between the opposing tendencies of Cr and Ni in stabilizing cementite. In many respects, Ni and Si have identical behavior in the tempering process of the steel (although the degree may be quite different), e.g., as discussed before, both of them raise the C activity and both of them destabilize cementite by promoting graphitization. The expanded occurrence of ϵ-carbide (Stage I tempering) in Si modified steels is well documented(30,36,37,84). Several models were porposed(84,92) to explain the ϵ-carbide stabilization and the inhibiton of cementite growth in the presence of Si or Ni. What is not clear is whether ϵ-carbide is directly stabilized by Si or indirectly stabilized due to the postponement of the onset of cementite nucleation. While the proposed models fail to solve this problem, they, nevertheless, present a convincing argument, especially the one by Owen(92), in explaining the inhibition of cementite growth. According to Owen(92), as cementite grows, increasing amounts of Si are rejected into the matrix which creates a Si concentration spike discouraging any C migration to the carbide due to the repellent interaction between C and Si(84). For further growth of the carbide, this Si concentration spike has to be dissipated which is rather slow at low temperatures. A similar explanation may be advanced for carbide growth in the presence of appreciable amounts of Ni in the alloy. King and Glover(84) report that the kinetics of ϵ-carbide precipitation (Stage I tempering) are also slowed down by the presence of graphitizing elements such as Ni and Si due to increased activitation energy for this process.

In the present study, ϵ-carbide is the predominant carbide at 200°C tempering in the 5 Ni modified alloy (Figs. 8, 9) although cementite precipitation occurred as early as 300°C tempering (Fig. 13). Since Ni is not a very strong graphitizer, it is suggested that the overwhelming influence of Cr in stabilizing cementite caused it to occur at 300°C tempering.

Regarding the observation of the alloy carbide M_7C_3, unfortunately, there is very little information available in the literature on the influence of various alloying elements on the formation and growth of this carbide. Seal and Honeycombe(88) and Rao et al.(33) discussed its formation in the ternary Fe-Cr-C alloys. It has been shown(88,25) that addition of strong carbide forming elements such as Mo, Nb, Ti to the ternary Fe|Cr|C steels can retard softening and this effect is suggested to be the result of these elements in restricting the diffusion of Cr in ferrite and thus the rate at which Cr_7C_3 coarsens(88). Therefore, it is not clear how and why higher Mn and Ni additions to the ternary alloy promote the formation of M_7C_3 (Figs. 12, 13, 15). The absence of any secondary hardening peak in the hardness vs. tempering temperature curves (Fig. 30) for all the curves can be explained by the fact that Mn is only a very mild carbide former and Ni is not a carbide former at all.

B. Thermal Stability of Retained Austenite

Whereas identifcation of retained austenite and studies on its stabilization in medium C, low alloy steels are in the very beginning stages, its decomposition following tempering is even much less studied. Most of the earlier studies on retained austenite decomposition were conducted with high C steels (>0.55 w/o C) wherein large quantities of austenite are retained.(8) Even here very little careful metallography was carried out. The austenite decomposition reaction was variously characterized as lower bainitic, upper bainitic or even pearlitic.(8) More recently, however, Speich and Leslie(74) characterized the decomposition reaction as bainitic. There is practically no work done in the past on the mechanism of decomposition of the specific type of retained austenite during tempering, viz., the interlath film morphology occurring in the structural steels of interest.

Thomas(70) has pointed out that some of the factors which promote austenite stabilization in the first place, viz., segregation of C and accommodation of transformation by plastic deformation in austenite, will also contribute to its instability during tempering. This is because the increased supersaturation of C in austenite promotes its decomposition to $\alpha+M_3C$ due to higher driving force available. So also, the dislocation substructure generated in austenite can promote heterogeneous nucleation of M_3C and thereby the decomposition reaction $\gamma\rightarrow\alpha+M_3C$.

In the present studies, the retained austenite is stable to 200°C tempering in all the alloys (Figs. 20, 22, 29) but in the Mn modified alloys the austenite undergoes decomposition following 300°C tempering (Figs 23, 24, 29). This is a temperature which is above the bulk M_s temperatures for 1 Mn and 2 Mn alloys and about the same as the bulk M_s temperature for 0.5 Mn modified alloy (Table I). If we invoke the possibility of some segregation and solute enrichment during tempering in austenite, then the decomposition temperature could lie in the upper bainitic transformation region for all the alloys. What is even more significant is that the decomposition occurs at a temperature where significant matrix cementite coarsening is also observed (Section A (ii), Figs. 11, 12). The elongated carbide stringers occurring at the lath boundaries following the decomposition, Figs. 23, 24, are quite typical of upper bainitic transformation.(4,10,33) Also, the analysed selected area diffraction patterns of Figs. 11, 23 and 24 reveal an orientation relationship between the interlath cementite and matrix which does not conform to the well established Bagaryatskii orientation relationship,(67,68) between the ferrite and cementite. Instead a new orientation relationship, viz.,

$$[\bar{1}25]_{\text{cementite}} \parallel [111]_{\text{ferrite}}$$
$$(1\bar{2}1)_{\text{cementite}} \parallel (1\bar{1}0)_{\text{ferrite}}$$
$$(3\bar{1}1)_{\text{cementite}} \parallel (3\bar{2}\bar{1})_{\text{ferrite}}$$

is obtained from Figs. 23 (c) and (d). Previous crystallographic studies(67,68) of the orientation relationships between bainitic carbide and ferrite have suggested that these carbides precipitate directly from austenite in upper bainite and therefore, the orientation relationship need not conform to the Bagaryatskii relation which is established for carbide precipitation from ferrite (for e.g., tempered martensite). Another observation of significance to the present discussion is that cementite is generally accepted to be the carbide phase in the upper bainitic product.(93,67) In view of these observations, the present results on the differences in the transformation characteristics of retained austenite in 5 Ni modified and 2 Mn modified alloys can be explained as follows. The difficulties involved in the formation and growth of cementite in the presence of graphitizing elements such as Si, Ni, Al has already been dealt with in the previous section. If the retained austenite were to transform by upper bainitic transformation, cementite formation and growth are important. The reason why retained austenite would prefer to transform by an upper bainitic transformation appears to be the much lowered accommodation necessary for this type of transformation due to the fact that carbide can be precipitated directly from γ. Thus, higher temperatures are necessary in the presence of Ni to transform retained austenite to isothermal decomposition products. In the present study, untransformed retained austenite was observed in 5 Ni alloys at as high temperatures as 400°C, Fig. 29. With the limited metallography carried out with 500°C tempered structures, no retained austenite could be observed in the 5 Ni alloy (Fig. 18). Further work to characterize the decomposition products of austenite in specimens tempered between 400°C and 500°C is necessary in order to understand fully the mechanism of retained austenite decomposition in this alloy.

C. Tempered Martensite Embrittlement

The occurrence of tempered martensite embrittlement in the quaternary alloys has already been referred to in the results section and Figs. 48 and 49 summarize the microstructural evolution, the micromechanisms of fracture and the correpsonding mechanical properties, of this phenomenon in two Mn modified alloys. Tempered martensite embrittlement (TME) or, 500°F embrittlement has been recognized for a long time(8,94-96,74) but the factors contributing to this phenomenon are not clearly resolved.(97-99) A sudden drop in a high strain rate toughness parameter, for example Charpy-V-Notch impact energy tested at room temperature following tempering in the range 250-450°C is generally regarded as the manifestation of the embrittlement; although, depending on the severity of this embrittlement, it is also shown to manifest itself in other low strain rate toughness parameters such as tensile ductility(98,100) and plane strain fracture toughness.(99) Both the origin of TME(98,99) as well as the fracture path(100) and failure mode(98,99) are points of debate. There is widespread confusion in the literature regarding these two aspects primarily because a wide spectrum of alloy compositions and C contents are employed with varying structures which can in a significant way affect the fracture path in embrittled alloy.(100) Secondly, a systematic unified approach wherein careful microstructural investigation is coupled with mechanical property and fractography analyses is lacking. Both transgranular(99) and intergranular failure modes have been associated with this embrittlement.(98,101,102) Previous work on TME can be broadly divided into two groups, viz., one group holding the view that segregation of impurities, regardless of their origin, to boundaries/interfaces is the primary cause(101-103) of TME and the other group strongly supporting the view that precipitation of brittle carbide phases at boundaries/interfaces/dislocations is the principal cause(96,97,99) of TME. At this moment it is also important to recognize another well established embrittlement(15,29,74) observed in certain quenched and tempered alloy steels and in steels doped intentionally with impurities such as Sb, P, As and Sn, i.e., temper embrittlement. This reversible embrittlement occurring between 370°C and 565°C is generally accepted to result from segregation of impurities to the prior austenite grain boundaries resulting in a loss of cohesion at these boundaries and the consequent intergranular fracture. In the foregoing discussion, it will be shown that depending on alloy compos it is possible to observe both TME and temper embrittlement in the same alloy and that the latter is more severe than the former.(100) It appears that some of the confusion and debate over the mechanism of TME in the past investigations also stems from the overlapping influence of temper embrittlement in those steels which were used to investigate TME.

Concerning the association between microstructure and TME, Lement et al(104) attributed the toughness degradations to the precipitation of cementite at the martensite packet boundaries whereas Klinger et al(105) suggested that the formation of cementite at prior austenite grain boundaries and the consequent intergranular fracture caused the embrittlement. Support for the assocation of TME with carbide precipitation can also be derived from the work of Delisle and Galibois(96) who concluded that the aligned carbides that result following embrittling tempering reduce the mobility of dislocations. The general drawback of all the above studies is the absence of high resolution electron metallographic characteriziation of microstructure over a range of tempering temperatures.

It is interesting that the influence of retained austenite in TME has been suggested as early as back in 1924 by Grossman(94) who, from thermal contraction-tempering temperature studies, envisaged the possibility of the preservation of austenite during quenching and its subsequent transformation during tempering causing the deleterious effect on toughness. More recently, McMahon and Thomas(18) observed a loss in toughness which they showed was correlated with the decomposition of austenite with the formation of interlath carbide films.

The results obtained in this investigation show a more definitive indication of the clear association between the retained austenite instability leading to interlath cementite and the TME. A monotonic increase was found in the volume fraction of retained austenite in the as-quenched structures as a result of quaternary alloy additions of Mn up to 2 w/o to the ternary Fe-4Cr-0.3C alloy (Figs. 19, 21, 27, 28). Similarly, the 5 Ni alloy also showed substantially increased quantities of retained austenite (Figs. 20, 28) as compared to the base alloy. In the Mn modified alloys as well as the base ternary alloy, this retained austenite is unstable to 300°C tempering and all of it is practically decomposed (Figs. 23, 24, 29) leading to the precipitation of interlath stringers of carbide (cementite), the thickness of which increased with initial amount of retained austenite (Figs. 23, 24). The accompanying variations in toughness are presented in Figs. 39, 34, 40. It is clear that the % reduction in area, a measure of tensile ductility, shows two minima, viz., one at 300°C (transgranular fracture), for the 2 w/o Mn modified alloy whereas no indication of a minimum in this property is discernible for the 0.5 Mn modified alloy, Fig. 34 (a). However, the Charpy impact toughness, Figs. 39 and 40, clearly reveals toughness minima at 300°C tempering for the base and 0.5 Mn alloys while for the 2 w/o Mn alloy the minimum occurs only at 500°C, although severe toughness degradation occurs in this alloy following

300°C tempering. Fractography (Fig. 44) revealed that the predominantly dimpled rupture at 200°C, Figs. 44 (a) and (c), in all the Mn modified alloys is replaced by quasi-cleavage at 300°C tempering, Figs. 44 (b) and (d), which indeed reveal parallel ridges indicative of a fracture path along interlath boundaries which are weakened by the precipitation of coarse carbides. Interestingly, the inter-ridge spacing measured from the fractographs is of the same order as the lath width (Table VIII) measured from transmission electron micrographs, Figs. 23 and 24. The 2 Mn modified alloy showed increasingly brittle fracture for tempering above 300°C and at 500°C, the fracture was completely intergranular (Figs. 45 (b) and 49) typical of emper embrittled structures. Transmission electron microscopy did not reveal any grain boundary precipitation that could be linked to this embrittlement at 500°C tempering although some interlath cementite still persisted at this temperature, Fig. 26. The Charpy impact behavior of the 2 Mn alloy appears to be the result of an overlapping influence of both TME (transgranular cleavage fracture) and temper embrittlement (intergranular fracture). In contrast, in the 5 Ni alloy, with only very little retained austenite having undergone decomposition even at tempering temperatures as high as 400°C (Figs. 25 and 29), the interlath precipitation of cementite is minimal, Fig. 25. Concomitant with this, the impact toughness of the 5 Ni alloy showed only a mild embrittlement and the tensile ductility vs. tempering temperature did not reveal any embrittlement at all, Figs. 41, 34 (b). The degree of embrittlement in the 2 Mn and 5 Ni alloys is compared in Fig. 41. Fractography, Fig. 46, of 5 Ni alloys revealed no significant changes in failure mode as a function of tempering temperature and the predominantly ductile dimpled rupture failure mode is evident at all tempering temperatures.

The present results show that the nature of toughness measurements in terms of strain rate and local stress conditions can be important to be able to detect any embrittlement minimum in that property. The 2 Mn alloy had a higher percentage of retained austenite and, therefore, would produce a higher volume fraction of interlath carbides (i.e., coarser) following its decomposition. Thus a more severe embrittlement is expected in the 2 Mn alloy compared to 0.5 Mn alloy which is substantiated by the occurrence of toughness minima in both the reduction in area as well as the impact toughness for the former. The strain rate in a tensile or K_{IC} test is about a million times smaller than that in an impact test and a higher strain rate is known to increase DBTT. At very low strain rates (such as in a tensile test), a toughness minimum may not be detected unless the embrittlement is very severe, compare Figs. 34 (a) and (b). The mechanisms whereby the brittle, coarse particles can reduce ductility and toughness are already discussed in connection with design guidelines. The failure stress, σ_F, can be directly related(99) to the width of carbide assuming carbide cracking occurs and treating the propagation of this cracked nucleus as that of a Griffith crack,

$$\sigma_F = \left[\frac{2E\gamma_p}{\pi(1-\nu^2)a}\right]^{\frac{1}{2}} \qquad (1)$$

where the terms have their usual meaning and 'a' in this case is the half width of the carbide. It is apparent from the above equation that the failure stress and consequently the toughness(108) are inversely related to the square root of the carbide thickness. Furthermore, the ease of cracking in the carbide itself is related inversely to the size of the carbide(43). In addition, Cochrane(106) and others(17) have found that the impact transition temperature increases directly with carbide thickness. TME has been observed(70) in several experimental steels but not in Fe|Mo|C steels in which no retained austenite was detected(21). This is consistent with earlier observations made by Irvine et al(107) who reported strikingly few carbide films at martensite lath boundaries in tempered steels containing Mo compared to several other alloy steels. Thus, TME appears to be a more general phenomenon(70) in alloys having appreciable amounts of retained austenite while temper embrittlement is specific to a few alloy compositions. Whatever the benefits of retained austenite to toughenss, following its decomposition, the toughness properties could be worse than not having it in the first place.

A major point of debate concerning TME is the fracture path(99,100) in the embrittled steels. The present investigation has shown that the fracture is transgranular with respect to prior austenite but is clearly intergranular with respect to the individual martensite laths (Figs. 44 and 49). The importance of a proper choice of composition (and hence microtructures) in arriving at the above conclusions can be understood from a critical analysis of the recent work by King et al.(99) on the occurrence of TME in a plain C steel. In the investigation under discussion, the authors chose a 0.6 w/o C alloy. Although King et al.

did not report any transmission electron microscopy, others have shown(7.) that the martensite morphology is mixed in the above steel with about 25 percent plate martensite, close to 8 percent retained austenite and the rest lath martensite. The evidence for substantial amounts of plate martensite in the structure can also be derived from the above authors' observation of microcracks. The morphology of retained austenite occurring in plate martensite is quite unlike that in the lath martensites found in the quaternary alloys. The expected differences are illustrated in the schematic diagram of Fig. 50. The island morphology of retained austenite, Fig. 50 (a), in plate martensite is expected to give rise to a carbide morphology and distribution shown in Fig. 50 (b) upon tempering. This is quite different from that occurring in lath martensite, Fig. 50 (d) following austenite decomposition. In the former, the islands containing coarse carbides should provide easy crack paths and thus, the fracture surface should contain facets of cleavage fracture which indeed appears to be the case from the published fractograph, Fig. 4, of the above paper. This led the authors to erroneously generalize a fracture path that is transverse to individual martensite crystals in a steel subject to TME. It is clear from the above discussion that a detailed microstructural characterization is vital for pinning down the origin of TME.

Grain refining is expected to lower the ductile to brittle transition temperature.(47,48) Grain refining also increased the amounts of retained austenite in the quaternary alloys (Figs. 27 and 28) which is shown in the above discussion to cause severe embrittlement following its decomposition. The results of these two mutually opposing tendencies is such that embrittlement vanished in the slow strain rate tensile ductility, Fig. 34 (b), but persisted in the high strain rate impact toughness, Fig. 40.

B. Correlation of Microstructure and Mechanical Properties

It is pointed out in the general introduction that the shear transformation is characterized by numerous structural variations and that, even a qualitative understanding of the structure-property relations is extremely complex and incomplete in spite of the numerous investigations in the past.(18-20) Therefore, an attempt is made here to propose a qualitative relationship between the mechanical behavior and the corresponding systematic changes in microstructure in a drive to unambiguously assess the role of certain microstructural features and explain the origin of superior properties in the experimental quaternary alloys wherein the impurity levels are carefully controlled. The experimental quaternary alloys are characterized by sufficient hardenability to avoid any isothermal decomposition products such as proeutectoid ferrite, pearlite or bainite as evidenced by careful extensive electron metallography (Figs. 6-9) and therefore, the effect of these on the microstructure need not be considered here.

In the present investigation coarse alloy carbides are dissolved in all the alloys during the initial high temperature austenitization (austenitizing temperature 1100°C). The size of the carbides is an important parameter in controlling the flow and fracture behavior(42-44,17 as already discussed in the previous section. Since these coarse carbides are present from previous treatments, they will probably be incoherent with the austenite and during the subsequent austenite-martensite shear transformation, since these are brittle and non-deformable particles, carbide/matrix interface cracking or residual stress build up at this interface can result and these conditons favor fast, brittle fracture, reducing the toughness and ductility. High temperature austenitization in addition to eliminating undissolved coarse carbides also results in coarse prior austenite grain sizes (Figs. 4 and 5). Carlson et al(58) have investigated the influence of austenitizing treatment on the mechanical properties of Fe-4Cr-C medium C steels and found that the strength level remains constant throughout the austenitizing temperature whereas the plane strain fracture toughness shows significant improvement up to 1,[illegible]°C above which it shows slight deterioration. These investigators attributed the improvement in properties largely to the lowering of undissolved alloy carbide content up to about 11[illegible]°C austenitization although several recent investigators([illegible]) advanced many other reasons for this improvement. Lai et al([illegible]) attributed this improvement in K_{IC} with austenitizing temperature to a decrease in the amount of substructural twinning and an increase in the volume fraction of retained austenite. Clark et al([illegible]) offered an alternate explanation for this improvement based on the proposal that a higher austenitizing temperature coupled with a fast quenching rate to suppress any segregation of embrittling constitutents leads to a decrease or elimination of quench cracks. However, Rao and Thomas(32) showed that quench cracking in these alloys has a different origin and in any case the above explanation fails to account for the absence of continued improvement in toughness properties(33,58) in these alloys above a certain temperature which coincides with a sharp decrease in the volume fractions of undissolved alloy carbides. More recently, Ritchie et al.(108) advanced a model according to which the notch root radius has an important bearing on the toughness parameter evaluated. These investigators were able to show that in 4340 steel the increased characteristic distance available with coarser prior austenite grain sizes with higher austenitizing temperatures would result in superior K_{IC} values (sharp crack) but poor impact energy values (blunt crack). However, the generality of this model can be questioned particularly in the case of the quaternary alloy steels under investigation since these alloys contain a large amount (4 w/o) of the carbide forming element Cr. Furthermore, several recent investigations(109,110) showed that fracture toughness (K_{IC}) increases with a decrease in prior austenite grain size. An important observation made by Dahl and Kretzschmann(110) is that at small plastic zone sizes at the crack tip as are common with the ultra-high strength structural steels, the fracture toughness is independent of grain size. In contrast it is well established(47,48) that the Charpy impact toughness is very sensitive to the prior austenite grain size. The lowering of ductile to brittle transition temperature with grain refinement and the consequent improvement in impact toughness is quite well known(111) for some time. Thus, from the above discussion, it appears that the generally attractive combinations of properties achieved with the non-conventional austenitizing in the experimental alloys (Figs. 35 and 37) could be the results of an overwhelming beneficial influence of the elimination of undissolved alloy carbides on fracture toughness and in the case of impact energy (Fig. 37), the behavior appears to be a compromise between the beneficial effect of lowering of undissolved carbide content and the unfavorable influence of coarse γ grain size.

Since the quaternary and the base alloys are heat-treated so as to dissolve all the alloy carbides (i.e., homogeneous austenite phase before quenching) it will be easier to correlate the mechanical property variations to the microstructural changes. The Mn modified alloys will be discussed first and later on the effect of 5 Ni addition to the ternary alloy will be considered. As shown in Figs. 6 and 7 there are no differences in either the martensite morphology or substructure (which is essentially dislocated) as a result of Mn addition up to 2 w/o. The most significant structural change as a result of increasing amounts of Mn addition is the increase in the retained austenite volume fraction (Figs. 21, 27 and 28) and the startling improvement in the impact toughness and plane strain fracture toughness with 2 % Mn is evident from the Figs. 35, 36 and 38. An added advantage of starting with a medium C matrix (0.3 w/o) is that substantial enrichment (i.e., up to ~30%) in austenite of C is possible before significant amounts of twinned martensite can form. Previous work showed(4) that twinning is very pronounced if C is > 0.4 w/o. In a previous section, it was also shown that in the Mn modified alloys substantial C segregation to austenite is not probable and that the stabilization of austenite is related to the increased chemical stabilization due to the presence of fcc stabilizer, Mn, and to the increased accommodation in austenite. As pointed out earlier, several investigators(18,23,30,35-38) associated improved mechanical properties to the presence of retained austenite although in most instances,(30,35,37) the improvement can not be singly attributed to the presence of retained austenite. The continuous interlath film morphology of retained austenite in the alloys under investigation would prevent propagation of a crack nucleated in the relatively brittle martensite to the adjacent martensite lath, i.e., the networks of retained austenite would help to break the continuity of the brittle phase martensite. Since fracture properties are of main concern in the present investigation, attention will be focussed on the mechanisms whereby retained austenite could provide resistance to the initiation and propagation of cracks. Suggested mechanisms of increased crack propagation resistance in the presence of retained austenite include: (i) crack branching,(112) resulting in a more tortuous crack propagation and the consequent increased energy expended, (ii) crack blunting,(113) as a result of plastic flow in austenite resulting in a decrease in stress concentration requiring higher applied stresses for unstable fracture and (iii) transformation induced plasticity (TRIP)(114) in which case, as the name suggests, the transformation of retained austenite to martnesite under stress/strain in the plastic zone ahead of a crack relieves the stress concentration. In all the three cases, the effectiveness of retained austenite in providing for improved toughness properties increases with its stability to transformation under mechanical stress/strain.

Besides the above direct effects of austenite on toughness, there are indirect benefits. Retention of austenite at lath boundaries prevents brittle lath boundary carbide formation(88,4) in the as-quenched as well as quenched and tempered structures if the tempering temperature is below instability temperature for austenite. Another significant benefit arising from retention of austenite is that, as will be shown in the next part, the γ/α boundary is highly coherent. In contrast, in the absence of γ, two adjacent laths impinge laterally to form rotation boundary thus creating high energy interfaces for crack propagation and/or segregation and precipitation.

Gerberich(113) proposed a fracture concept based on critical displacement for treating two phase structures wherein a tough unidirectional phase is dispersed in a relatively brittle matrix, Fig. 51. The situation is very similar to the one under discussion since within a martensite packet, the retained austenite films can be considered unidirectional (Figs. 19, 22 and 55). In the above treatment, the Hahn and Rosenfield fracture criterion showing the equivalence of the critical displacement ν^* to fracture toughness, K_c, given by

$$K_C = (2\nu^*\sigma_{ys}E)^{1/2} \tag{2}$$

was used where the other terms have their usual meaning. Other equations are available(113) to determine the displacement at the crack tip, ν_c and at any distance, ν_x, in front of the crack tip as shown in Fig. 51. As the material is loaded, when $\nu_c > \nu^*_{M1}$ the crack moves from position 1 to position 2 where it encounters the tough second phase. If $\nu_{c2} < \nu^*_{M2}$ (Fig 51) then the crack will be arrested provided the width of the M_2 phase (tough phase) is sufficiently large. This is so because, if M_2 is very thin, then the displacement at the distance x, (representing the dimension of the second phase) in front of the crack may be larger than the critical displacement for failure in the brittle material. If $v_x > v^*_{M1}$, then failure will proceed in the brittle material. This model brings out two very important points: (i) the thicker the austenite films (hence higher the volume fraction), higher will be its crack blunting ability and (ii) some degree of ductility in martensite is needed in order to prevent brittle failure in martensite even in the presence of austenite.

This model very nicely explains the observed improvement in fracture toughness and impact toughness values with increasing Mn (Figs. 35, 37) particularly after 200°C tempering (Figs. 36, 38 and Tables II and III). This is so, because in the higher Mn alloys, auto-tempering did not take place (Figs. 7 and 55) due to low M_s temperature and a low temperature tempering is necessary in order to induce some plasticity. It has been also reported(30,37) that such low temperature tempering augments the mechanical stability of austenite.

The advantages of grain refining are discussed in the beginning. In order to combine the benefits of high temperature austenitization, i.e., reduce coarse undissolved alloy carbide volume fraction and maintain a fine γ grain size, double treatments (Fig. 1) are necessary. The increased volume fraction of γ as a result of grain refining is evident from a comparison of Figs. 27 and 28 and the corresponding improvement in fracture and impact properties can be seen from a comparison of Figs. 36 and 38 and Tables II through IV. However, the strength properties are somewhat lower probably due to the increased amount of retained austenite.(115)

In the 5 Ni modified alloy, there are two variations in the microstructure compared to the base alloy, viz., some substructural twinning (Fig. 8) and increased amount of retained austenite, (Figs. 28 and 21). The detrimental effects of twinning on toughness have already been discussed and the somewhat poorer toughness properties in this alloy compared to some of the Mn modified alloys (Figs 35 - 38) is attributed to the presence of substructural twinning. Although the toughness of 5 Ni alloys are somewhat lower than that of the Mn steels, their toughness and strength combinations are quite attractive as shown in Figs. 35 and 37.

The desirable microstructural features for good strength and toughness combinations as concluded from this investigation are schematically illustrated in Fig. 52. By adhering to the design guidelines, microstructures are developed in quaternary alloys which have toughness to strength combinations much superior to the equivalent commercial alloys, shown in Figs. 53 (a) and (b).

PART 2.

MORPHOLOGY, CRYSTALLOGRAPHY AND FORMATION OF DISLOCATED (LATH) MARTENSITES IN STEELS

I. INTRODUCTION

It is now known that there are two basic morphologies of bulk martensite in ferrous alloys:(4,6) dislocated lath martensite and twinned plate martensite. Although the morphology and crystallography of plate martensites are well understood, the same is not true for the dislocated lath martensites occurring in the technologically more important medium and low carbon steels.(3,4,6,116) This part of the investigation is concerned with a detailed electron diffraction and microscopy examination of dislocated lath martensites in an effort to characterize the morphology and crystallogrpahy in greater detail than has been done previously and to better understanding of the austenite→martensite transformation mechanism. This work has been partly stimulated by the fact that small amounts of retained austenite have been detected (Part 1) in many lath martensites during an extensive alloy design program on dislocated martensitic steels.(4,34) Consequently, the unique orientation relationships can be obtained directly by utilizing selected area diffraction analyses of the lath bundles and their surrounding austenite. Such analysis is more precise at high voltages due to the reduction of spherical aberration. This method serves to eliminate controversies that must arise if indirect methods of habit plane analysis were to be used.(116-124) These usually involve the determination of the habit plane in martensite and converting it back to austenite using either the known traces of austenite or the presupposed orientation relationships. There is a wide scatter in the existing data as can be seen from Table V.

Another important aspect of the debate surrounding the lath martensite is the mechanism of its formation. Some of the earlier investigators considered that the packet is a fundamental nucleation and growth unit and the laths and cell boundaries form after transformation as accommodation relaxation in the martensite.(76,125) Others concluded that the laths are fundamental nucleation events and growth units and some cell structure originates in the austenite ahead of a growing martensite lath/plate and is inherited by the subsequently formed martensite.(126) The present study aims to resolve this conflict.

II. EXPERIMENTAL

The steels used for this part of the investigation are given in Table VI. Iron-nickel binary alloys in the form of 5 mil thick sheets encapsulated in evacuated quartz tubes, were austenitized 1 hr. at 1100°C and quenched into iced water. The carbon steels were austenitized in bulk for 1 hr. followed by quenching into iced water. Different austenitizing temperatures were used to change grain sizes. Details about the heat-treatment and specimen preparation are described in Part 1. Thin foils were examined in the Philips EM 301 (100 KV) and Hitachi HU 650 electron microscopes (500 KV).

III. RESULTS

A. Morphology and Cell Structure of Martensite

The martensite packet size was found by optical microscopy to increase with austenitizng temperature and prior austenite grain size (Table VII) but did not show the same rate of increase as the prior austenite grain size when the austenitizing temperature was increased from 870 to 1200°C. There was no noticeable variation in the average lath width as a function of prior austenite grain size.

Transmission electron micrographs taken at 100 KV and 500 KV revealed that the laths are parallel with reasonably straight boundaries and a high dislocation density (Figs. 54 and 55). Although there were no significant differences in lath morphology or substructure as a function of carbon content, retained austenite could only be detected in the carbon containing alloys (cf. Figs. 54 and 55)., in agreement with Yeo.(77) Fig. 55 gives evidence of retained austenite in the ternary Fe-4Cr-0.3C alloy(127) (Figs. 55 (a) through (c)) and quaternary Fe-4Cr-2Mn-0.3C alloy (Figs. 55 (d) through (f)). Indexed diffraction patterns clearly reveal the austenite zones (110) (Fig. 55 (c)) and (211) (Fig. 55 (f)). A detailed discussion of the occurrences of retained austenite has already been dealt with in part 1.

B. Crystallography of the Transformation

1. Relative Orientations of Adjacent Laths

Fig. 54 is an example of a detailed analysis of parallel laths. The SAD patterns and regions from where the patterns are obtained in the bright-field image are identified by 1, 2, 3 etc. The $[110]_\alpha$ crystal direction remains parallel in all the laths in this packet, indicating that these laths are separated by $[110]_\alpha$ rotation boundaries. Using sterographic analysis, Fig. 56 , it is found that the lath 5 is rotated 180°C with respect to lath 1 indicating that the shear components are opposite and accommodative. Thus, within the packet, the relative orientations of laths is such as to minimize the overall shape deformation. It is possible that adjacent laths can be twin related(124) in which case a 180° rotation of shear vector is obtained in a single step at adjacent laths. But twin related laths were found to occur infrequently in the carbonless alloys. However, in carbon containing alloys twin related or near twin related adjacent laths is a common occurrence. In addition, the presence of carbon appears to bring about the 180° rotation of the shear vector with less number of laths than without carbon. Moreover, the rotation axis for producing adjacent lath orientations is not uniquely $[110]_\alpha$, since $[100]_\alpha$ is also occasionally observed.

2. Austenite/Martensite Orientation Relationships

The ternary Fe-4Cr-0.3C alloys showed mostly the K-S (Kurdjumov-Sachs) relation (Fig. 55(c)) while alloys modified with 2% Mn and 5% Ni (alloys 5 and 6) frequently revealed the N-W (Nishiyama-Wasserman) relation (Fig. 55(f)). In Fig. 55(c) there are two martnesite zones, $[100]_\alpha$ and $[111]_\alpha$, and yet a single $[110]_\gamma$ zone. Out of the four possible orientation relationships between fcc austenite and bcc martensite,(72) viz., Bain, Pitsch, K-S and N-W, only K-S and N-W relations are widely recognized(74,1,83,117) to occur in the ferrous systems under investigation. The K-S and N-W relations are related simply by a 5.26° rotation around the normal of a close packed plane in either crystal structure,(128,129) Fig. 57. In the light of these comments, the results presented in the SAD pattern of Fig. 55 (c) need to be re-examined. Considering only one martensite crystal variant at a time, the $[111]_\alpha$ and $[110]_\gamma$ combination results in K-S relation, but if $[100]_\alpha$ and $[110]_\gamma$ are considered, the result is the N-W relation, Fig. 58. It is clear, therefore, that this is an ambiguous pattern for orientation relationship analysis although this is not apparently well recognized by other workers.(35,124,129) The particular combination of orientations {$<100>_\alpha$, $<111>_\alpha$ and $<110>_\gamma$)} was frequently observed in the present investigation as well as several past investigations.(124,129) The inability of the previous investigators to identify retained austenite led them to misinterpret the two matrix orientaions as the result of adaptation of two different variants of K-S relation in adjacent laths of a packet. In the absence of retained austenite reflections, the resulting diffraction pattern corresponding to Fig. 55 (c), would be as depicted in Fig. 58 consisting of only martensite reflections. Quite obviously, these two matrix orientations do not exactly fit into two variants of the K-S relation and in an effort to find an unique, single orientation relationship, some Russian investigators(129) concluded on the basis of elaborate matrix computations that the orientation relationship is exactly intermediate between

K-S and N-W. This conclusion can not be disproved as long as only matrix martensite reflections are recorded, Fig. 58. However, the present investigation using direct evidence of retained austenite reflections, Fig. 55 (c), has shown that what is in fact happening is that both K-S and N-W orientation relationships are alternating within the same packet and that the orientation relationship between a particular martensite crystal (lath) and parent austenite is <u>either</u> K-S or N-W but <u>not</u> intermediate. In the present study, evidence for the K-S relation as the dominant orientation relationship is obtained from several other unambiguous diffraction patterns. Similarly, the dominant orientation relation in the quaternary alloys (alloys 5 and 6 in Table VI) is the N-W, Fig. 55 (f). In this figure, although, there are again two martensite orientations, viz., $[110]_\alpha$ and $[311]_\alpha$ and a single austenite orientation, $[211]_\gamma$, it can be shown that neither of the matrix orientations belongs to a K-S variant. The $[110]_\alpha$ and $[311]_\alpha$ crystal directions in this figure are not exactly twin related but rotated ~6° about $[110]_\gamma$ direction.(14) It was pointed out(14,129) that the appearance of twin orientations of martensite crystals is evidence that the orientation relationship during $\gamma \rightarrow \alpha$ transformation is very close to precise K-S. Twin orientations of martensite crystals corresponding to the different variants of an orientation relationship are analytically impossible for N-W.

3. <u>Trace Analysis</u>

Fig. 59 (c) shows the trace analysis directly in austenite from which it can be seen that the habit plane in austenite is very close to the $(111)_\gamma$ within the limits of the accuracy of the electron metallographic trace analysis (2^{o}). This habit plane in the parent phase agrees with several earlier investigators (Table V). A determination of the habit direction of the laths in austenite indicates that it falls closely along $[1\bar{1}0]_\gamma$. Fig. 59 (a) shows the scatter when trace analysis is done only in martensite and emphasizes the advantages of detecting and utilizing the retained austenite. Fig. 59 (b) shows the trace analysis of the long axes of laths; these are always in $<111>_\alpha$ within experimental error.

C. High Resolution Lattice Imaging

The advantages of employing high resolution lattice imaging to the study of phase transformation(130) is beginning to gain recognition. An attempt is made here to apply this powerful technique to study various interfaces such as, lath, packet boundaries in martensite as also the most important austenite/martensite interface. The difficulties involved in lattice imaging ferrous martensites are already dealt with in the literature(131) and very preliminary results are shown in Fig. 60(a) and (b) which is a $\{110\}_\alpha$ lattice image in a martensite region of fine grained Fe-4Cr-5Mn-0.3C alloy (alloy 5). It is seen that the martensite packet boundary extends over a region larger than could be measured from a conventional bright field micrograph, Fig. 60(a). The dark contrast observed at the boundary which can be resolved in the conventional bright field image is not a true indication of the actual location or extent of the boundary as $\{110\}_\alpha$ fringes can be seen beyond this contrast.

Also, from the visibility of the fringes, it can be seen that the boundary is not straight, but wavy. In Fig. 60(b) several end-on dislocations can be seen within the martensite region and the considerable bending of lattice plane around dislocations is evident.

As a next step in this analysis, lattice imaging of the austenite/martensite interface is attempted. The main difficulty in simultaneously imaging lattice fringes in austenite and martensite across the interface (as is required to study the interface depicted in Fig. 62) is that the austenite is non-magnetic and the martensite is magnetic. Thus, the objective lens astigmatism correction for optimum resolution is different for lattice imaging austenite and martensite. However, with appropriate objective lens defocus and astigmatism corrections, a compromise conditon can be obtained whereby lattice fringes in both phases can be formed. Initial success indicates that the lattice fringes on either side of the boundary undergo considerable bending and some interfacial dislocations were also detected.

IV. DISCUSSION

Because packet size increases at constant lath width (Table VII), the aspect ratio of the laths increases with prior austenite grain size. A constant aspect ratio with increasing packet size would result in a higher volume dependent strain energy.

Regarding relative orientation of adjacent laths, Kelly(132) showed that those variants that are exactly twin related have shears which are equal and opposite. The present observations suggest that the orientatons of the laths are those which result from minimization of the overall shape deformation and its accommodation over a group of laths. Analysis of several adjacent laths in a packet was necessary to reach this conclusion, see for example Fig. 54. It is also shown that, in general, a gradual change in orientation to minimize shape deformation is preferred to a twin orientation of the adjacent laths. Fig. 61 depicts schematically three possible cases of accommodation within a martensite packet and their corresponding displacement profile. The situation where a single shear is operative throughout the width of packet is shown in case I (Fig. 61) where the large accommodation necessary is evident from the displacement profile. This is an energetically very unfavorable situation and the shape deformation can be minimized considerably by breaking the original packet into sub-units, or laths, such that several shear vectors operate within a given packet. In addition, instead of being random, if these shear vectors are arranged such that over a group of laths, the shear vector completes a 2π rotation case II, then the corresponding accommodation is considerably reduced. This is what is happening in Fig. 54. Instead of a multi-step orientation process, this minimizaton of shape deformation can also be obtained in a two step twinning process wherein, the adjacent laths are twin related, case III. Twinning in this case does not imply physical twinning but describes a situation where the relative orientaton of adjacent laths corresponds to a twin relation. The occurrence of twin related adjacent laths is a point of considerable debate(124) and in the present investigation twin related adjacent laths were observed occasionally in all the specimens but their occurrence increased with the presence of interstititial C. As discussed before, the SAD pattern of Fig. 55 (f) reveals two diffraction zones, viz., $<110>_\alpha$ and $<311>_\alpha$ corresponding to a near twin related orientation of adjacent ltahs shown in the bright-field micrograph, Fig. 55 (d). The presence of carbon also appears to reduce the number of laths required to achieve a 180° rotation of the shear vector, for example, in Fig. 55 (c), the 180° rotation achieved in a group of three adjacent laths. It thus appears that the increasing dilatation component of the strain energy with increasing C requires(32) complete accommodtation over fewer number of laths with a tendency for adjacent twin relation. There are a few examples(6) in the literature of the cooperative accommodation in the formation of martensite in some non-ferrous systems. The presence of multiple shears wherein the $<112>$ shear direction alternates among the three variants in the close packed plane during the fcc→hcp martensitic transformation in Co and Co-Ni alloys is thought to be resposible for the much reduced net shape strain and the consequent strain energy.

The habit plane by <u>direct</u> trace analysis is shown to be $\{111\}_\gamma$. Some of the scatter in the habit plane analysis by indirect methods may be due to the presence of ledges in the austenite-martensite interface as shown in Fig. 62(a). From this figure, the microscopic habit plane remains $\{111\}_\gamma$ but the macroscopic habit plane of any $(hk\ell)_\gamma$ can be generated by varying ledge density, ledge morphology, or both as shown in Figs. 62 (b) and (c). The martensite laths would thicken by propagation of these ledges into the surrounding austenite.

The identification of retained austenite around the lath boundaries supports the view that these laths are indeed individual nucleation events. The proponents of the idea that a packet is a fundamental growth unit(76,125) derive their support largely from the observation that surface relief experiments reveal upheavals over distances which are often 5 to 6 lath widths. However, as shown by the present study, adjacent laths may be rotated with respect to a common axis. Therefore, although all the individual laths undergo shear, they contribute to surface relief only over distances which are 5 to 6 laths in width. From these arguments, it appears that the so-called laths are really <u>small platelets</u> as shown in Fig. 63 with b > a > c where 'b' is the long axis, Fig. 55 (d). In the case of carbon steels, the laths are separated by thin films of austenite which may be stabilized to some extent due to the segregation of carbon from the adjoining laths as indicated in the diagram. For the first time, it is identified in this study that austenite/martnesite phases can obey both K-S and N-W orientation relations within the same packet. There is no a priori reason why this cannot happen. On the other hand, a hypothesis can be advanced to explain this on the basis that the two orientation relations give better flexibility in terms of increased variants available during martensite nucleation.

SUMMARY AND CONCLUSIONS

Both a fundamental study of the "lath" martensite formation as well as microstructure-property relations have been carried out in the present investigation and the following conclusions are drawn from this study.

1. Some alloy design considerations for optimizing strength-toughness combinations in high strength structural steels were critically assessed and based on these quaternary alloy additions of Mn and Ni were made to the base Fe/4Cr/0.3C steel and optimizing heat-treatments were chosen resulting in the design of superior experimental steels.

2. From the microstructural study of the quaternary alloys, the following observations are made:

   (a) The single high temperature austenitization produced a homogeneous austenite phase free from undissolved coarse alloy carbides in all the alloys.

   (b) Additions of up to 2 w/o Mn did not alter the substructure of martensite which is mainly dislocated. However, increasing Mn suppressed auto-tempering concomitant with very low M_s temperatures in these alloys.

   (c) Interrupted quenching following high temperature austenitization was required in order to avoid quench-cracking in 5 Ni modified quaternary alloys. Addition of 5 w/o Ni to the ternary alloy resulted in about 10% of the martensite laths containing twinned substructures. This is concluded to be due to the indirect influence of Ni in promoting the twinning propensity of C and Cr.

(d) From a study of the retained austenite, the following conclusions were made:

(i) There is a monotonic increase in the volume fraction of retained austenite with Mn as shown by both transmission and electron metallography as well as careful x-ray diffraction analysis. The stabilizing mechanisms for austenite are discussed and it is concluded that chemical stabilization as a result of excessive C segregation can not be the dominant stabilizing mechanism in Mn modified alloys.

(ii) The 5 w/o Ni addition resulted in the highest amount of retained austenite particularly following M_s-M_f hold. This is attributed to enhanced roles of thermal and chemical (C segregation) stabilizations in this treatment.

(iii) The morphology of retained austenite in all the alloys is of the continuous interlath film type, the thickness of which increased with its volume fraction.

3. Non-conventional double treatments were designed in order to take advantage of high temperature austenitization and fine grain size and the following conclusions on structure are arrived at:

(a) There is roughly a ten-fold refinement in grain size following the double treatments and the substructure of martensite essentially remained the same as single treated alloys.

(b) The volume fraction of retained austenite increased in all the alloys compared to their single treatments.

4. The following conclusions were made from the mechanical property measurements:

(a) The fracture toughness and impact toughness increase with Mn additions. This is attributed to increased retained austenite. Grain-refining further increased the toughness properties of the 2 Mn and 2 Ni modified alloys which is attributed to the combined influence of increased retained austenite and fine grain size.

(b) For the 2 Ni modified alloy, the somewhat inferior toughness properties is attributed to the small but significant fraction of substructural twinning in these alloys. The higher amount of retained austenite in this alloy appears to have compensated for this loss in properties as the 2 Ni alloy showed superior strength-toughness combinations.

(c) The origin of the beneficial influence of retained austenite is attributed to the following:

(i) Continuous interlath film morphology forming networks around the comparatively brittle phase martensite breaking the continuity of this brittle phase.

(ii) Heat-treatments to check excessive carbon enrichment in austenite.

(iii) fcc stabilizers in austenite which improve its mechanical stability.

(iv) Careful control of austenite composition to avoid excessive twinning if it were to TRIP.

(d) Several possible mechanisms of the beneficial effect of retained austenite on toughness properties have been considered but this study could not reveal a single dominant mechanism.

5. Tempering between room temperature and 300°C resulted in a rapid drop in strength with increasing Mn additions. This is

attributed to the rapid [illegible] in the range [illegible] in all the alloys [illegible] attributed [illegible] [illegible] calculated, [illegible].

4. Both tempered martensite embrittlement (TME) and temper embrittlement were observed in the 2Mn containing alloy while only TME is observed in all the others. Temper embrittlement in the 2Mn alloy at [illegible] °C is characterized by an intergranular fracture path probably due to segregation effects. The micro-structural features could be attributed to [illegible]. The following conclusions are made about TME:

(a) TME occurs in the range [illegible] °C depending on alloy composition.

(b) TME is coincident with decomposition of interlath retained austenite into stringers of coarse cementite at these boundaries and the severity of TME increases with initial retained austenite volume fraction and the extent of its decomposition.

(c) The fracture path during TME is intergranular not with respect to prior austenite grains but clearly with respect to individual martensite crystals (laths).

(d) Gran-refining although ineffective in eliminating TME, nevertheless reduces its severity. This is concluded to be due to the mutually opposing tendencies of fine grain size and increased retained austenite following grain refinement.

(e) The decomposition reaction of retained austenite is concluded to be upper bainitic.

(f) Graphitizing alloying elements such as Ni, Al and Si which destabilize M_s are beneficial [illegible] to [illegible]°C and above.

(c) TMF does not necessarily [illegible] with [illegible] fracture mode from [illegible] particle to M_s in the martensitic matrix.

2. From a fundamental study of Fe-Ni-C lath martensites [illegible], the following conclusions are drawn:

(a) The aspect ratio of the lath martensite [illegible] with [illegible] austenite grain size. This [illegible] than if the aspect ratio were to be [illegible].

(b) The orientation of adjacent laths is [illegible] of minimization of the overall shape deformation. This is not normally achieved by a single step twin mechanism, [illegible] through a multi step orientation process involving rotation of adjacent laths along a common axis such that the shear vector completes a 2π rotation in a group of adjacent laths (several cycles possible within a packet). The presence of carbon promotes a single step twin mechanism and reduces the number of laths required to produce a 2π rotation.

(c) Both $\{110\}_\alpha$ and $\{331\}_\alpha$ habit planes are observed.

(d) Carbon is essential in stabilizing austenite. In alloys with similar M_s-M_f temperatures, retained austenite is found only in carbon containing alloys.

(e) Either K-S or N-W orientation relationship between fcc austenite and bcc martensite was observed to be dominant depending on composition. Significantly, the present study revealed that proposed intermediate K-S and N-W orientation

[illegible]

[illegible]

substrate within the same [illegible].

[illegible] the austenite

martensite interface may be [illegible] that the

"[illegible]" and "[illegible]" [illegible] to be differ-

ent. Critical lattice images of the [illegible] interface re-

vealed clearly [illegible] nature of [illegible].

[illegible] It is concluded that martensite laths are thin platelets

and that individual laths and not the packets are the fundamental

nucleation events.

ACKNOWLEDGMENTS

The author extends his sincere appreciation and deep gratitude to Professor Gareth Thomas for his unfailing support, encouragement and expert guidance throughout the course of this investigation. Thanks are also due to Professors I. Finnie and J.W. Morris, Jr. for their critical review of this manuscript.

The assistance provided by the support staff of the Materials and Molecular Research Division of the Lawrence Berkeley Laboratory is gratefully acknowledged. The author recognizes in particular the help provided by Carolyn Gosnell, Gloria Pelatowski, Don Krieger, Lee Johnson, and Ed Edwards. Thanks are also due to Shirley Ashley, Paula Conant, Lorine Hesleph, Michele Marram, and Teri Tanasovich for typing this manuscript. Dr. Asada and Daido Steel Company graciously supplied the alloys used in this research. Dr. R.L. Miller of the U.S. Steel Research Laboratories kindly performed the x-ray volume fraction analysis of austenite.

The author is greatly indebted to his parents and grandparents for their help in making this possible.

The author is also grateful to Mr. Tom Rabe for his help with the manuscript preparation and to Mr. Mark Carlson for the use of some of his unpublished data.

Finally, the author remains forever obligated to his wife for her help, cooperation, understanding and enjoyable companionship.

This research was supported by the U.S. Department of Energy.

Appendix I.

Critical Flaw Size-Fracture Toughness Relations in Some Ultra-High Strength Steels

In order to ensure that a critical part in an assembly, machine, or any other structure does not fail in service, extensive proof testing is carried out before that part is put in service. Ultra-high strength steels in structural applications suffer from the limitation that they do not allow their full strength to be realized due to their poor toughness to strength ratio which in turn results in extremely small critical flaw sizes for catastrophic failure. Experimental limitations make the detection of such tiny cracks extremely difficult. The following table (Table A1) of critical flaw sizes at certain applied stresses gives an idea of the utilization factor of the steels' yield strengths. The assumed yield strengths are 260,000 psi for the ultra-high strength steel and 200,000 psi for the high strength steels and these are computed for a safety factor of 1. Assuming catastrophic propagation of existing flaws in the material under service load as the failure criterion, and using the relation between critical flaw size a_{cr} and applied stress σ from fracture mechanics (eq. A1), the critical flaw sizes were computed and plotted in Fig. A1

$$K_{IC} = 1.1\sqrt{\pi}\,\sigma\sqrt{\frac{a_{cr}}{Q_{cr}}}$$

where Q_{cr} is the flaw-shape parameter. For an elliptical flaw, Q_{cr},

Table A1. Critical flaw sizes for various applied stresses.

APPLIED STRESS σ (ksi)	ULTRAHIGH STRENGTH STEELS			HIGH STRENGTH STEELS		
	$\sigma/\sigma_{y.s.}$	CRITICAL FLAW SIZE, a_{cr} (in.)		$\sigma/\sigma_{y.s.}$	CRITICAL FLAW SIZE, a_{cr} (in.)	
		K_{IC} = 40 ksi-in$^{1/2}$	K_{IC} = 80 ksi-in$^{1/2}$		K_{IC} = 100 ksi-in$^{1/2}$	K_{IC} = 200 ksi-in$^{1/2}$
100	0.385	0.042	0.168	0.5	0.263	1.052
120	0.462	0.029	0.117	0.6	0.183	0.731
140	0.538	0.021	0.086	0.7	0.134	0.537
160	0.615	0.016	0.066	0.8	0.103	0.411
180	0.692	0.013	0.052	0.9	0.081	0.325
200	0.769	0.011	0.042	1.0	0.066	0.263

XBL 761-6269

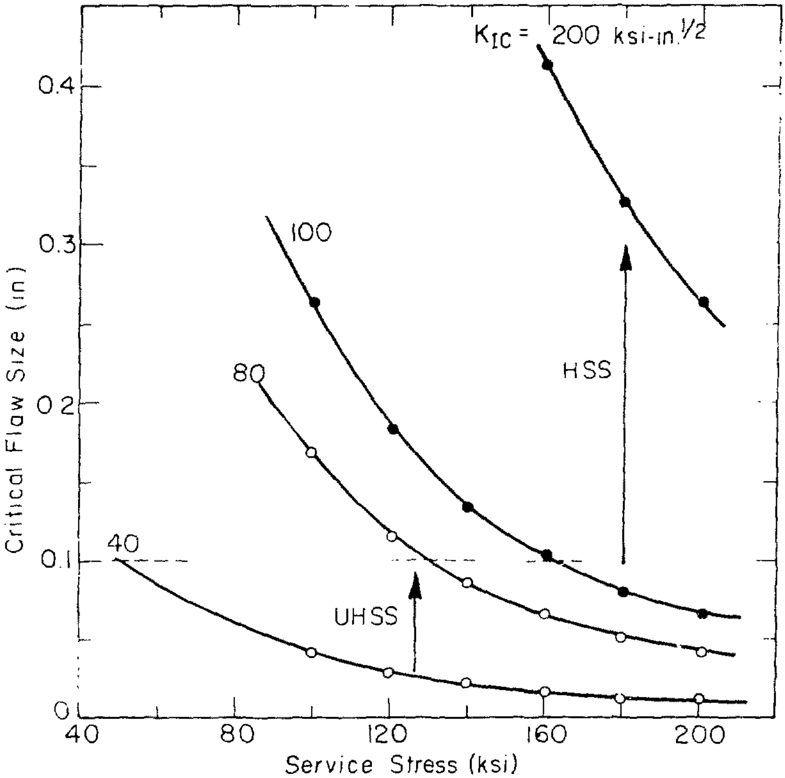

XBL 761-6271

Fig. A1. Critical flaw size vs. service stress for two ultra-high strength and two high strength steels.

varies as the ratio of minor axis to major axis. For a circular flaw, $Q_{cr} \approx 2.5$. Assuming $Q_{cr} \equiv 1$ (conservative) and neglecting plastic zone correction,

$$a_{cr} = \frac{1}{1.21\pi} \left(\frac{K_{IC}}{\sigma} \right)^2 \qquad (A1)$$

It is clear from the above equation, at a given applied stress, σ, a_{cr} is dependent only on the K_{IC} value of the steel. The improvement in applied stress that can be tolerated by a steel by an increase of its K_{IC} is apparent from Fig. A1. Assuming the detection limit to be 0.1" for a critical crack, the utilization limit of the yield strength for the ultra-high strength steel can be increased from a mere 20% to about 50% by doubling its K_{IC} from 40 to 80 Ksi-in1/2. On the other hand, for the high strength steel, as much as 80% of its yield strength can be used at a K_{IC} of 100 Ksi-in1/2 and 100% yield strength utilization can be achieved in this steel by a small increase in K_{IC}.

Appendix 2.

Method for Obtaining Calculated K_{IC} Values From Apparent Toughness (K_Q)

The ASTM validity criteria(57) for determining fracture toughness relate the specimen geometry to the measured toughness K_Q and the material yield stress σy. When the crack length C and the specimen thickness B both exceed 2.5 $(K_Q/\sigma y)^2$, K_Q is said to be a valid estimate of the plane strain fracture toughness, K_{IC}. K_Q is calculated from the equation,

$$K = \frac{P_Q}{B\sqrt{W}} f(C/W) \qquad \text{(A2)}$$

where f(C/W) is the specimen compliance function for the testing geometry and W the specimen width and the method to arrive at P_Q from the load-displacement curve is dealt in detail in the ASTM standards.(57) In the present investigation, equivalent-energy method described by Chell et al(133) was used to calculate K_{IC} from K_Q wherein the invalidity is due to smaller specimen thicknesses. Fig. A2 reproduced from Ref. 133 shows the normalized load-displacement curve wherein the displacement can be considered to be the external crack opening displacement δ for a compact tension specimen (see Fig. 2 of main body). Large specimens fail on the linear part of the normalized load-displacement curve, say at A in Fig. A2, where linear elastic fracture mechanics is applicable. Smaller specimens fail well into the non-linear part of the curve, at say, B. Considering a fracture test on a specimen that fails at the point B, according to the equivalent-

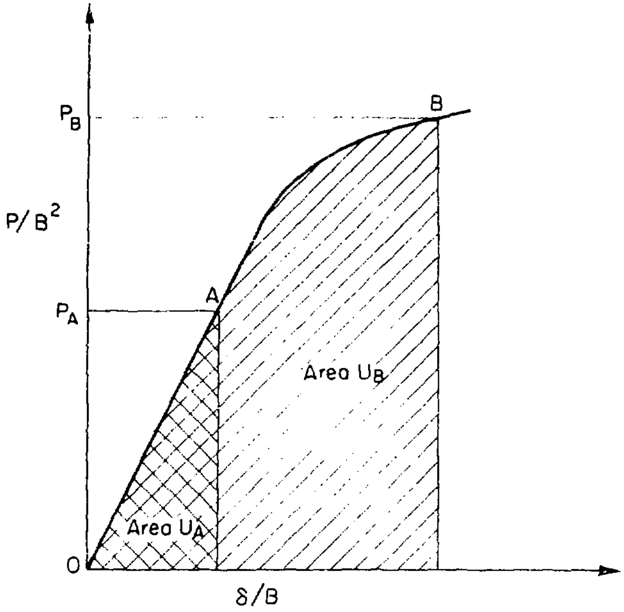

XBL 782-4553

Fig. A2. Normalized load-displacement curve(133).

energy method the toughness, K_{IC} is obtained from

$$K_{IC} \text{ (calculated)} = \frac{P_A}{B\sqrt{W}} f(C/W) \sqrt{\frac{U_B}{U_A}} \qquad \text{(A3)}$$

where P_A is any load which lies on the linear part of the load-displacement curve, Fig. A2, P_B, the maximum load recorded up to failure and U_B and U_A are the areas under the load-displacement curve up to the points B and A, respectively.

Sample Calculation: 2 Mn modified quaternary alloy, single treated, quenched and 200°C tempered condition with K_Q = 126 KSI-in1/2, Table II

Specimen Thickness B = 0.846"; W = 2.000"; C/W = 0.500; f (C/W) = 9.6 from Ref. 57. Maximum load, $P_B = 17.64 \times 10^3$ lbs. Load chosen in the elastic region, $P_A = 9.6 \times 10^3$ lbs.

Area under A, U_A = 318 units.

Area under B, U_B = 1797 units.

Using eqn. (A3) above, the plane strain fracture toughness is calculated to be 183 KSI-in 1/2.

References

1. "Phase Transformations", 1970; Metals Park, Ohio (Amer. Soc. Metals)

2. D. H. Jack and J. Nutting: Intl. Met. Reviews, 1974, 19, p. 90

3. G. Thomas: Met. Trans., 1971, 2, p. 2373

4. G. Thomas: Iron and Steel Intl., 1973 _, p. 451

5. S. K. Das and G. Thomas: Met. Trans., 1970, 1, p. 325

6. C. M. Wayman: Metallography, 1975, 8, p. 105

7. R. V. Fostini and F. J. Schoen: "Transformation and Hardenability in Steels", Symposium, Climax Moly Co., Ann Arbor, 1967, p. 195

8. E. C. Bain and H. W. Paxton: "Alloying Elements in Steels", 2nd Edition, ASM, Metals Park, 1966

9. R. A. Grange: Met. Trans., 1973, 4, p. 2231

10. M. Raghavan and G. Thomas: Met. Trans., 1971, 2, p. 3433

11. S. Jin and D. Huang: Met. Trans. A, 1976, 7A, p. 745

12. K. Shimizu, M. Oka and C. M. Wayman: Acta Met., 1970, 8, p. 1025

13. S. R. Pati and M. Cohen: Acta Met., 1969, 17, p. 189

14. G. R. Speich and P. R. Swann: JISI, 1965, 203, p. 480

15. C. J. McMahon, Jr.: "Temper Embrittlement in Steel", p. 127, STP No. 407 ASTM, Philadelphia, 1968

16. E. Nes and G. Thomas: Met. Trans. A, 1976, 7A, p. 967

17. M. Holzmann and J. Man: JISI, 1971, 209, p. 836

18. J. McMahon and G. Thomas: Proc. Third Intern. Conf. on Strength of Metals and Alloys, Inst. of Metals, London, 1973, 1, p. 180

19. G. E. Pellissier: Engineering Fracture Mechanics, 1968, 1, p. 55

20. E. R. Parker and V. F. Zackay: Engineering Fracture Mechanics, 1973, 5, p. 147

21. R. Clark and G. Thomas: Met. Trans., 1975, 6A, p. 969

22. D. Huang and G. Thomas: Met. Trans., 1971, 2, p. 1587

23. G. Thomas: Battelle Colloquium on Fundamental Aspects of Structural Alloy Design, R.I. Jaffee and B.A. Wilcox (eds.), Plenum Pub. Co., 1977

24. B. N. P. Babu: D. Eng. Thesis, Univ. of Calif., Berkeley, 1974, LBL Report No. 2772

25. R. W. K. Honeycombe: "Structure and Stength of Alloy Steels", Climax Moly. Co., London, 1975

26. G. P. Contractor: J. of Metals, 1966, 18, p. 1

27. I-Lin Cheng and G. Thomas: Transactions of the ASM, 1968, 61, p

28. F. J. Irvine, F. B. Pickering and T. Gladman: JISI, 1967, 205, p. 161

29. B. C. Woodfine, JISI, 1953, 173, p. 229

30. M. S. Bhat: Ph.D. Thesis, Univ. of Calif., Berkeley, Feb. 1977, LBL Report No. 6046

31. A. A. Scheinker and C. S. Kontovich: "Inhibition of H_2 Embrittlement in 4340 Steel by Ce and La additions". Reported at AIME Fall 1977 meeting in Chicago

32. B. V. Narasimha Rao and G. Thomas: Mat. Sci. and Engin., 1975, 20, p 195

33. B. V. Narasimha Rao, R. W. Miller and G. Thomas: Proc. 16th Intl. Heat Treatment Conf, The Metals Society, London, 1976, p. 75

34. B. V. Narasimha Rao, J. Y. Koo and G. Thomas: EMSA Proceedings, 1975, p. 30, Claitors Publishing Div. Baton Rouge

35. G. Y. Lai, W. E. Wood. R. A. Clark, V. F. Zackay and E. R. Parker: Met. Trans., 1974, 5, p. 1663

36. G. Kohn: Ph. D. Thesis, Univ. of Calif., Berkeley, Nov. 1976, LBL Report No. 5466

37. R. M. Horn: Ph. D. Thesis, Univ. of Calif., Berkeley, Dec. 1976, LBL Report No. 5787

38. V. F. Zackay, E. R. Parker and W. E. Wood: Proc. 3rd Intl. Conf. on Strength of Metals and Alloys, Inst. of Metals, London, 1973, 1, p. 175

39. S. K. Das and G. Thomas: Trans. of the ASM, 1969, 62, p. 659

40. P. M. Kelly and J. Nutting: JISI, 1961, 197, p. 199

41. D. Hull, Acta Met., 1960, 8, p. 11

42. R.B. Nicholson: Proc. "Effect of Second Phase Particles on the Mechanical Properties of Steel," Iron and Steel Inst., London, 1971, p. 1

43. R. F. Decker: Met. Trans., 1973, 4, p. 2495

44. T. B. Cox and J. R. Low: Met. Trans., 1974, 5, p. 1457

45. G. R. Brophy and A. J. Miller: Trans. ASM, 1949, 41, p. 1185

46. C. W. Marshall, R. F. Hehemann and A. R. Troiano: ASM Trans., 1962, 55, p. 135

47. A. H. Cottrell: Trans:: AIME, 1958, 212, p. 192

48. N. J. Petch, Phil. Mag., 1958, 3, p. 1089

49. G. Clark, R. O. Ritchie and J. F. Knott: Nature Phys. Sci. (London), 1972, 239, p. 104

50. R. A. Grange: Met. Trans., 1971, 2, p. 65

51. G. M. Sinclair and W. J. Craig: Trans ASM, 1952, 44, p. 929

52. W. Jolley: JISI, 1968, 206, p. 174

53. J. D. Bolton, E. R. Petty and G. B. Allen: Met. Trans., 1971, 2, p. 2915

54. G. Krauss and A. R. Marder: Met. Trans., 1971, 2, p. 2343

55. R. L. Miller: Trans. ASM, 1964, 57, p. 892

56. R. L. Miller: Talk presented at the Metals Show and Materials Engineering Congress, Oct. 1973, Chicago

57. Standard Method of test for "Plane Strain Fracture Toughness of Metallic Materials", designation E 399-72, Annual ASTM standards, 1973, p. 960

58. M. Carlson, B.V.N. Rao, R. O. Ritchie and G. Thomas: Proc. Intl. Conf. on Strength of Metals and Alloys, Nancy, France, 1976, p. 509

59. H. W. Paxton: "The Formation of Austenite", Symposium: Transformation and Hardenability in steels, Climax Moly Co., 1967, Ann Arbor, p. 3

60. G. R. Speich and A. Szirmae: Trans. of AIME, 1969, 245, p. 1063

61. Standard Methods for "Estimating the Average Grain Size of Metals," designation E112-63, Annual ASTM Standards, 1973, p. 419

62. Y. V. Murty, T. Z. Kattamis, R. Mehrabian, and M. C. Flemings: Met. Trans., 1977, 8A, p. 1275

63. B. J. Schulz and C. J. McMahon: Met. Trans., 1973, 4, p. 2485

64. R. O. Ritchie and J. F. Knott: Met. Trans., 1974, 5, p. 782

65. N.P. Allen et al.: JISI, 1953, 174, p. 108

66. S. Murphy and J. A. Whiteman: Met. Trans., 1970, 1, p. 843

67. D. Huang and G. Thomas. Met. Trans., 1977, 8A, p. 1661

68. D. N. Shackleton and P. M. Kelly: Acta Met., 1967, 15, p. 979

69. D. J. Dyson and K. W. Andrews: JISI, 1969, 208, p. 208

70. G. Thomas. Met. Trans., 1978, 9A, p. 439

71. D. S. Sarma and S. R. Keown: Met. Trans., 1975, 6A, p. 934

72. T. Maki and C. M. Wayman: Acta Met., 1977, 25, p. 681

73. W. S. Owen, E. A. Wilson and T. Bell: High Strength Materials, V. F. Zackay ed., p. 167, John Wiley and Sons, New York, 1965

74. G. R. Speich and W. C. Leslie: Met. Trans., 1972, 3, p. 1043

75. O. Johari and G. Thomas: Acta Met., 1965, 13, p. 1211

76. M. J. Roberts: Met. Trans., 1970, 1, p. 3287

77. R. B. G. Yeo: Trans. AIME, 1962, 224, p. 1222

78. "Transformations in Metals," P.G. Shewmon, McGraw-Hill Book Co., 1969

79. E. P. Klier and A. R. Troiano, Metals Technology, 1945, 12, p. 1

80. C. S. Ansell, S. J. Donachie and R. W. Messler, Jr., Met. Trans., 1971, 2, p. 2443

81. B. Edmondson and T. Ko: Acta Met., 1954, 2, p. 235

82. "Cobalt Containing High-Strength steels": Cobalt Monograph series, Cobalt Information Center, Columbus, 1974

83. B. V. Narasimha Rao: M. S. Thesis, Univ. of Calif., Berkeley, June 1975, LBL No. 3794

84. H. W. King and S. G. Glover, JISI, 1960, 196, p. 281

85. R. P. Brobst and G. Krauss: Met. Trans., 1974, 5, p. 457

86. W. C. Leslie and R. L. Miller: Trans. ASM, 1964, 57, p. 972

87. W. W. Gerberich, G. Thomas, E. R. Parker and V. F. Zackay: Proc. 2nd Intl. Conf. on the Strength of Metals and Alloys, Asilomar, 1970

88. A. K. Seal and R. W. K. Honeycombe: JISI, 1958, 188, p.9

89. B.J. Reisdorf: Trans. AIME, 1963, 227, p. 1334

90. Metals Handbook, Vol. 8, American Soc. for Metals, Metals Park 1973

91. S. Björklund, L. F. Donaghey, and M. Hillert: Acta Met., 1972, 20, p. 867

92. W. S. Owen, JISI, 1954, 177, p. 445

93. R. F. Hehemann, K. R. Kinsman, and H. I. Aaronson: Met. Trans., 1972, 3, p. 1077

94. M. A. Grossman: "Brittle Range in Low Alloy Steels", Iron Age, July 1924

95. J. M. Capus and G. Mayer: JISI, 1958, 188, p. 255

96. G. Delisle and A. Galibois: JISI, 1969, 207, p. 1628

97. B. R. Banerjee: JISI, 1965, 203, p. 166

98. G. Berry and R. Brook, Metal Sc., 1975, 9, p. 467

99. J. E. King, R. F. Smith and J. F. Knott: Fracture 1977, Univ. of Waterloo, 1977, 2, p. 279

100. B. V. Narasimha Rao and G. Thomas: Intl. Journ. of Fracture, 1977, 13, p. 705

101. C. J. McMahon, C. L. Braint and S. K. Banerji: Fracture 1977, Univ. of Waterloo, 1977, 1, p. 363

102. E. B. Kula and A. A. Anctil: J. Materials, 1969, 4, p. 817

103. J. R. Rellick and C. J. McMahon: Met. Trans., 1974, 5, p. 2439

104. B. S. Lement, B. L. Averbach and M. Cohen: Trans. ASM, 1954, 46, p. 851

105. L. J. Klinger, J. W. Barnett, R. P. Frohmberg and A. R. Troiano: Trans. ASM, 1954, 46, p. 1557

106. R. C. Cochrane: Proc. "Effect of Second Phase Particles on the Mechanical Properties of Steel", The Iron and Steel Institute, London, 1971, p. 101

107. K. J. Irvine, F. B. Pickering, and J. Garstone: JISI, 1960, 196, p. 66

108. R. O. Ritchie, B. Francis and W. L. Server, Met. Trans., 1976, 7A, p. 831

109. F. Stonesifer and R. W. Armstrong: Fracture 1977, Univ. of Waterloo, 1977, 2, p. 1

110. W. Dahl and W. Kretzschmann: Fracture 1977, Univ. of Waterloo, 1977, 2, p. 17

111. R. W. Armstrong: Advances in Material Research, H. Herman Ed., 1970, 4, p. 101

112. D. Webster: Met. Trans., 1971, 2, p. 2097

113. W. W. Gerberich: Trans. AIME, 1967, 239, p. 753

114. V. F. Zackay, E. R. Parker, J. W. Morris, Jr., and G. Thomas: Materials Sc. and Engin., 1974, 16, p. 201

115. S. K. Hwang: Ph. D. Thesis, Univ. of Calif., Berkeley, 1977, LBL no. 6603

116. A. B. Grenninger and A. R. Troiano: Trans. AIME, 1940, 140, p. 307

117. D. S. Sarma, J. A. Whiteman and J. H. Woodhead: Metal Sci. J., 1976, 10, p. 391

118. R. F. Mehl, C. Barrett, and D. W. Smith, Trans. AIME, 1933, 105, p. 215

119. F. J. Schoen, J. L. Nilles and W. S. Owen: Met. Trans., 1971, 2, p. 2489

120. A. R. Marder and G. Krauss: Trans. ASM, 1969, 62, p. 957

121. P. M. Kelly and J. Nutting: Proc. Roy Soc., 1960, A259, p. 45

122. T. Bell and W. S. Owen: JISI, 1967, 205, p. 428

123. J. D. Bolton and E. R. Petty: Metal Sci. J., 1971, 5, p. 166

124. J. M. Chilton, C. J. Barton and G. R. Speich: JISI, 1970, 208, p. 184

125. J. S. Pascover and S. V. Radcliffe: Acta Met., 1969, 17, p. 321

126. F. J. Schoen and W. S. Owen: Metallography, 1970, 3, p. 473

127. M. Carlson: M. S. Thesis (in progress), Univ. of Calif., Berkeley

128. K. W. Andrews, D. J. Dyson and S. R. Keown: "Interpretation of Electron Diffraction Patterns", Plenum Press, New York, 1967

129. M. P. Nemirovskiy and Yu. R. Nemirovskiy: Fiz. Metal. Metalloved., 1975, 39, p. 782

130. G. Thomas: Journal of Metals, 1977, 29, p. 31

131. J. Y. Koo and G. Thomas: "35th Ann. Proc. Electron Microscopy Soc. Amer", Boston 1977, G. W. Bailey (ed)., p. 118

132. P. M. Kelly: Acta Met., 1965, 13, p. 635

133. G. G. Chell, I. Milne and J. H. Kirby: Metals Technology, 1975, 2, p. 549

TABLE I.

ALLOY COMPOSITIONS AND TRANSFORMATION TEMPERATURES

Alloy Designation	Composition (wt%)					Measured Temp. (^oC)			
	C	Cr	Mn	Ni	Fe	M_s	M_f	A_s	A_f
A	0.29	4.0	---	---	Bal.	270	170	726	808
B	0.24	4.0	0.54	---	Bal.	305	190	728	762
C	0.24	4.1	1.0	---	Bal.	274	167	700	735
D	0.25	4.0	1.93	---	Bal.	253	164	655	685
E	0.27	3.8	---	5.0	Bal.	210	110	641	656

TABLE II.

MECHANICAL PROPERTIES OF SINGLE TREATED, COARSE GRAINED STEELS

Alloy	Tempering Temperature (^{o}C)	YS (KSI)	UTS (KSI)	% Reduction in Area	% Elongation Total (Uniform)	K_{IC} KSI-in 1/2	Charpy-V-Notch Energy ft-lbs
Fe-4Cr-0.3C	as-quenched	195	240	35.4	8.0 (3.0)	71	18
	200	189	230	45.5	11.0 (4.0)	76.5	30
	300	173	208	45.2	10.0 (3.3)	----	15
	400	169	202	48.3	11.0 (3.3)	----	15.5
	500	155	175	52.4	13.5 (4.4)	----	19.5
	600	110	129	78.6	17.0 (5.2)	----	36.5
+ 0.5 Mn	as-quenched	192	233	34.0	9.0 (3.5)	92.5	14.0
	200	175	214	47.0	11.0 (3.5)	117 (150)*	35.0
	300	170	204	50.0	10.8 (3.3)	----	14.0
	400	163	195	51.0	11.3 (3.6)	----	15.5
	500	150	172	60.0	13.5 (4.2)	----	19.5
	600	104	125	71.0	16.2 (5.4)	----	36.5
+ 1.0 Mn	as-quenched	198	240	28.5	6.4 (3.0)	85.5	11.5
	200	185	224	45.7	10.0 (2.7)	----	48.0
+ 2.0 Mn	as-quenched	207	265	33.0	8.5 (3.5)	59	3.4
	200	195	235	36.0	6.5 (2.5)	126 (180)*	40.0
	300	177	212	19.0	-------	----	18.5
	400	160	195	45.0	11.5 (4.0)	----	14.5
	500	150	175	24.0	12.5 (4.0)	----	4.0
	600	105	125	64.0	17.0 (6.0)	----	10.2

*K_Q values only, calculated K_{IC} in brackets.

TABLE III.

MECHANICAL PROPERTIES OF GRAIN REFINED (DOUBLE TREATED) STEELS

Alloy	Tempering Temperature (°C)	YS (KSI)	UTS (KSI)	% Reduction in Area	% Elongation Total	K_{IC} KSI-in 1/2	Charpy-V-Notch Energy ft-lbs
Fe-4Cr-0.3C	as-quenched	180	230	24.0	9.4	66.0	20.0
	200	187	227	32.0	9.0	----	20.5
+ 0.5 Mn	as-quenched	185	230	48.2	13.3	74.5	23.5
	200	186	222	49.1	13.7	82.5	32.5
+ 1.0 Mn	as-quenched	177	228	47.4	13.7	85.0	29.1
	200	185	223	50.0	13.9	110.0	40.0
+ 2.0 Mn	as-quenched	189	242	38.7	11.0	84.0	30.5
	200	184	230	50.8	15.4	126.0*	49.5
	300	182	215	58.5	14.6	----	29.5
	400	177	204	59.1	15.4	----	24.5
	500	161	160	60.3	21.0	----	17.0
	600	108	127	72.6	23.3	----	28.0

*K_Q only

TABLE IV.

MECHANICAL PROPERTIES OF 5 Ni MODIFIED ALLOYS

Treatment	Tempering Temperature (°C)	YS (KSI)	UTS (KSI)	% Reduction in Area	% Elongation Total (Uniform)	K_{IC} KSI-in 1/2	CVN Impact Energy ft-lbs
Single Treatment M_S-M_f holding Coarse grained Structure	as-quenched	195	275	25.0	9.0 (5.5)	89.5	19.5
	200	187	234	-	12.0 (5.0)	123.0	43.5
Double Treatment Fine grained Structure	as-quenched	200	280	44.5	11.1	75.0	27.0
	200	193	242	57.5	15.8	102.0	41.9
	300	183	218	58.7	15.3	----	41.0
	400	181	215	59.5	16.0	----	39.0
	500	172	195	64.0	18.1	----	48.5
	600	114	137	75.0	24.0	----	117.0

TABLE V.

SUMMARY OF CRYSTALLOGRAPHIC STUDIES IN LATH MARTENSITE

Investigator(s)	Habit Plane in Martensite	Habit Plane in Austenite	Ref.
Mehl et al.	------	$\{111\}_\gamma$	118
Greninger & Troiano	------	$\{111\}_\gamma$	116
Schoen et al.	------	$\{111\}_\gamma$	119
Marder & Krauss	------	$\{557\}_\gamma$	120
Kelly & Nutting	$<111>_\alpha$*	$<110>_\gamma$*	121
Bell & Owen	$\{110\}_\alpha$	------	122
Bolton & Petty	$\{110\}_\alpha$	------	123
Chilton et al.	$\{213\}_\alpha$	------	124
Sarma et al.	$\{213\}_\alpha$	------	117

*long direction of the needle/lath

TABLE VI.

CHEMISTRY OF THE ALLOYS AND THEIR Ms TEMPERATURES

Alloy #	Alloy Comp. (wt%), Nominal	Ms (^{o}C)
1)	Fe-12 Ni	300*
2)	Fe-15 Ni	250*
3)	Fe-20 Ni	165*
4)	Fe-4Cr-0.3C	320
5)	Fe-4Cr-5Ni-0.3C	210
6)	Fe-4Cr-2Mn-0.3C	253

*calculated

TABLE VII.

VARIATION OF MARTENSITE SIZE PARAMETERS WITH AUSTENITIZING TREATMENT

IN Fe/4Cr/0.3C Alloy

Austenitizing Temperature (°C)	Prior austenite grain size, μm	Martensite packet size, μm	Martensite lath width, μm
870	29	26	0.37
1000	111	31	0.35
1100	202	42	0.39
1200	254	47	0.39

Figure Captions

Fig. 1. Schematic illustration of heat-treatments employed in this study.

Fig. 2. Sketches of round tensile (A), fracture toughness (B), and impact toughness (C) specimens.

Fig. 3. Equilibrium pseudo-binary phase diagram of Fe-5Cr-C system.

Fig. 4. Optical micrographs of as-quenched steels: (a) and (b) are for 2 Mn modified alloy and (c) and (d) are for 5 Ni modified alloy. (a) and (c) are from single high temperature treated specimens whereas (b) and (d) are from grain-refined specimens.

Fig. 5. Prior austenite grain size as a function of alloying and heat-treatment.

Fig. 6. Bright field (a), dark-field (b) revealing auto-tempered ϵ-carbide in the single treated as-quenched 1 Mn modified alloy. The SAD pattern (c) containing streaked reflections from ϵ-carbide is indexed in (d).

Fig. 7. Bright-field micrographs (a) and (b) show the dislocated lath martensite structure devoid of any auto-tempered carbides in the as-quenched coarse grained structure of 2 Mn modified alloy.

Fig. 8. Bright-field micrographs (a) and (b) reveal the dislocated lath martensite while (c) and (d) show the presence of some substructural twinning in the 5 Ni modified alloy single treated and interrupted quenched to room temperature. Twinning reflections from (d) are shown in the SAD of (e) and suitably indexed in (f).

Fig. 9. Tempered ϵ-carbide observed in single treated 5 Ni modified alloy is shown in the BF micrographs (a) and (b).

Fig. 10. Bright-field (a), dark-field (b), selected area diffraction pattern (c) and the corresponding indexed pattern (d) revealing Widmanstatten cementite in the 200°C tempered specimens of 2 Mn modified alloy.

Fig. 11. Bright-field (a), dark-field (b), selected area diffraction (c) and the corresponding indexed pattern (d) revealing cementite precipitation in 0.5 Mn modified alloy tempered at 300°C.

Fig. 12. Morphology of cementite precipitation in 300°C tempered structures of 2 Mn modified alloy: bright-field (a) and dark-field (b) micrographs reveal typical widmanstätten platelets while bright-field (c) and dark-field (d) micrographs reveal on-going process of spheroidization of this carbide.

Fig. 13. Bright-field (a), dark-field (b), selected area diffraction pattern (c) and the corresponding indexed pattern (d) showing carbide precipitation in 300°C tempered, fine grained 5 Ni modified alloy. Retained austenite is identified by arrows in the DF micrograph (b).

Fig. 14. Bright-field (a), dark-field (b) revealing spheroidized cementite in 0.5 Mn modified alloy tempered at 500°C. (c) and (d) are the bright-field and dark-field micrographs showing interlath cementite in the same alloy.

Fig. 15. Bright-field (a), dark-field (b) showing presence of widmanstätten cementite and M_7C_3 precipitation in 2 Mn modified alloy tempered at 500°C. (d) is the analysis of the selected area diffraction pattern (c), which contains streaking presumably from M_7C_3 carbide.

Fig. 16. (a) BF, (b) DF, (c) SAD and (d) analysis revealing continued presence of fine widmanstätten cementite platelets in the 2 Mn alloy tempered at 500°C.

Fig. 17. (a) BF showing twinning, (b) DF showing twin boundary carbide precipitation and (c) DF revealing twins in bright contrast in 5 Ni alloy tempered at 500°C.

Fig. 18. (a) BF, (b) DF revealing both M_7C_3 and cementite in 5 Ni modified alloy tempered at 500°C. The SAD pattern shown in (c) is analysed in (d).

Fig. 19. Retained austenite in the as-quenched 1 Mn single treated alloy. (a) BF and (b) DF micrographs revealing austenite in bright contrast. Extensive retained austenite in this alloy is also shown in the BF (c) and DF (d) micrographs from a different area.

Fig. 20. Extensive retained austenite in the 5 Ni alloy (coarse grained) is revealed in the BF (a) and DF (b) micrographs. (c) is the DF micrograph of retained austenite from a different area of the specimen.

Fig. 21. DF comparison of the amount of retained austenite in the quaternary alloys. (a) base alloy, (b) 0.5 Mn alloy, (c) 1 Mn alloy, (d) 2 Mn alloy, (e) 5 Ni alloy, all coarse grained structures. The strong austenite reflections observed in the quaternary alloys can be seen from the indexed SAD pattern shown in (f).

Fig. 22. DF composite revealing continuous interlath films of retained austenite in the 1 Mn alloy (coarse grained) tempered at 200°C.

Fig. 23. Decomposition of retained austenite into interlath stringers of cementite in 300°C tempered 0.5 Mn alloy. (a) BF, (b) DF, (c) SAD and (d) analysis of this carbide.

Fig. 24. Decomposition of retained austenite into interlath stringers : cementite in 300°C tempered 2 Mn alloy. (a) BF, (b) DF, (c) SAD and (d) analysis of this carbide.

Fig. 25. (a) BF, (b) DF of γ, (c) SAD showing austenite reflections analysed in (d) in 300°C tempered 5 Ni alloy (fine grained).

Fig. 26. (a) BF and (b) DF revealing interlath cementite in coarse grained 2 Mn alloy tempered at 500°C.

Fig. 27. Variation in the volume fraction of retained austenite with Mn in single treated alloys.

Fig. 28. Volume fraction of retained γ vs. alloying in grain-refined steels. Also shows retained γ in 5 Ni alloy interrupted quenched (M_s-M_f) following single high temperature austenitization.

Fig. 29. % Retained γ vs. tempering temperature in 2 Mn and 5 Ni modified alloys.

Fig. 30. R_C hardness vs. tempering temperature.

Fig. 31. Strength vs. tempering temperature of single treated alloys.

Fig. 32. Strength vs. tempering temperature for grain-refined alloys.

Fig. 33. Strength vs. % Mn of the single treated, as-quenched alloys.

Fig. 34. % reduction in area vs. tempering temperature of the (a) single treated Mn modified alloys and (b) grain refined Mn and Ni modified quaternary alloys.

Fig. 35. Plane strain fracture toughness vs. yield strength.

Fig. 36. K_{IC} vs. w/o quaternary alloying for the grain refined structures.

Fig. 37. Impact energy vs. yield strength of single treated Mn modified alloys and grain refined Ni modified alloy.

Fig. 38. Impact energy vs. quaternary alloying for the grain-refined structures.

Fig. 39. Impact energy vs. tempering temperature for the single treated, coarse grained alloys.

Fig. 40. Comparison of impact energy as a function of tempering temperature for the coarse and fine grained structures of the 2 Mn alloy.

Fig. 41. Impact energy vs. tempering temperature for the grain refined 2 Mn and 5 Ni alloys.

Fig. 42. Ductile-brittle transition temperature curves for the base and quaternary steels.

Fig. 43. As-quenched CVN fractographs of coarse grained (a) 0.5 Mn (b) 2 Mn alloys.

Fig. 44. Fractographs of Fe-4Cr-0.3C + Mn alloys. (a) and (b) are from 0.5 Mn alloy at 200 and 300°C tempering respectively and (c) and (d) are from 2 Mn alloy at 200 and 300°C tempering respectively.

Fig. 45. CVN fractographs of coarse grained, 500°C tempered (a) 0.5 Mn and (b) 2 Mn alloys.

Fig. 46. CVN fractographs of grain refined 5 Ni modified alloy: (a) as-quenched, (b) 200°C tempered, (c) 400°C tempered and (d) 600°C tempered.

Fig. 47. Inclusion identification in coarse grained 2 Mn alloy: (a) Fractograph and (b) corresponding EDAX analysis of rounded inclusion (arrowed in (a)) in 200°C tempered structure and (c) fractograph and (d) EDAX analysis of rounded (arrowed in (c)) inclusion in 500°C tempered structure.

Fig. 48. Evolution of microsctructure and embrittlement during tempering of modified ultra-high strenght Fe-4Cr-0.3C steels.

Fig. 49. Fractography of the evolution of embrittlement during tempering of modified Fe-4Cr-0.3C steels.

Fig. 50. Schematic illustration of the morphology of retained austenite and martensite in high carbon, high alloy steels (a) and low carbon, low alloy steels (c). Morphology of fracture due to decomposition of retained austenite to carbide on tempering [(b) and (d)] depends on the initial microstructure (see text).

Fig. 51. Schematic of crack, displacements, and plastic zone in a two-phase material.

Fig. 52. Schematic showing desired duplex microstructure consisting of major phase martensite contributing to strength and minor phase retained austenite providing improved toughness.

Fig. 53. Comparison of toughness to strength relations in experimental quaternary alloys and equivalent commercial alloys. (a) Charpy impact energy vs. tensile strength and (b) plane strain fracture toughness vs. tensile strength.

Fig. 54. (a) Parallel laths in a packet martensite of binary Fe-12 Ni alloy. The $[110]_\alpha$ remains the same in all the laths of the region. BF micrograph. (b) Corresponding indexed SAD patterns with the electron zone axes shown in the top left circles.

Fig. 55. (a), (b) and (c): BF, DF and SAD pattern, respectively, revealing retained austenite in alloy 4 (Table VI). DF (b) is obtained using $(002)_\gamma$ reflection in (c). (d), (e), (f): BF, DF and SAD pattern showing retained austenite in alloy 6 (Table VI). DF (e) is obtained using $(02\bar{2})_\gamma$ reflection of the $[211]_\gamma$ zone. N-W orientation relationship is shown in (f).

Fig. 56. Stereographic analysis of relative rotations amongst the laths in a packet corresponding to Fig. 54. The axis of rotation, [110], is also the standard projection of the stereogram.

Fig. 57. Plotted composite austenite-martensite diffraction patterns revealing the relatively simple correspondence between the K-S and N-W orientation relationships between fcc austenite and bcc martensite.

Fig. 58. Detailed analysis of the diffraction pattern corresponding to Fig. 55 (c).

Fig. 59. Trace analysis of habit plane/direction for the martensite transformation, (a) analysis of plane in martensite showing $(011)_\alpha$ and $(133)_\alpha$ habits, (b) analysis of direction in martensite showing near $[111]_\alpha$ habit, (c) direct analysis of plane in parent austenite revealing near $(111)_\gamma$ habit.

Fig. 60. Lattice image micrographs (a) and (b) are obtained from Fe-4Cr-0.3C-5Ni alloy (grain refined): (a) shows $(101)_\alpha$ lattice fringes near a martensite packet boundary. The location of packet boundary as judged from contrast variation in conventional bright-field is indicated by arrows, (b) shows $(101)_\alpha$ lattice fringes within the martensite region. Several end-on dislocations can be seen and one of them is marked on the micrograph.

Fig. 61. Schematic representation of accommodation within a martensite packet: Case I represents no accommodation, Case II represents accommodation over a group of laths and Case III shows accommodation in adjacent twin related laths.

Fig. 62. (a) Suggested ledge model of the austenite/martensite interface, (b) and (c) show different ledge configurations leading to either different macroscopic and microscopic habit planes (b) or a single habit plane (c).

Fig. 63. Proposed morphology of lath martensite, b > a >> c. Arrows indicate carbon segregation into austenite (A) from adjoining martensite (M).

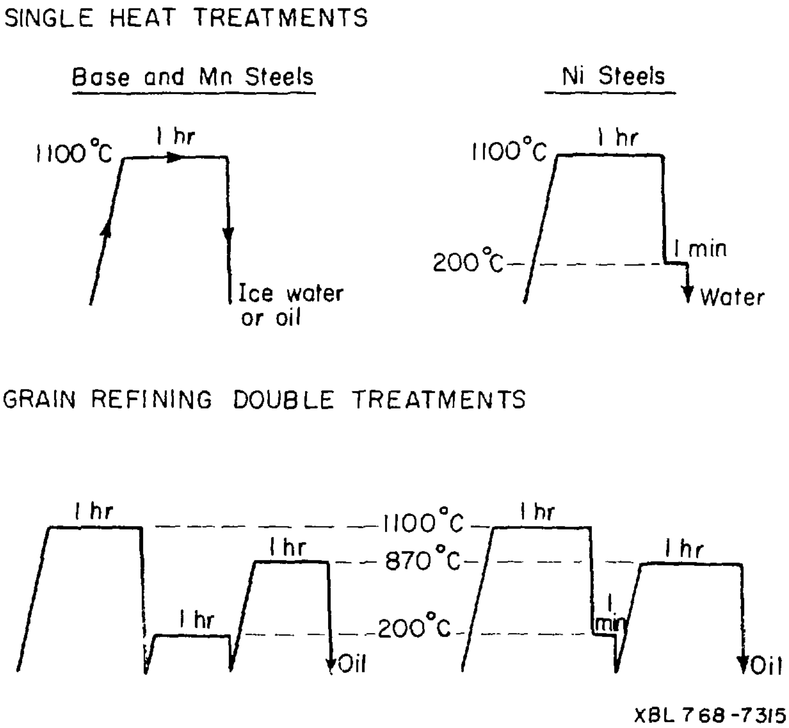
SINGLE HEAT TREATMENTS
Base and Mn Steels
1100°C
1 hr
Ice water or oil
Ni Steels
1100°C
1 hr
200°C
1 min
Water
GRAIN REFINING DOUBLE TREATMENTS
1 hr
1 hr
1 hr
1100°C
870°C
200°C
Oil
1 hr
1 hr
1 min
Oil
XBL 768-7315

Fig. 1

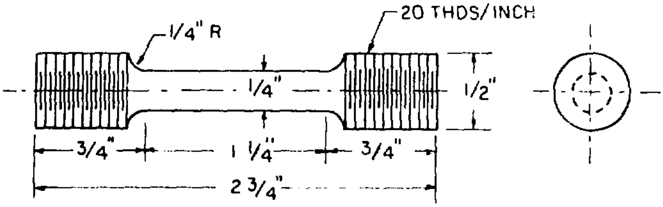

A. ROUND TENSILE SPECIMEN

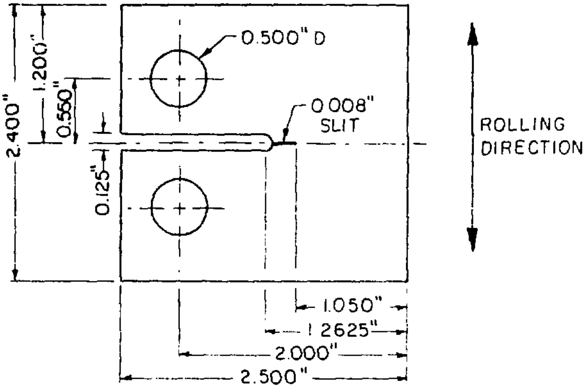

B. FRACTURE TOUGHNESS SPECIMEN

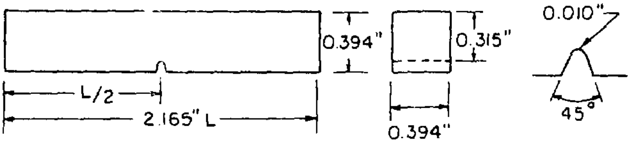

C. CHARPY V-NOTCH IMPACT SPECIMEN

XBL 754-6176

Fig. 2

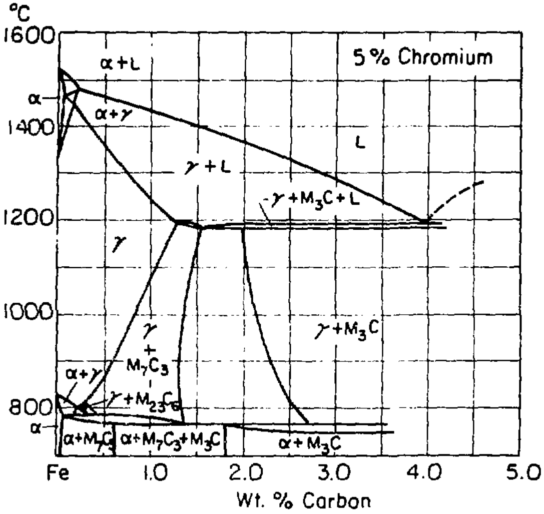

XBL 782-4554

Fig. 3

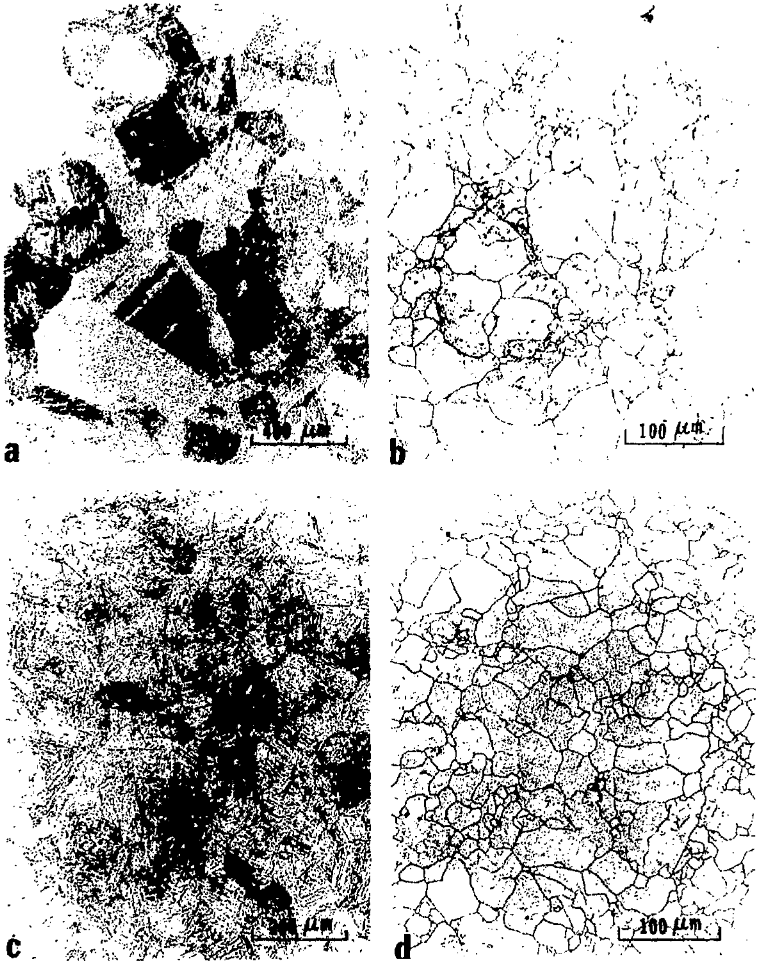

XBB 782-1185

Fig. 4

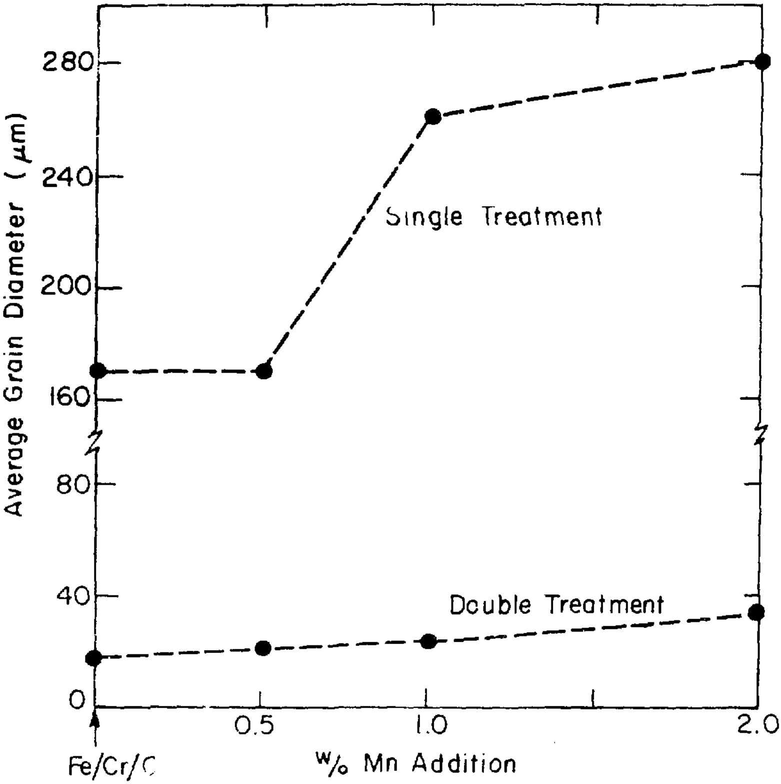

XBL 768-7313

Fig. 5

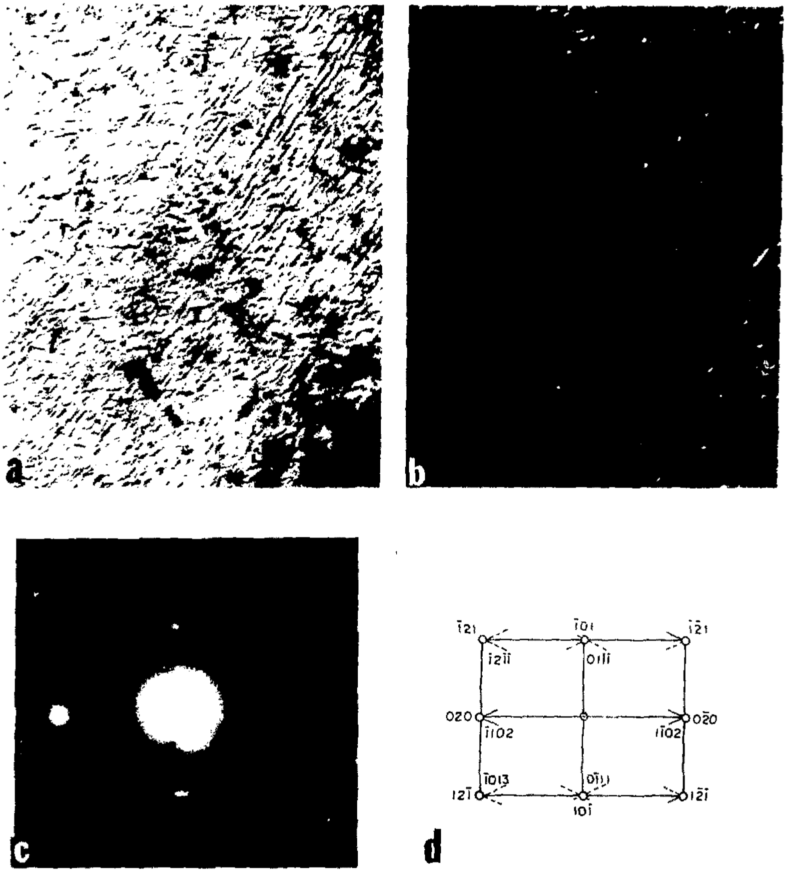

XBB 782-1180

Fig. 6

XBB 768-7131

Fig. 7

XBB 768-7133

Fig. 8 (a-d)

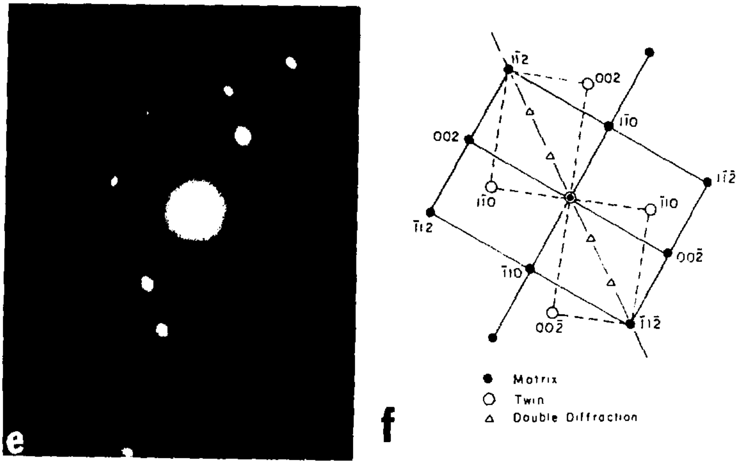

XBB 782-1179

Fig. 8 (e-f)

XBB 782-1182

Fig. 9

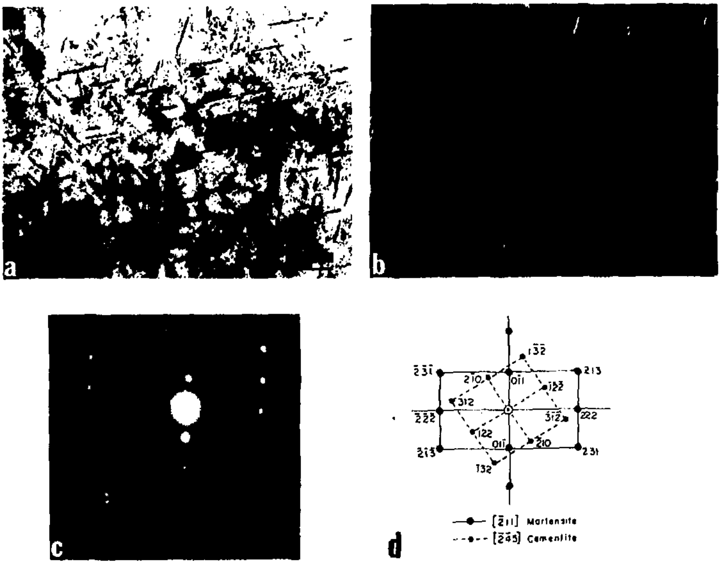

XBB 782-1175

Fig. 10

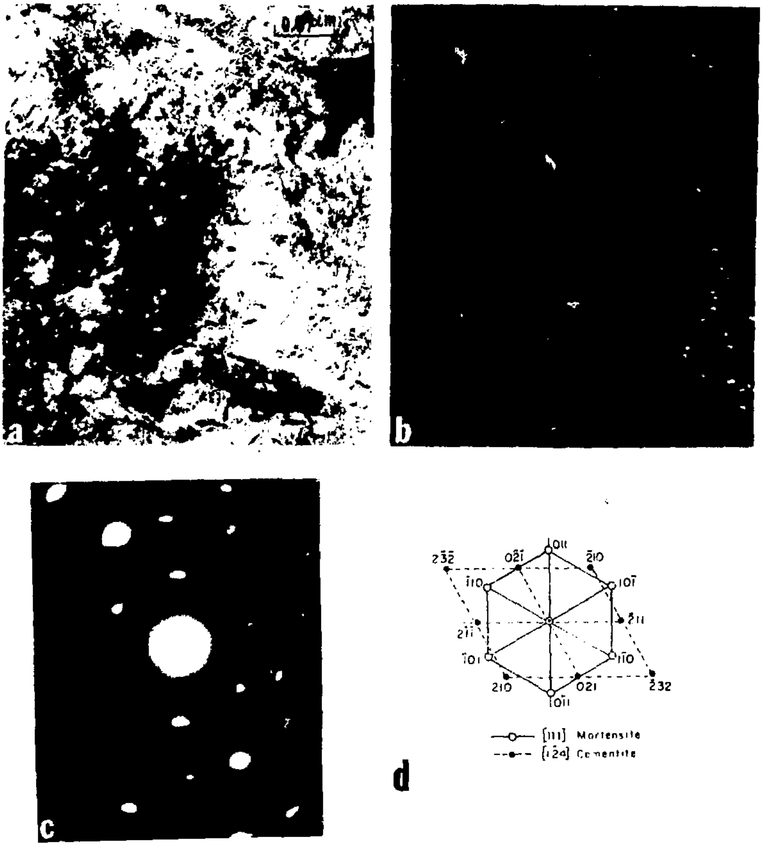

XBB 782-1177

Fig. 11

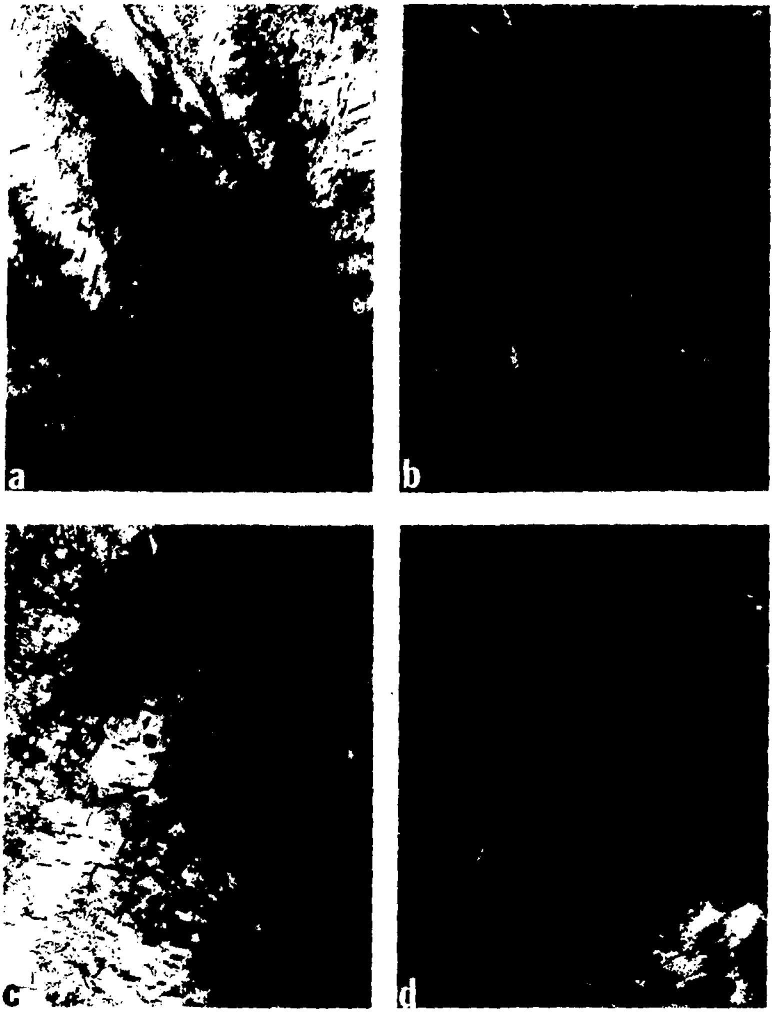

XBB 782-1186

Fig. 12

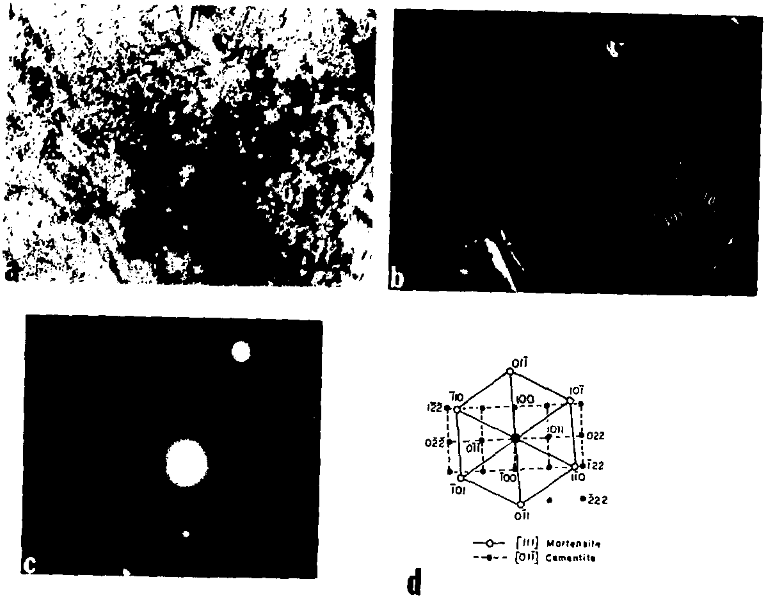

XBB 782-1173

Fig. 13

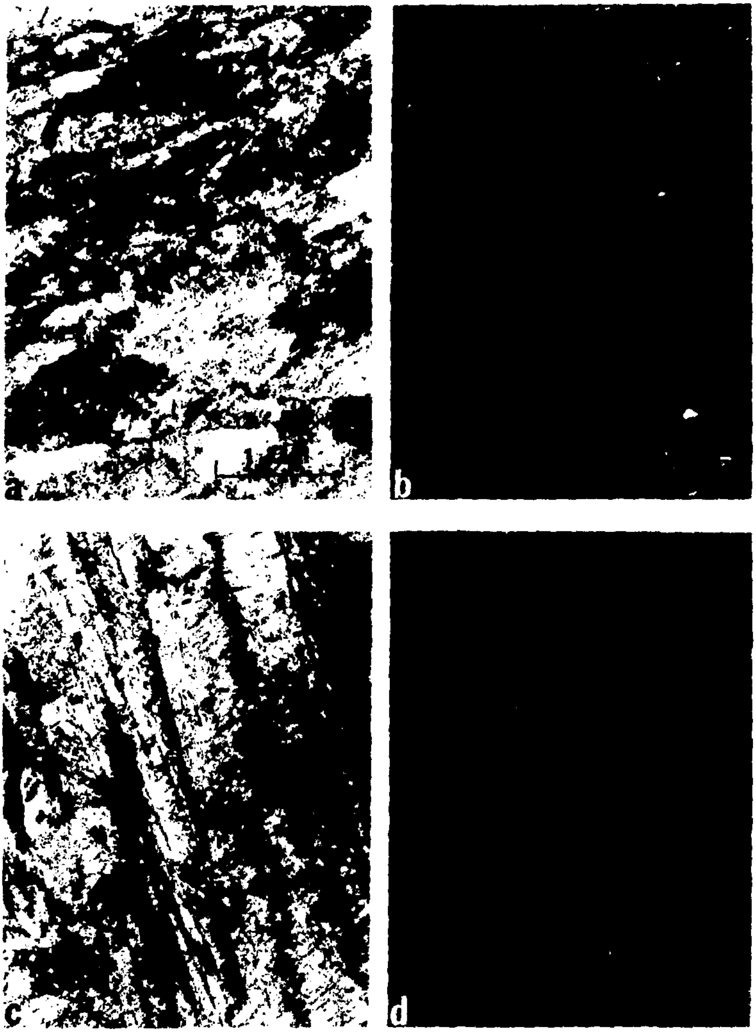

XBB 782-1056

Fig. 14

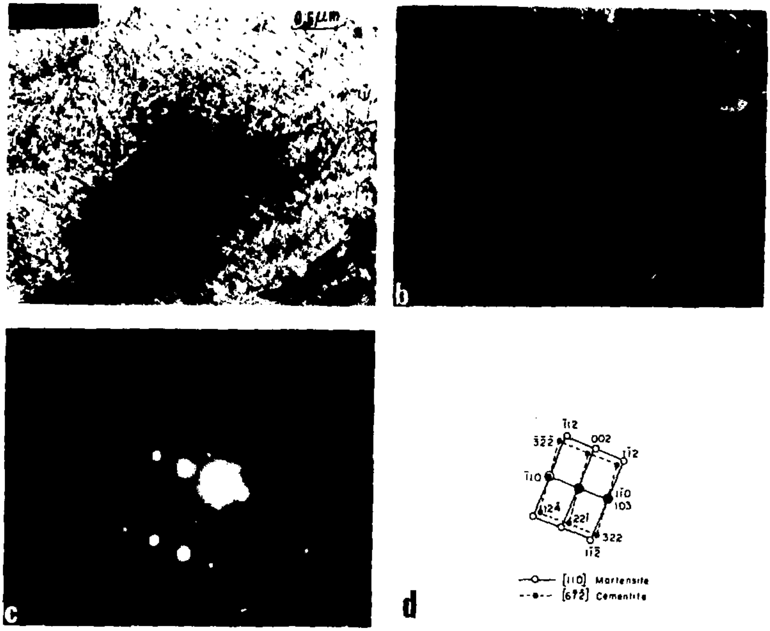

XBB 782-1171

Fig. 15

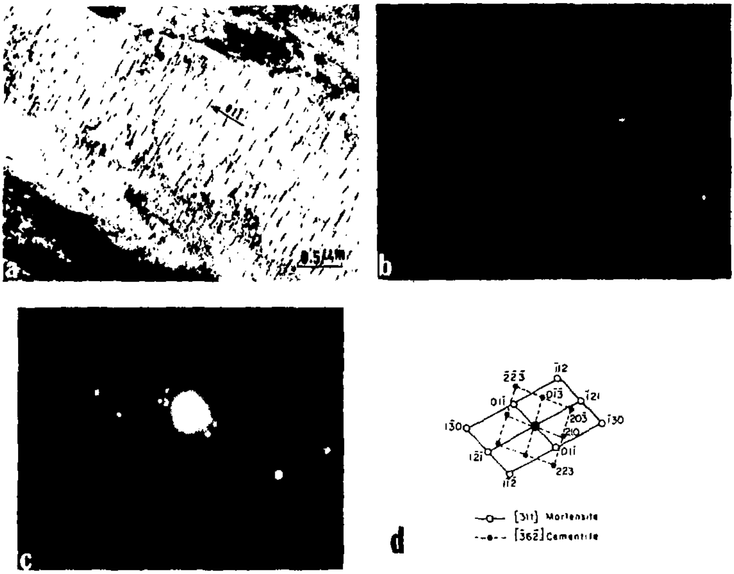

XBB 782-1176

Fig. 16

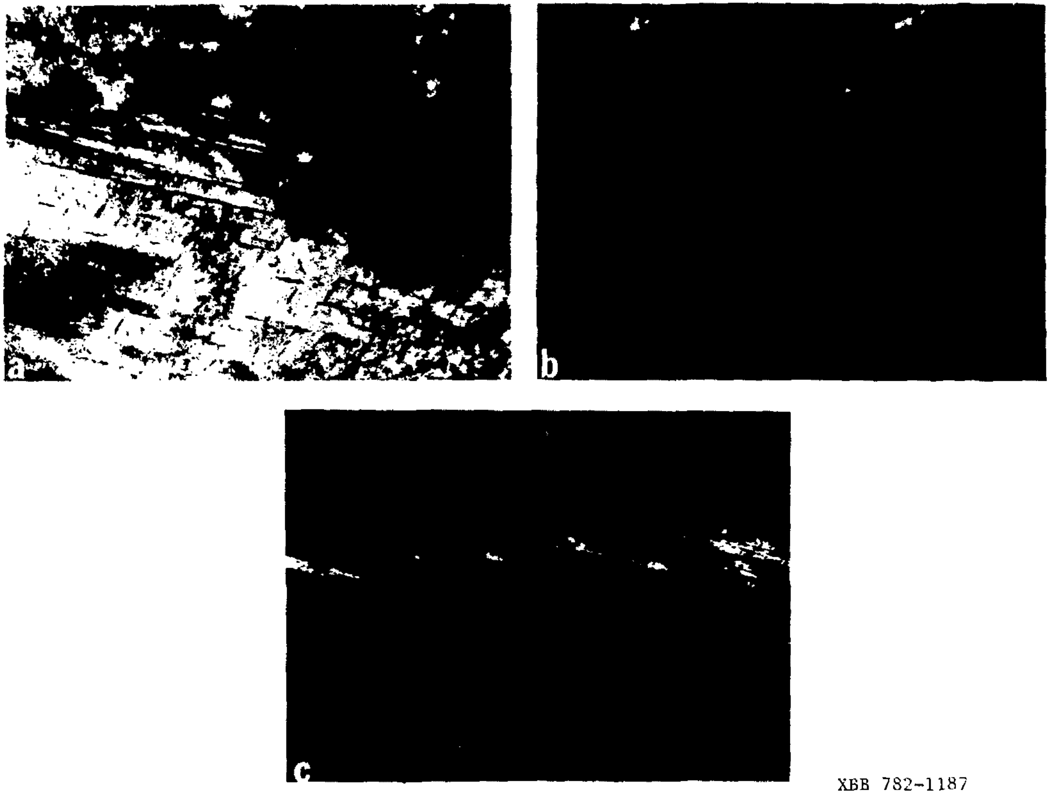

XBB 782-1187

Fig. 17

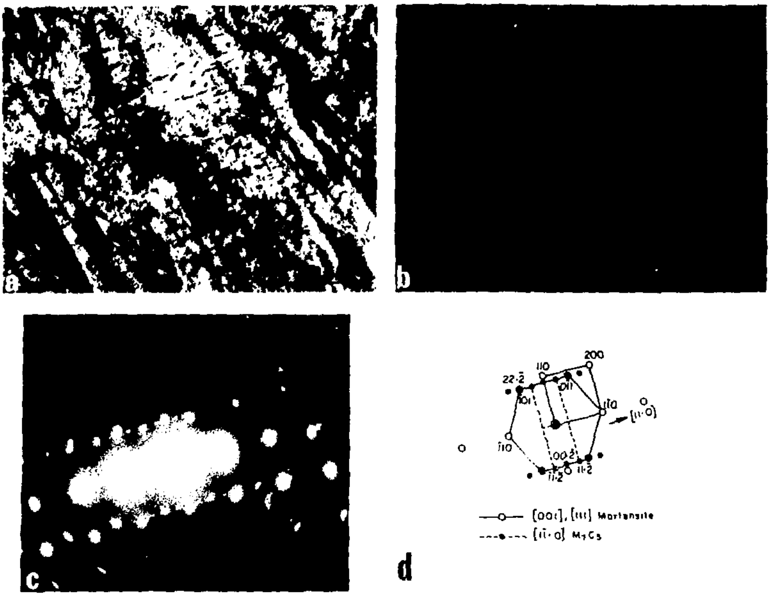

XBB 782-1172

Fig. 18

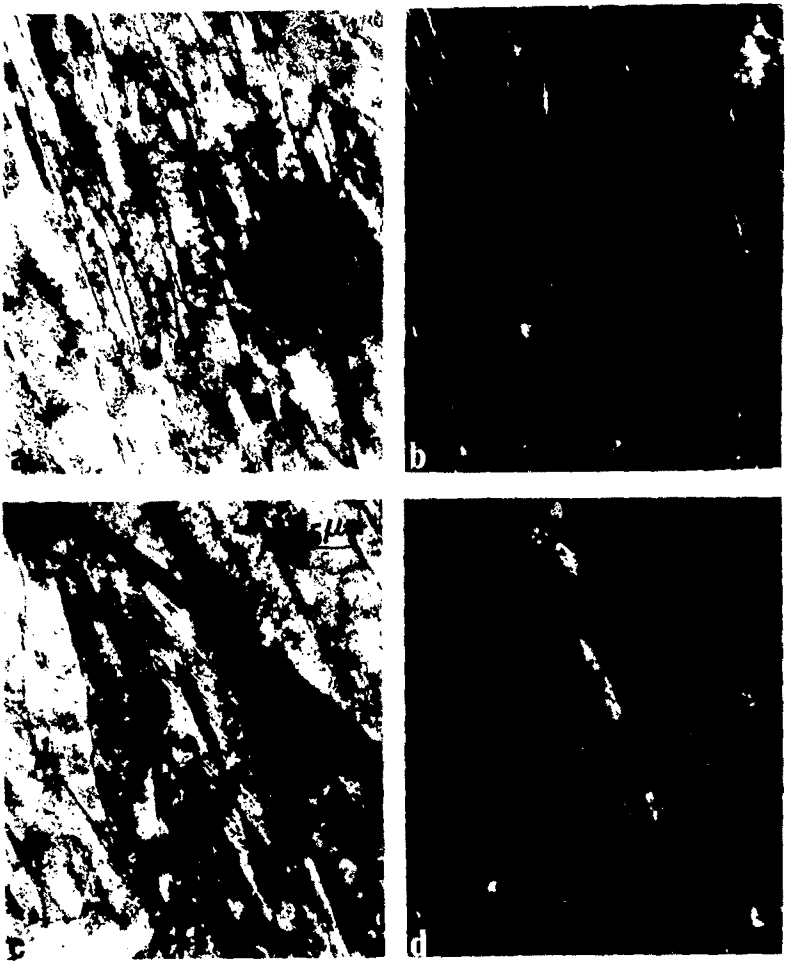

XBB 782-1055

Fig. 19

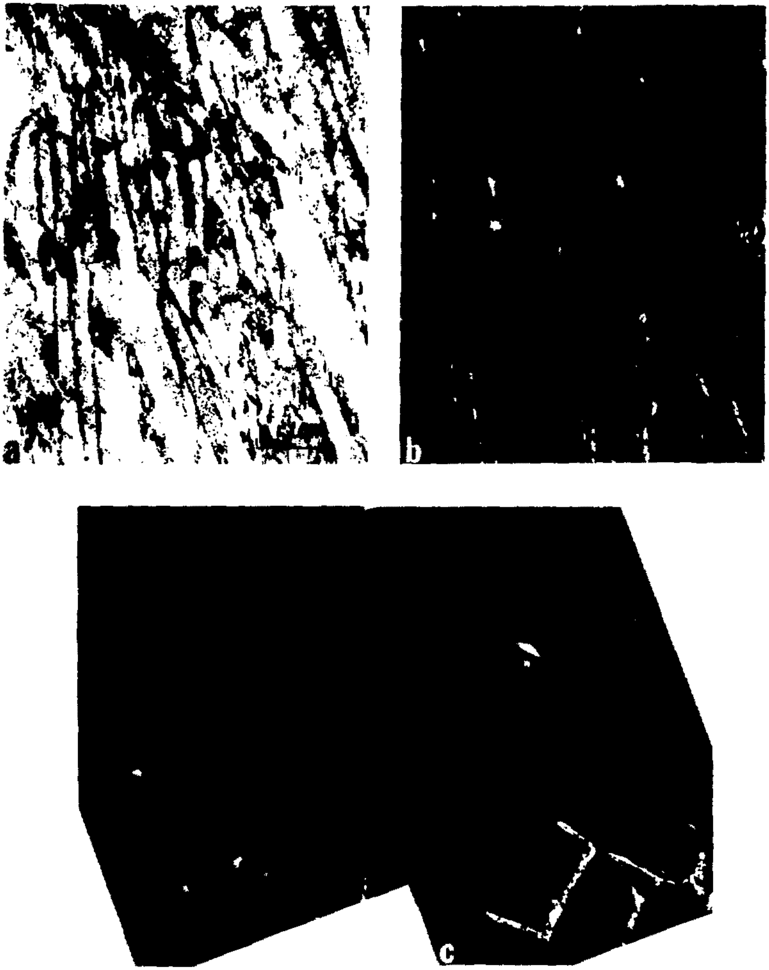

XBB 768-7130

Fig. 20

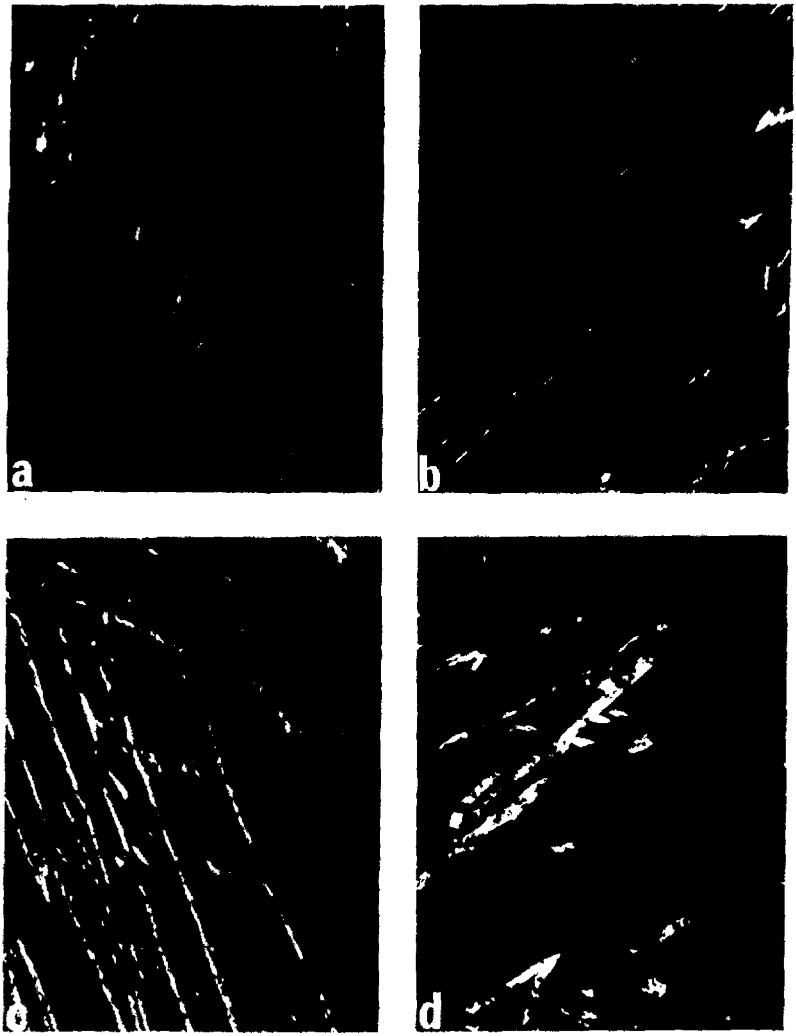

XBB 774-3111

Fig. 21 (a-d)

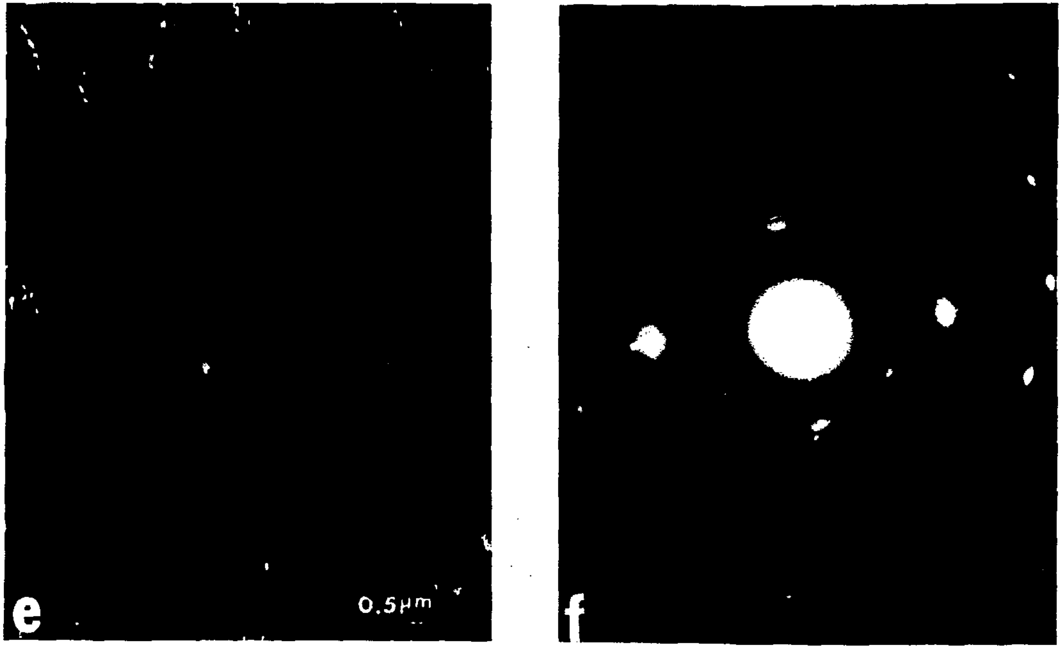

XBB 774-3112

Fig. 21 (e-f)

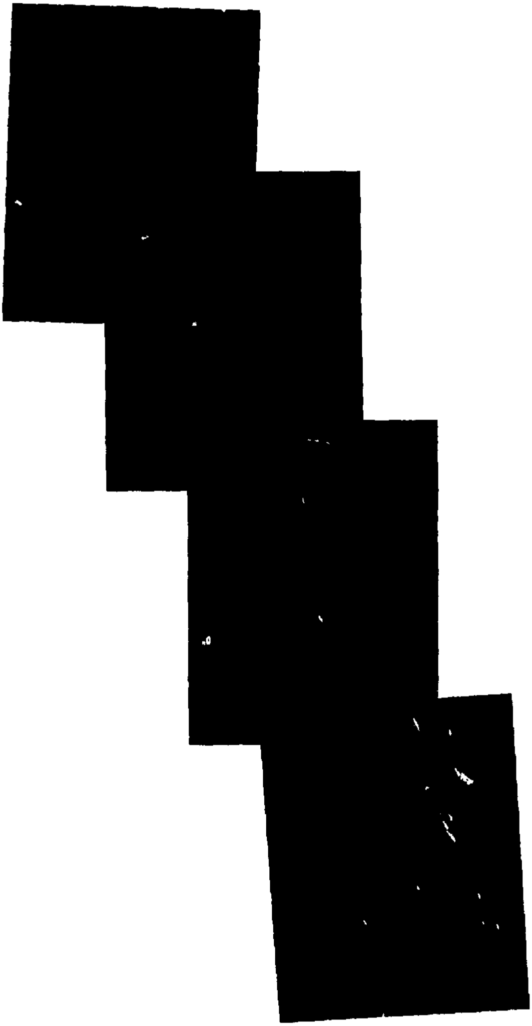

XBB 782-1054

Fig. 22

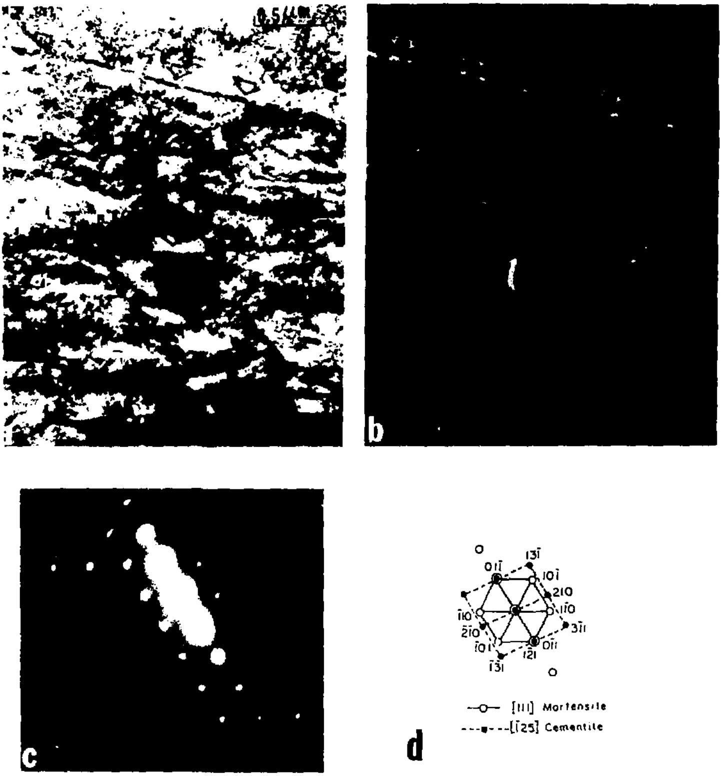

XBB 782-1178

Fig. 23

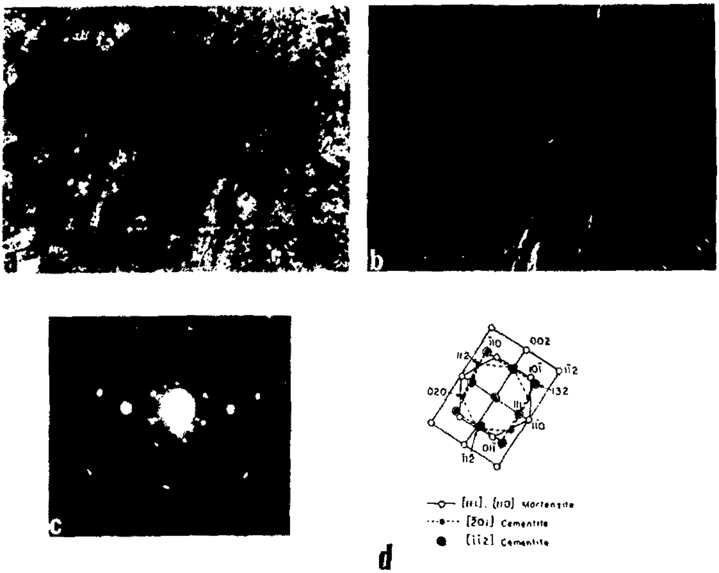

XBB 782-1174

Fig. 24

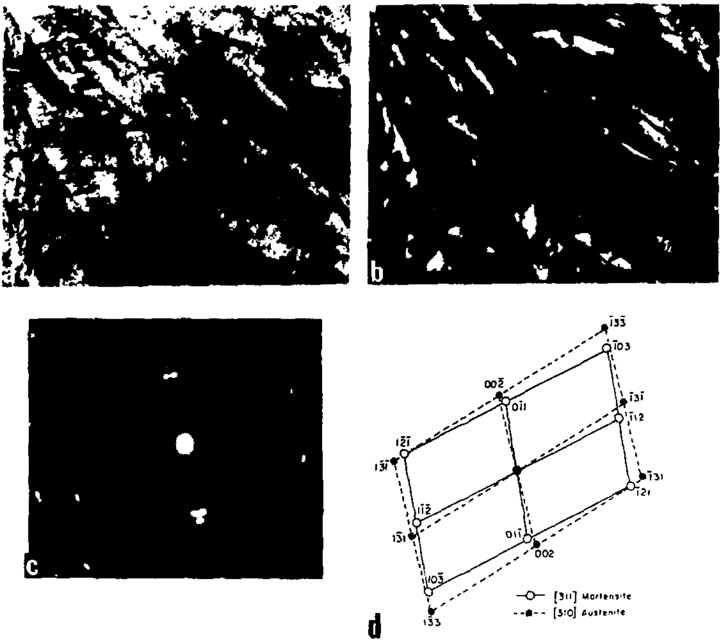

XBB 782-1181

Fig. 25

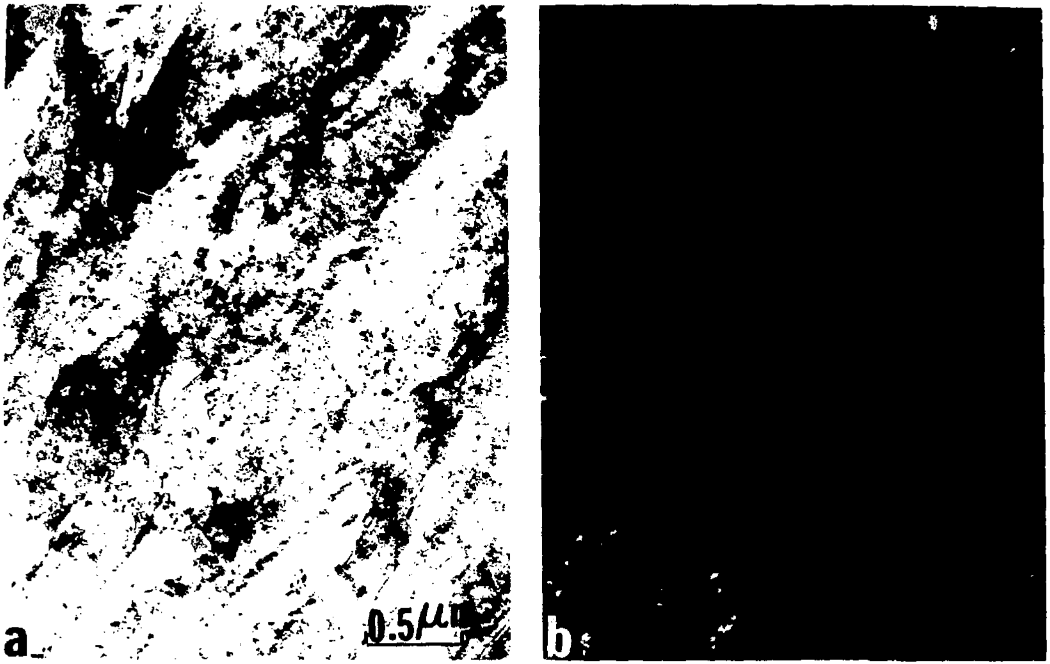

XBB 782-1057

Fig. 26

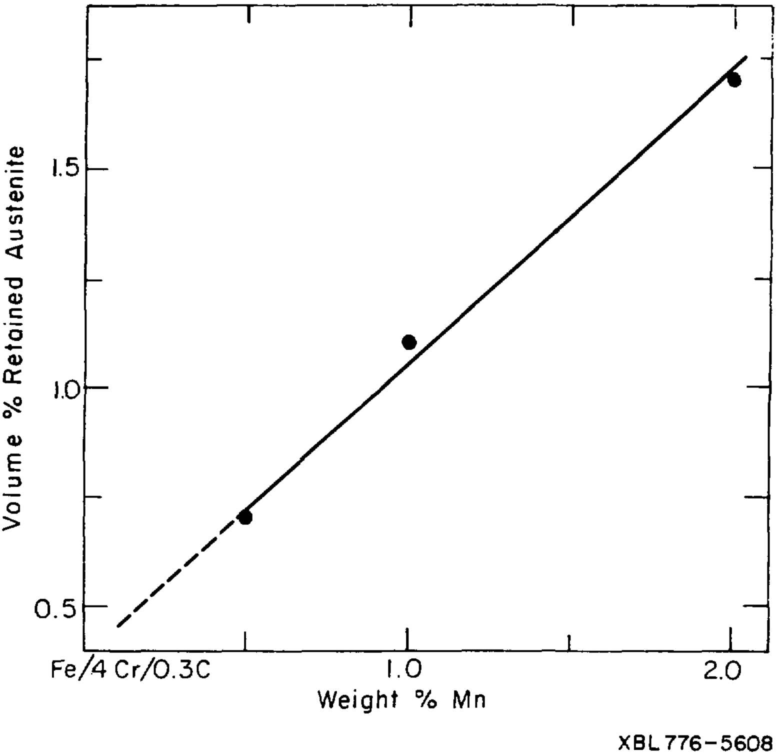
Volume % Retained Austenite
1.5
1.0
0.5
Fe/4 Cr/0.3C
1.0
2.0
Weight % Mn
XBL 776-5608

Fig. 27

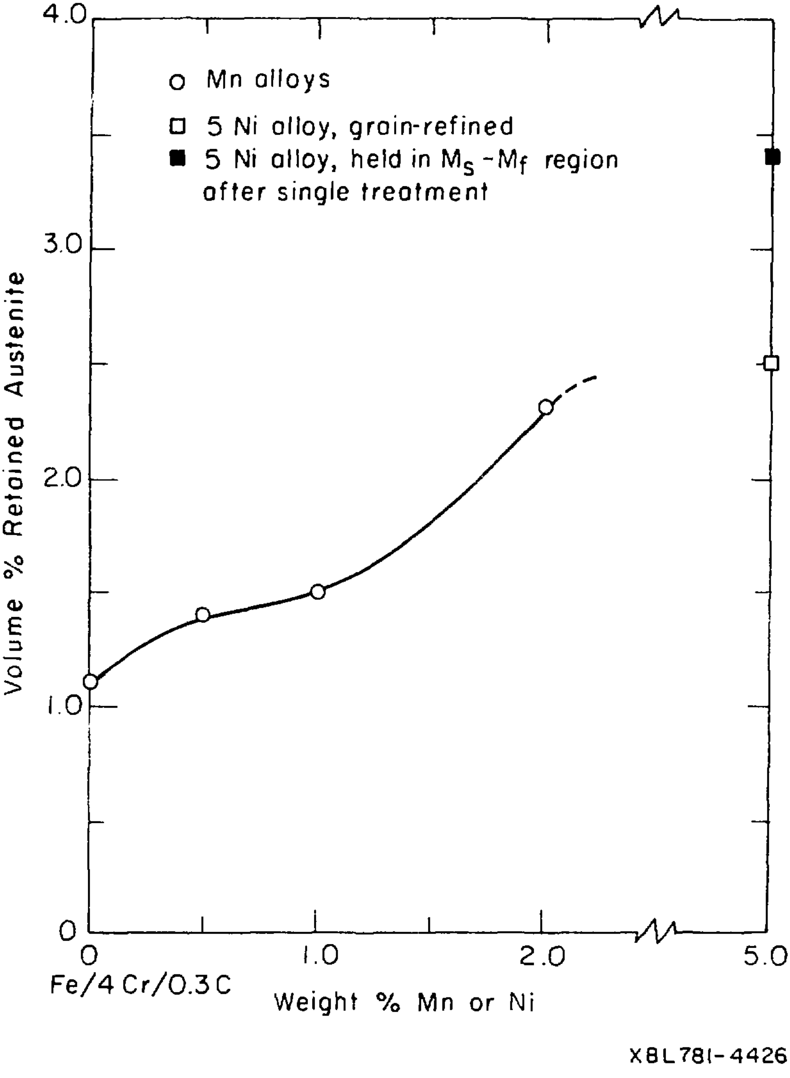
4.0
3.0
2.0
1.0
0
Volume % Retained Austenite
○ Mn alloys
□ 5 Ni alloy, grain-refined
■ 5 Ni alloy, held in M_s -M_f region after single treatment
0
1.0
2.0
5.0
Fe/4 Cr/0.3 C
Weight % Mn or Ni
XBL781-4426

Fig. 28

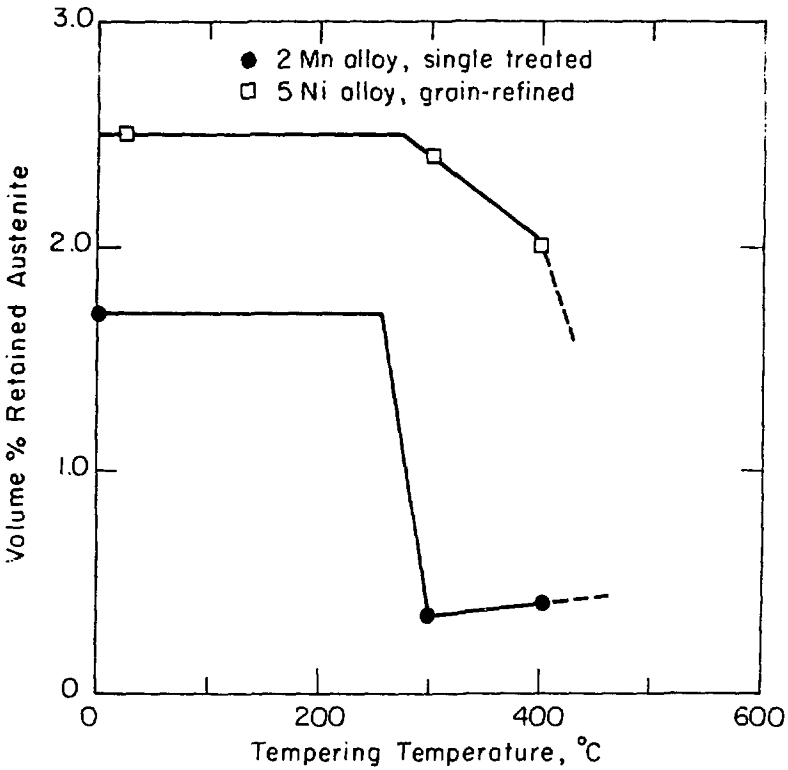

XBL781-4425

Fig. 29

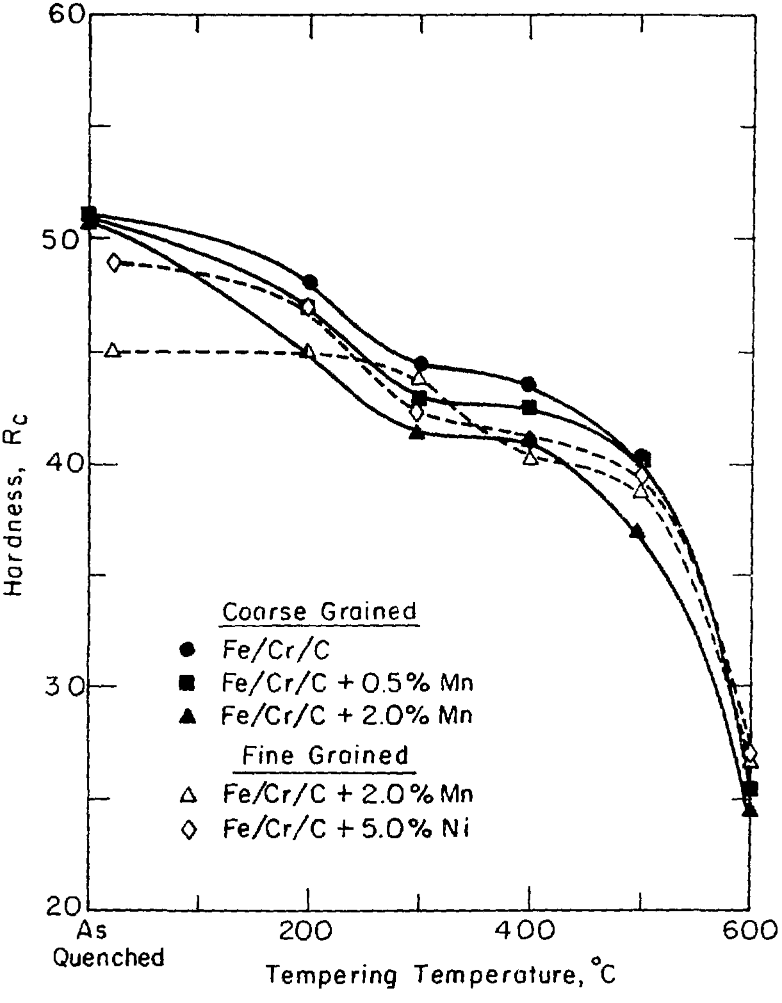

XBL781-4428

Fig. 30

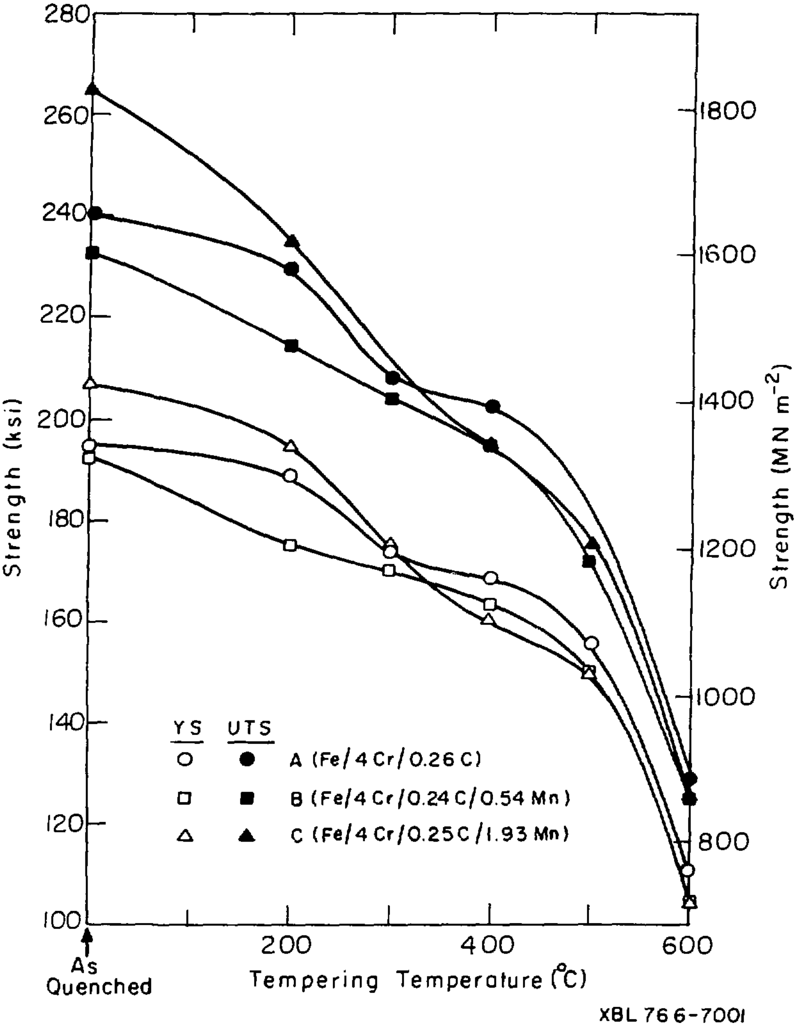
Strength (ksi)
280
260
240
220
200
180
160
140
120
100
Strength (MN m^{-2})
1800
1600
1400
1200
1000
800
200
400
600
As Quenched
Tempering Temperature (°C)
YS UTS
○ ● A (Fe/4 Cr/0.26 C)
□ ■ B (Fe/4 Cr/0.24 C/0.54 Mn)
△ ▲ C (Fe/4 Cr/0.25 C/1.93 Mn)
XBL 766-7001

Fig. 31

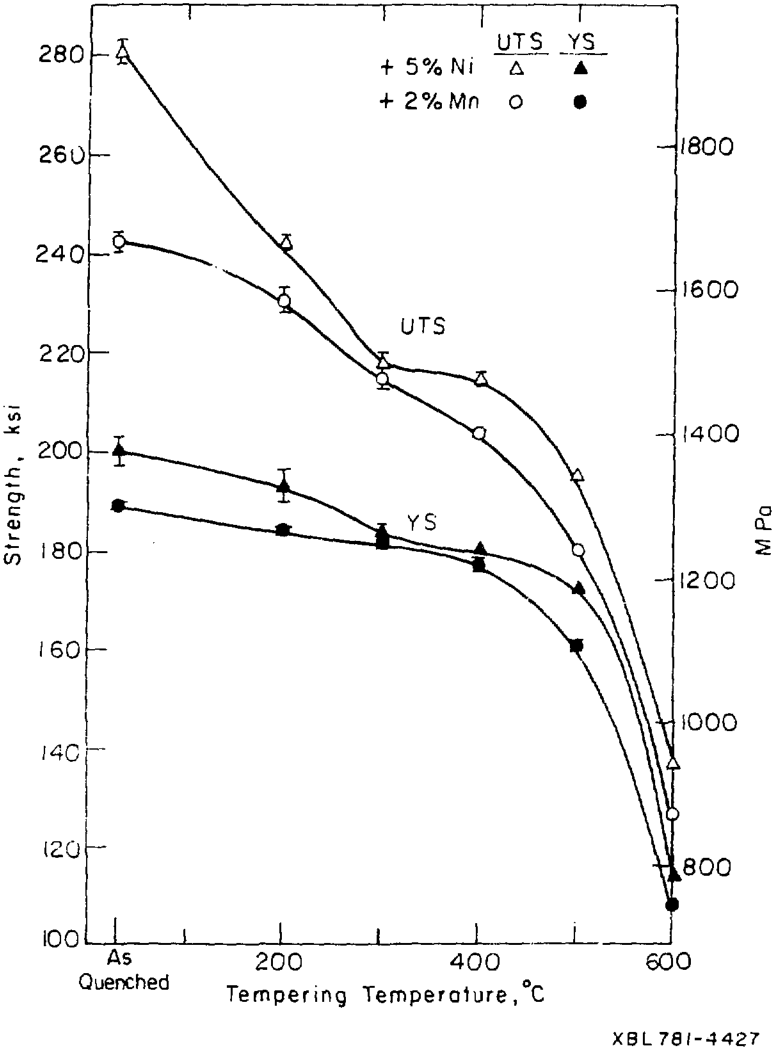
UTS
YS
+ 5% Ni
Δ
▲
+ 2% Mn
○
●
UTS
YS
Strength, ksi
280
260
240
220
200
180
160
140
120
100
MPa
1800
1600
1400
1200
1000
800
As Quenched
200
400
600
Tempering Temperature, °C
XBL 781-4427

Fig. 32

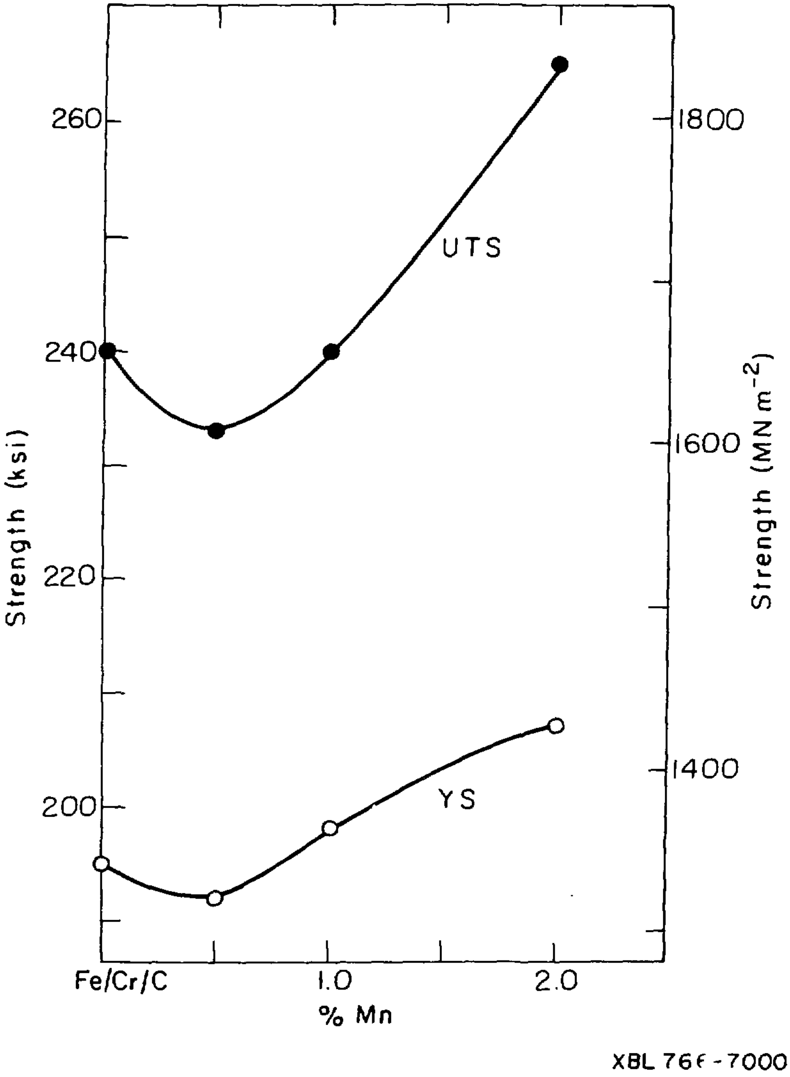
260
240
220
200
1800
1600
1400
UTS
YS
Strength (ksi)
Strength (MN m^{-2})
Fe/Cr/C
1.0
2.0
% Mn
XBL 766-7000

Fig. 33

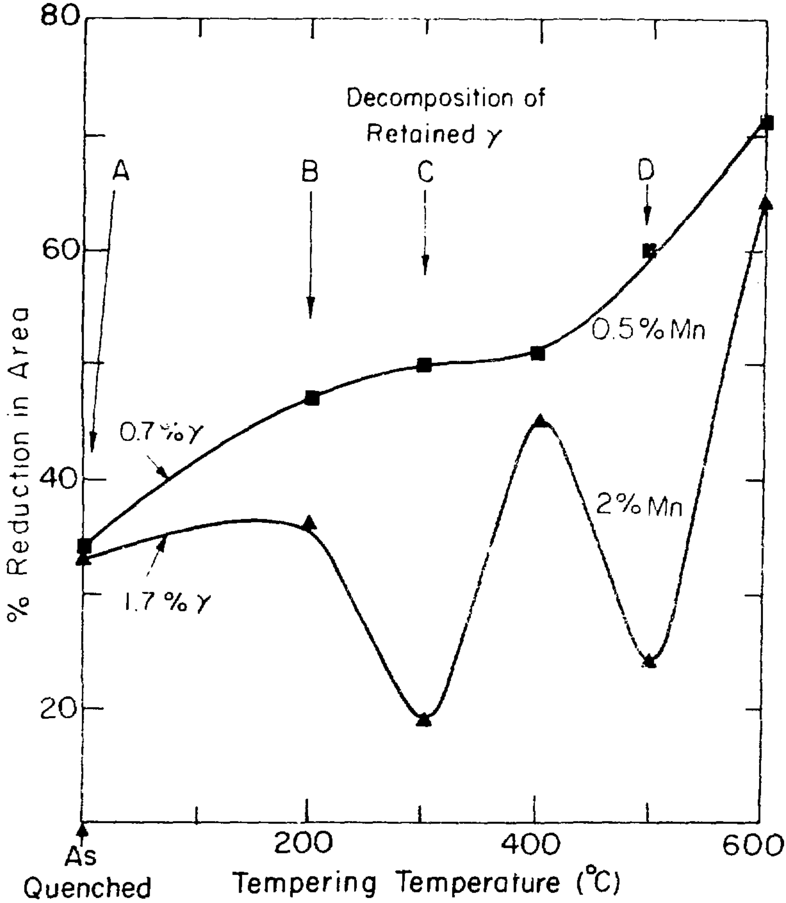

XBL776-5607

Fig. 34 (a)

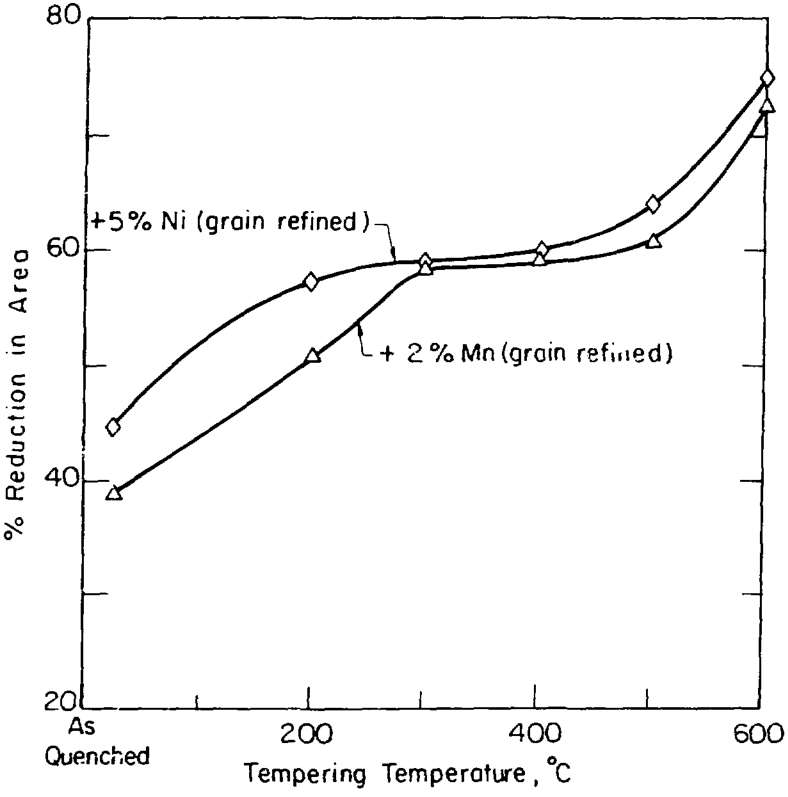

XBL 781-4436

Fig. 34 (b)

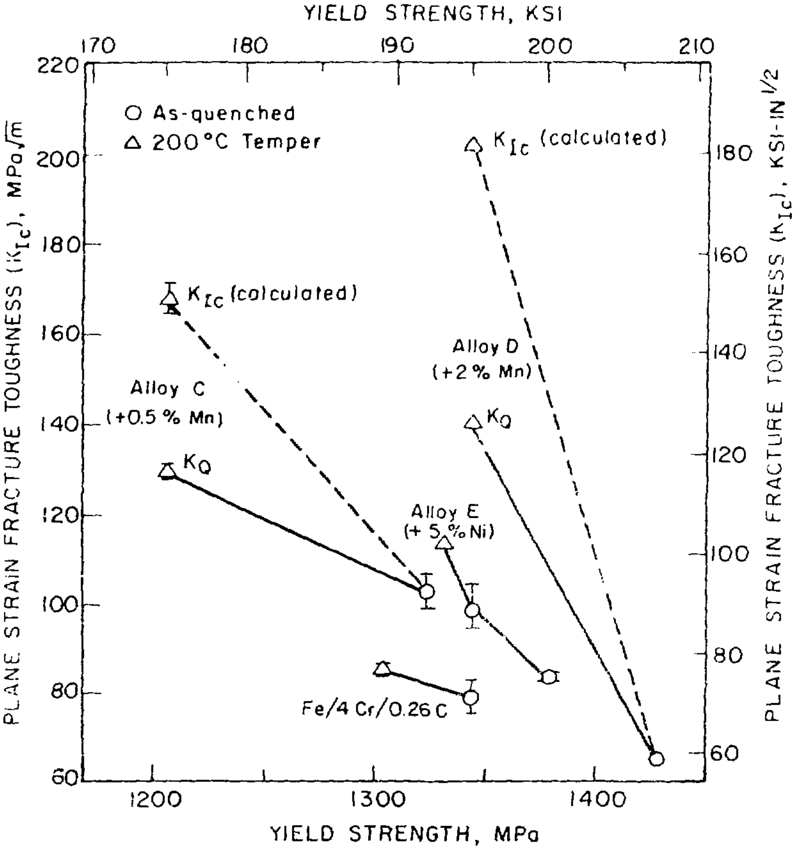
YIELD STRENGTH, KSI
170
180
190
200
210
220
200
180
160
140
120
100
80
60
PLANE STRAIN FRACTURE TOUGHNESS (K_{Ic}), MPa$\sqrt{m}$
PLANE STRAIN FRACTURE TOUGHNESS (K_{Ic}), KSI-IN$^{1/2}$
180
160
140
120
100
80
60
○ As-quenched
△ 200°C Temper
K_{Ic} (calculated)
K_{Ic} (calculated)
Alloy D
(+2 % Mn)
Alloy C
(+0.5 % Mn)
K_Q
K_Q
Alloy E
(+ 5 % Ni)
Fe/4 Cr/0.26 C
1200
1300
1400
YIELD STRENGTH, MPa
XBL 764-6733

Fig. 35

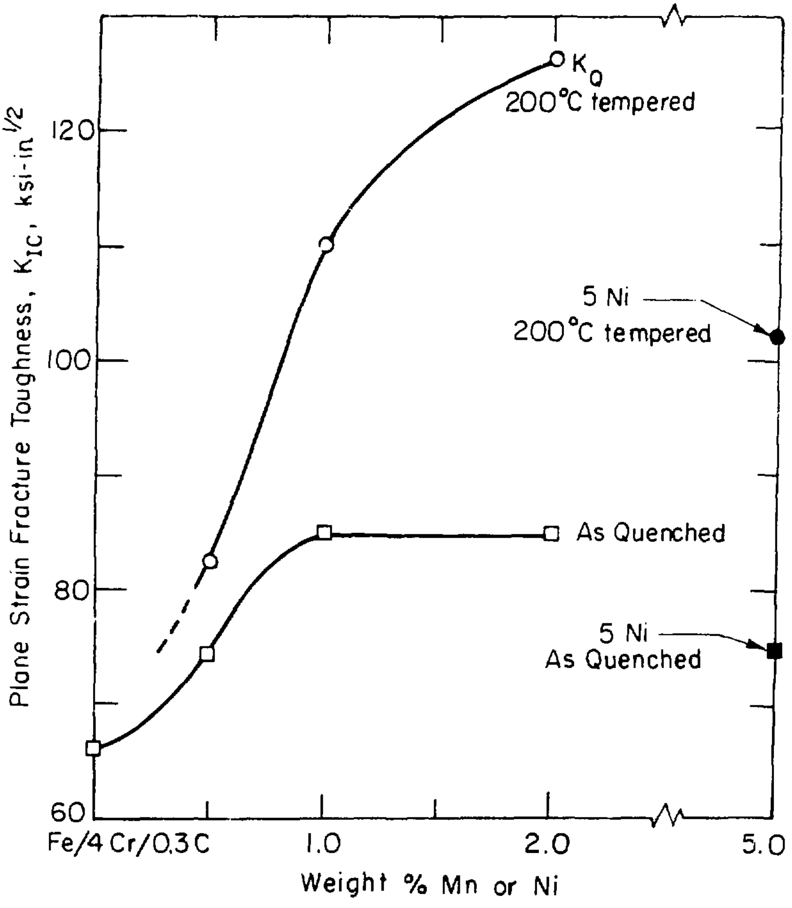

XBL 781-4437

Fig. 36

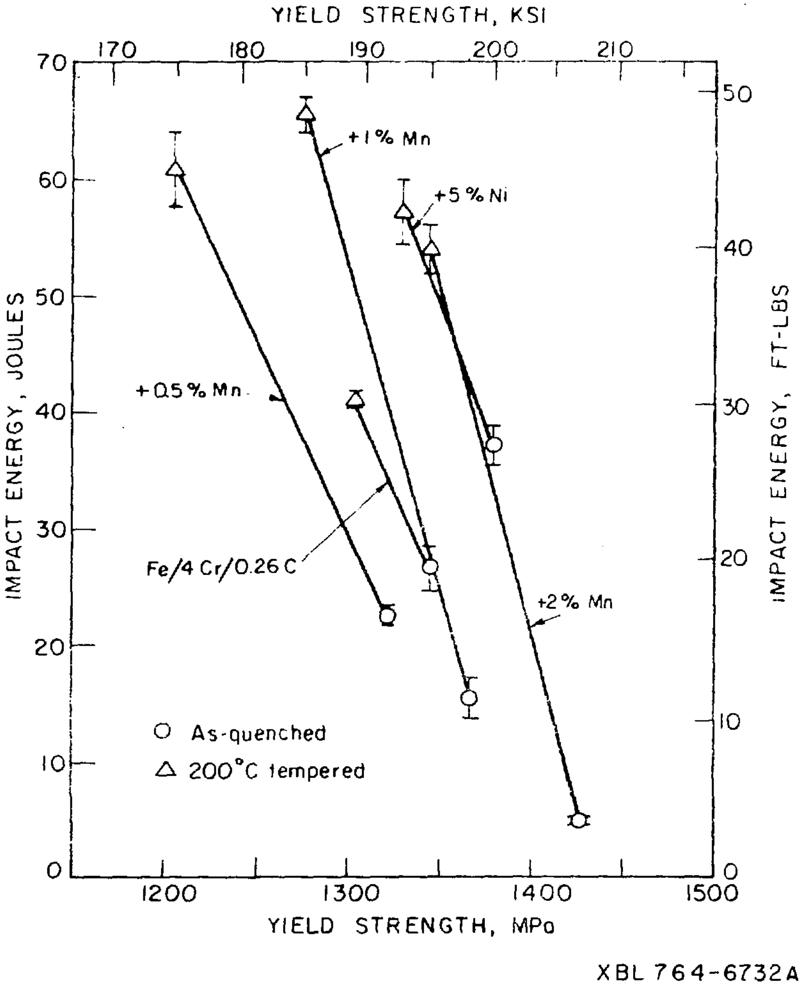
YIELD STRENGTH, KSI
170
180
190
200
210
70
60
50
40
30
20
10
0
IMPACT ENERGY, JOULES
50
40
30
20
10
0
IMPACT ENERGY, FT-LBS
+1% Mn
+5% Ni
+0.5% Mn
Fe/4 Cr/0.26 C
+2% Mn
○ As-quenched
△ 200°C tempered
1200
1300
1400
1500
YIELD STRENGTH, MPa
XBL 764-6732A

Fig. 37

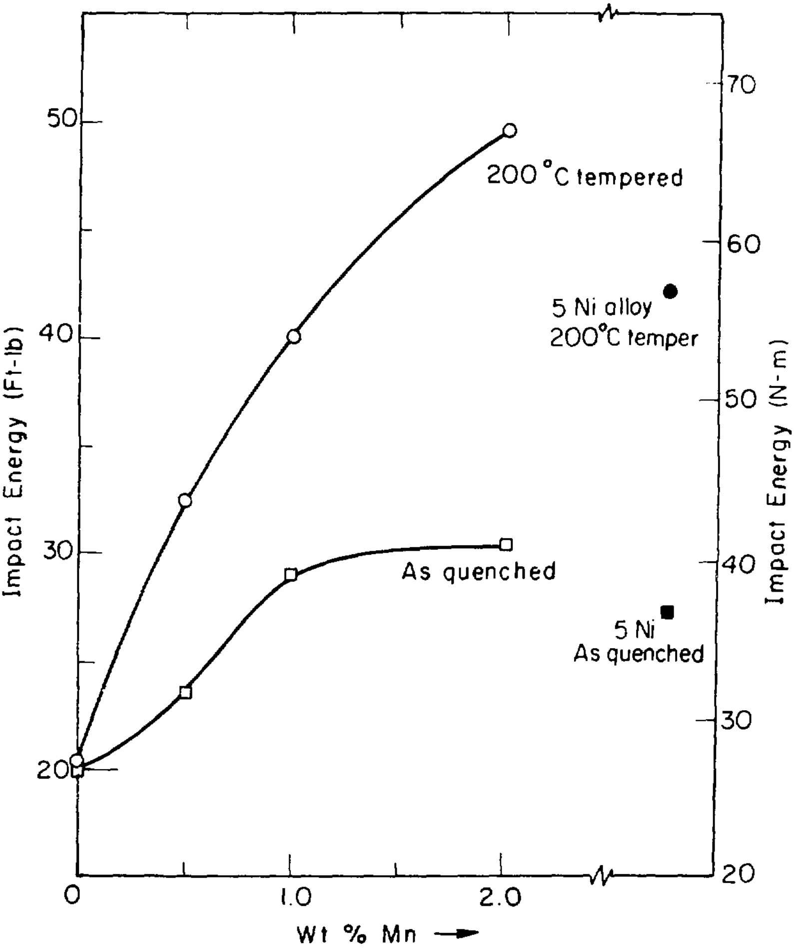

XBL 774-5303

Fig. 38

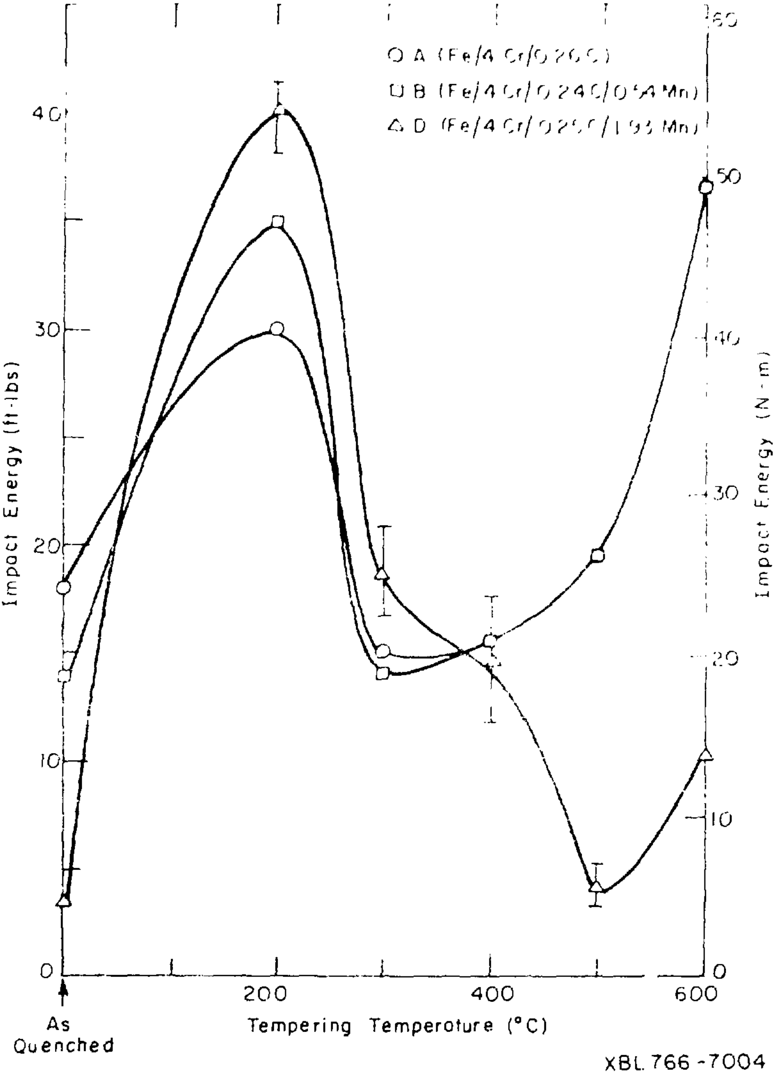

XBL 766-7004

Fig. 39

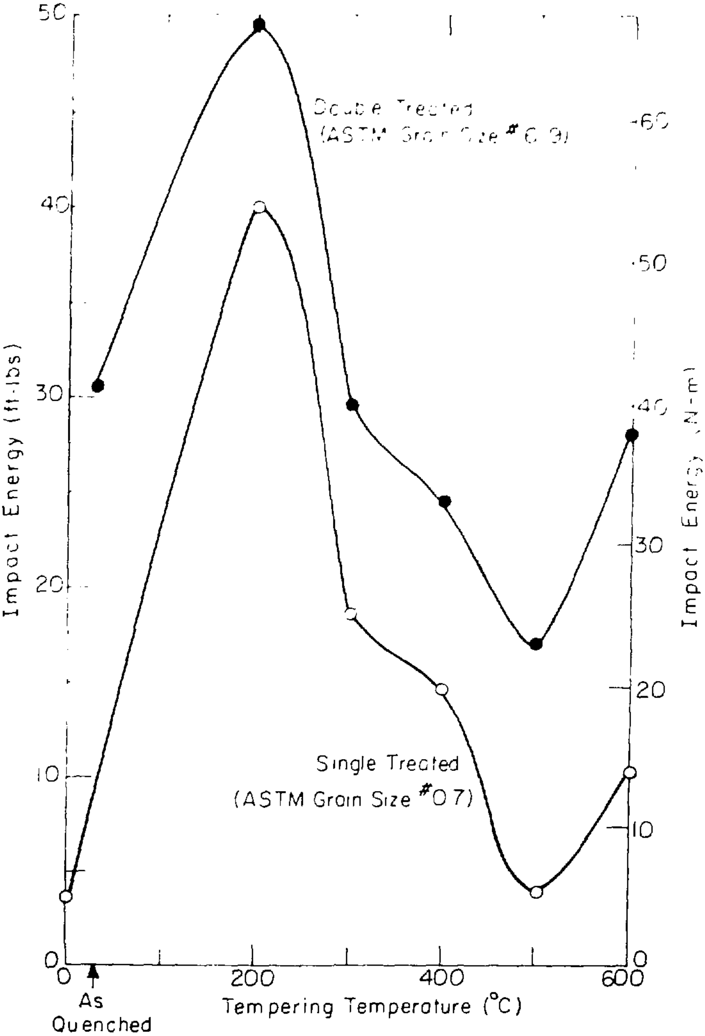

XBL 766-7002

Fig. 40

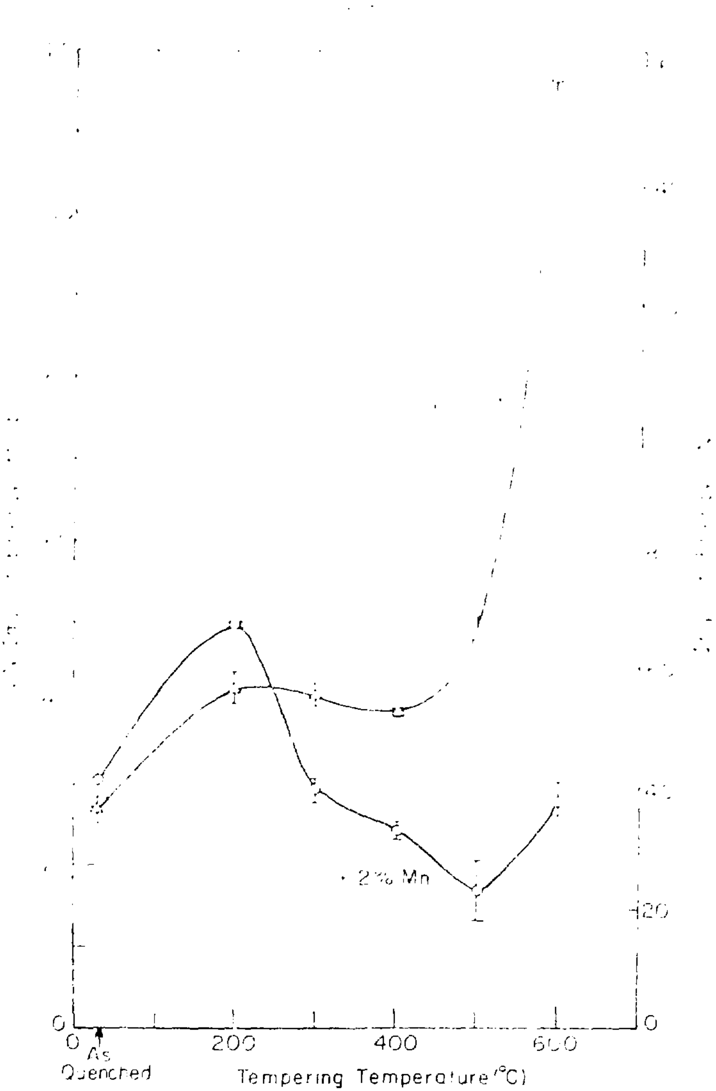

XBL 766-7006

Fig. 41

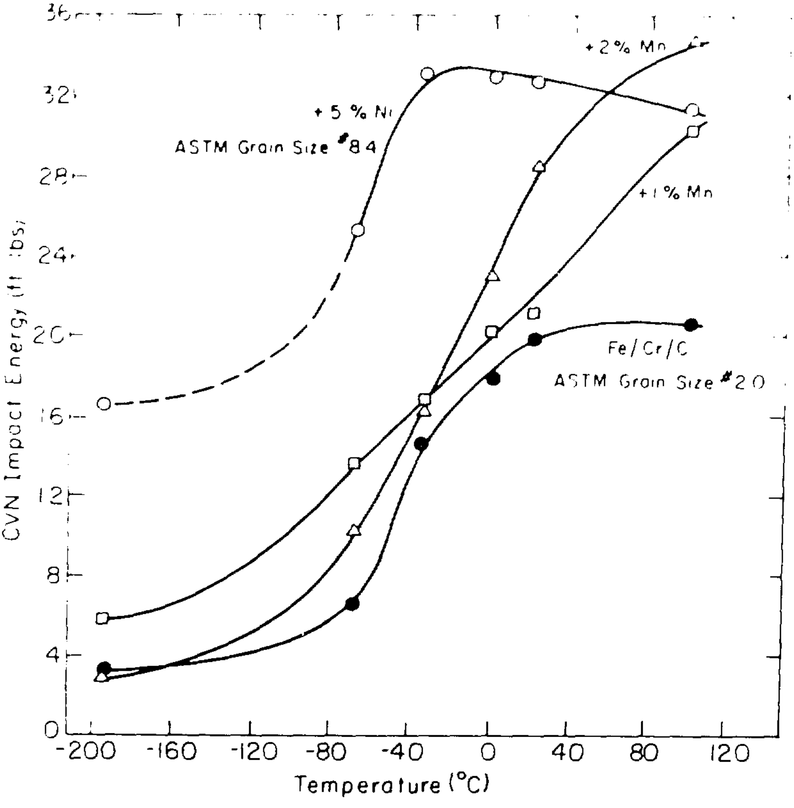

XBL 766-6999

Fig. 42

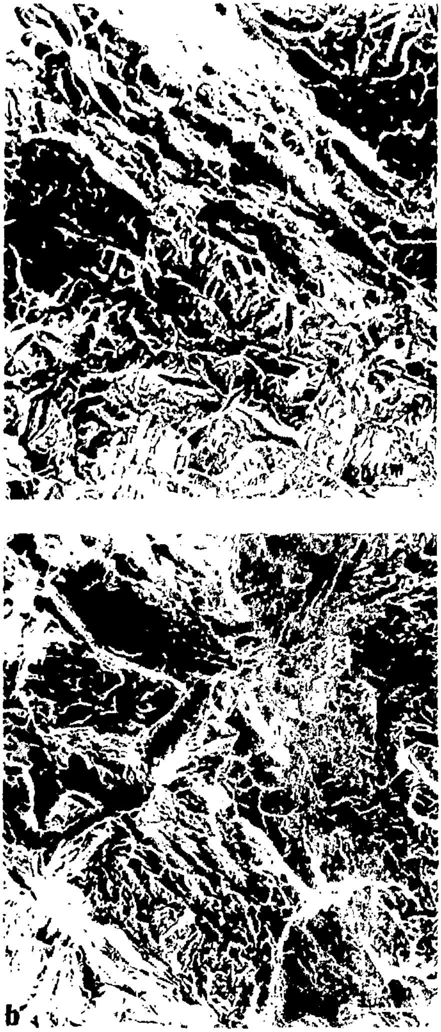

[illegible] 1058

Fig. 18

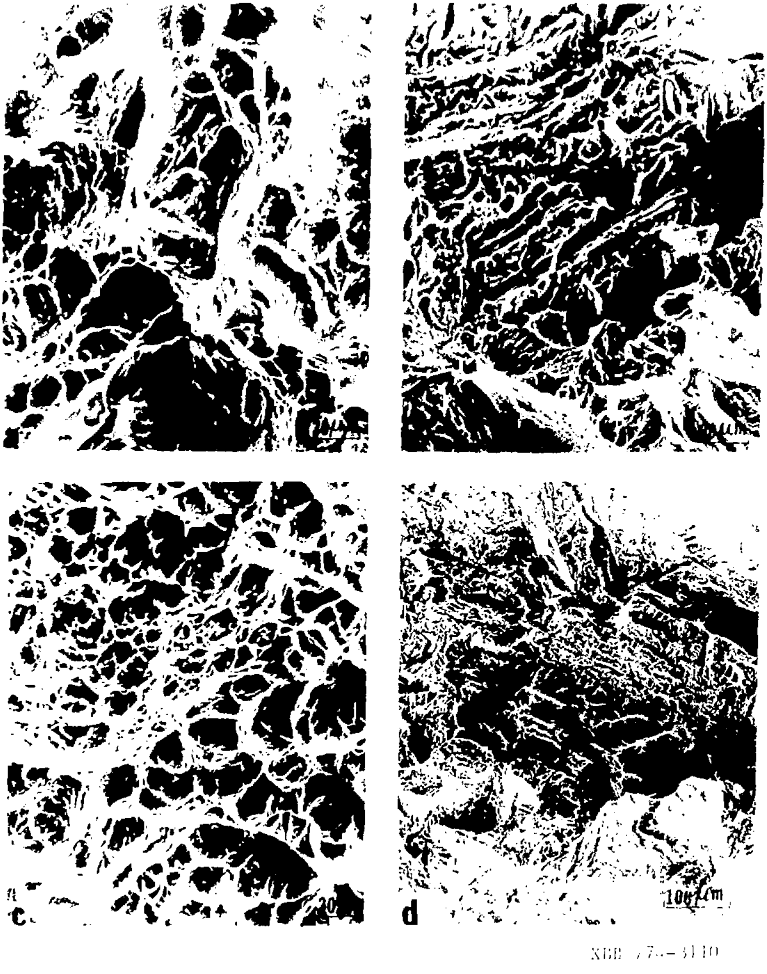

XBB 774-3110

Fig. 44

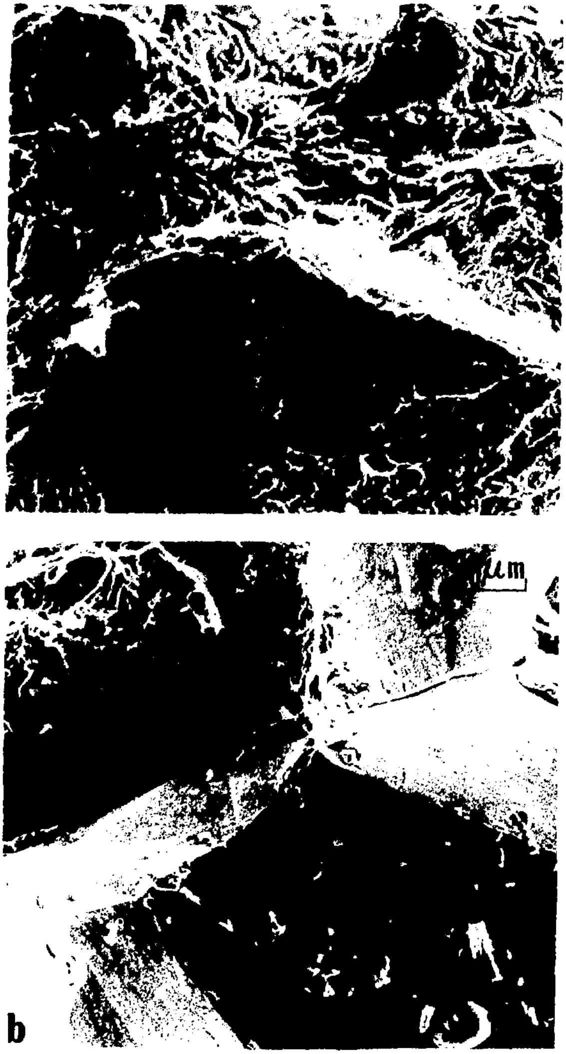

XBB 776-6056

Fig. 45

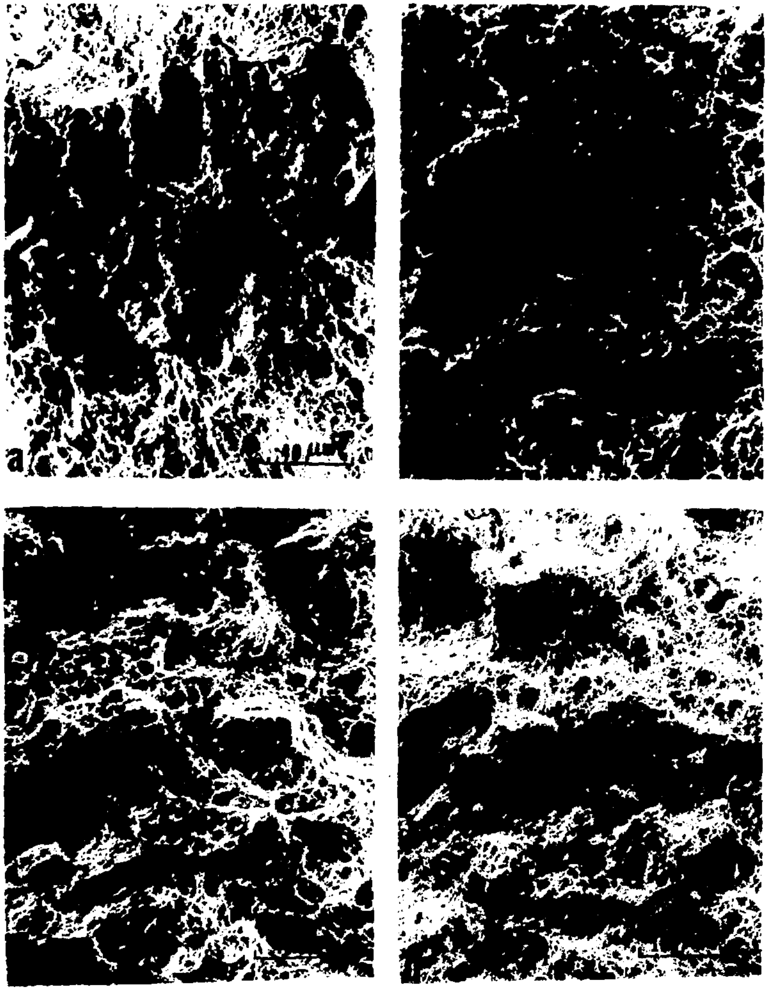

XBB 782-1184

Fig. 46

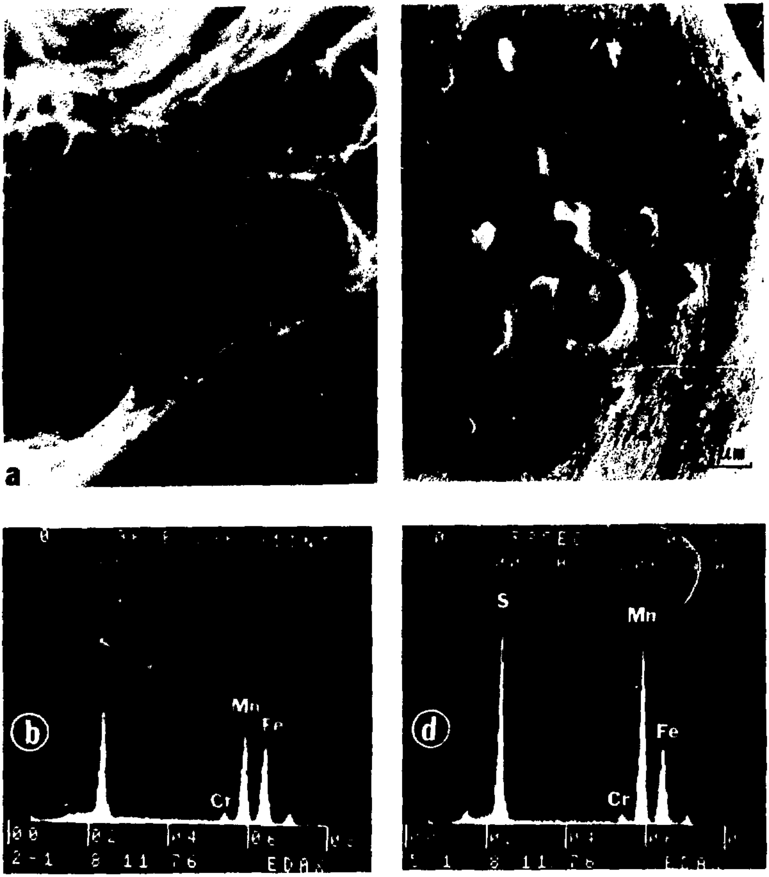

XBB 782-1183

Fig. 47

Evolution of Microstructure and Embrittlement During Tempering of Modified Ultra-high Strength Fe-4Cr-0.3 C Steels

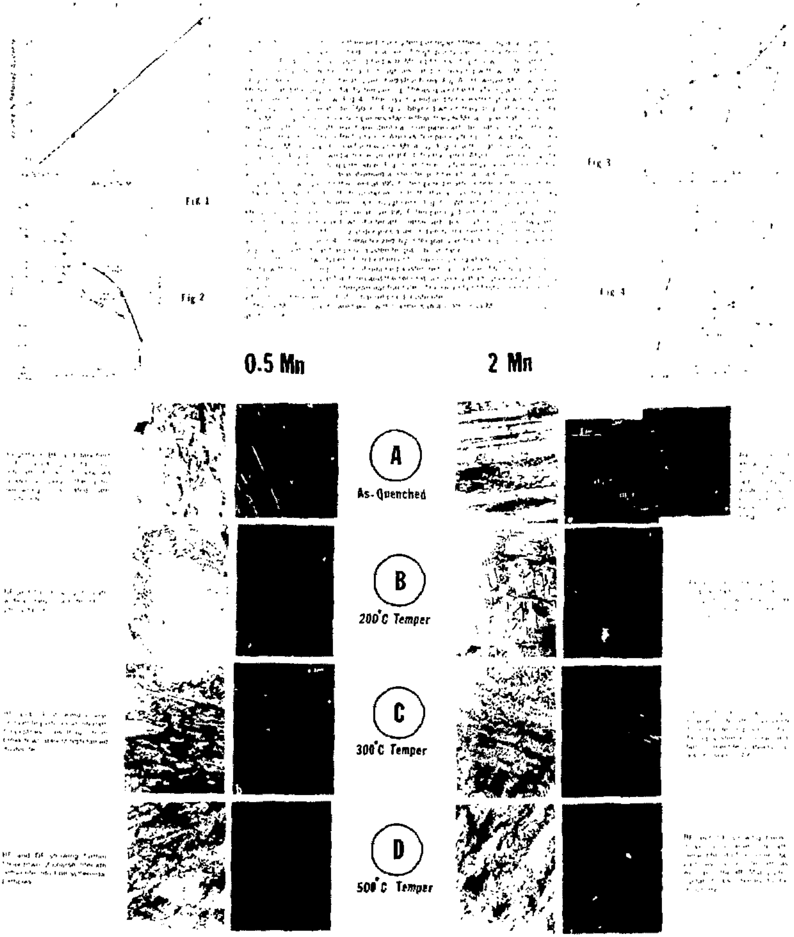

XBB 776-6136

Fig. 48

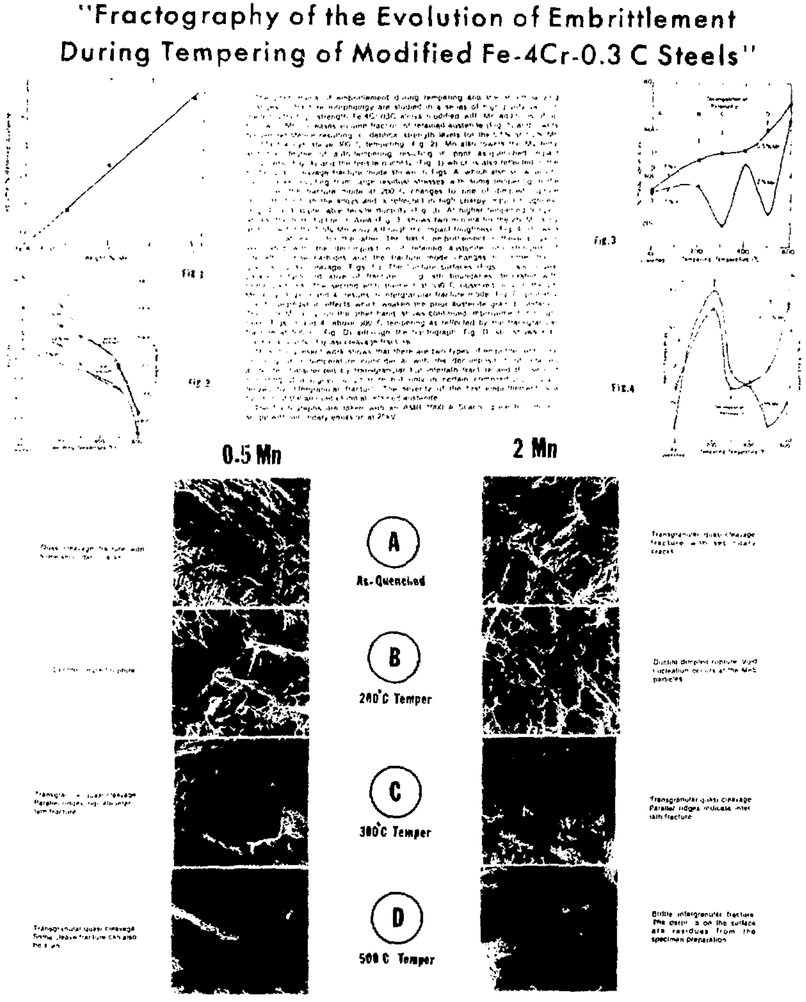

"Fractography of the Evolution of Embrittlement During Tempering of Modified Fe-4Cr-0.3 C Steels"

Transgranular quasi cleavage fracture with [illegible] cracks

Ductile dimpled rupture. Void nucleation occurs at the MnS particles

Transgranular quasi cleavage. Parallel ridges indicate inter lath fracture

Brittle intergranular fracture. The [illegible] on the surface are residues from the specimen preparation

XBB 776-6137

Fig. 49

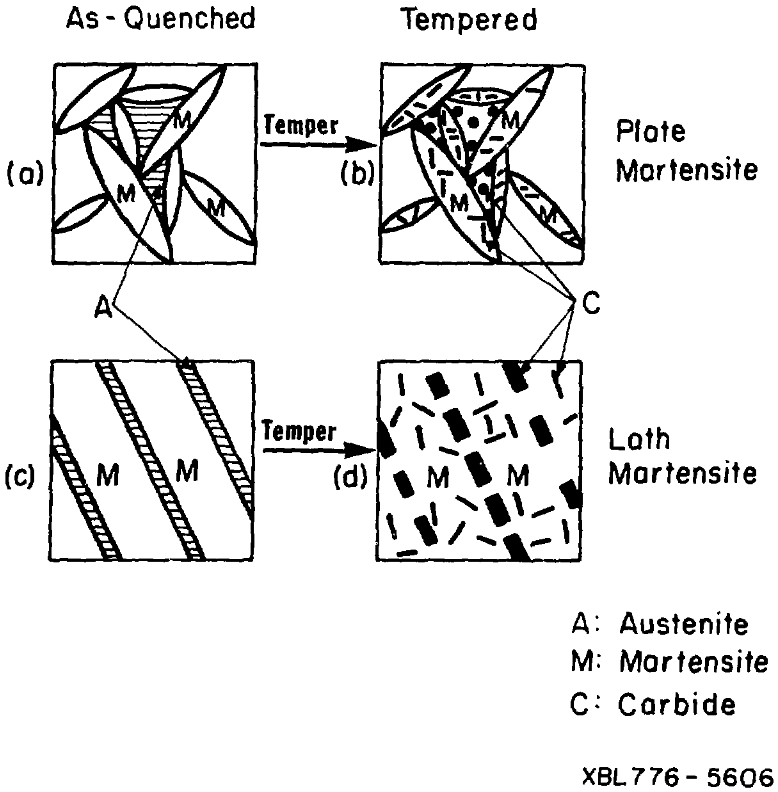
As - Quenched
Tempered
(a)
(b)
(c)
(d)
Temper
Temper
M
A
C
Plate Martensite
Lath Martensite
A: Austenite
M: Martensite
C: Carbide
XBL 776 - 5606

Fig. 50

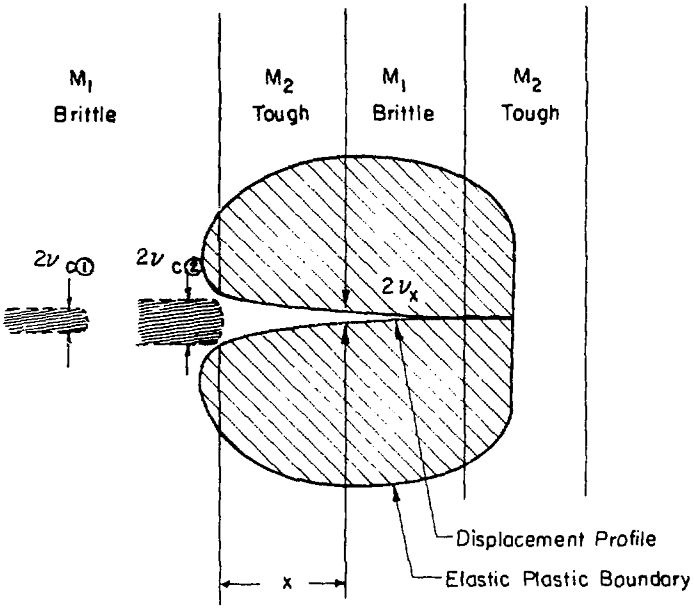

XBL 782-4552

Fig. 51

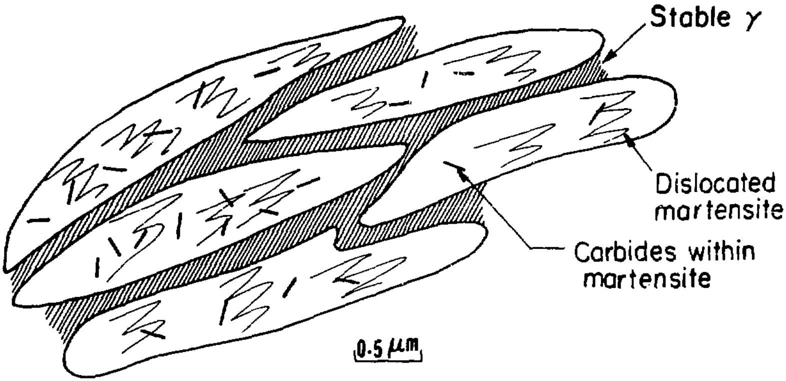

XBL 7711-10457

Fig. 52

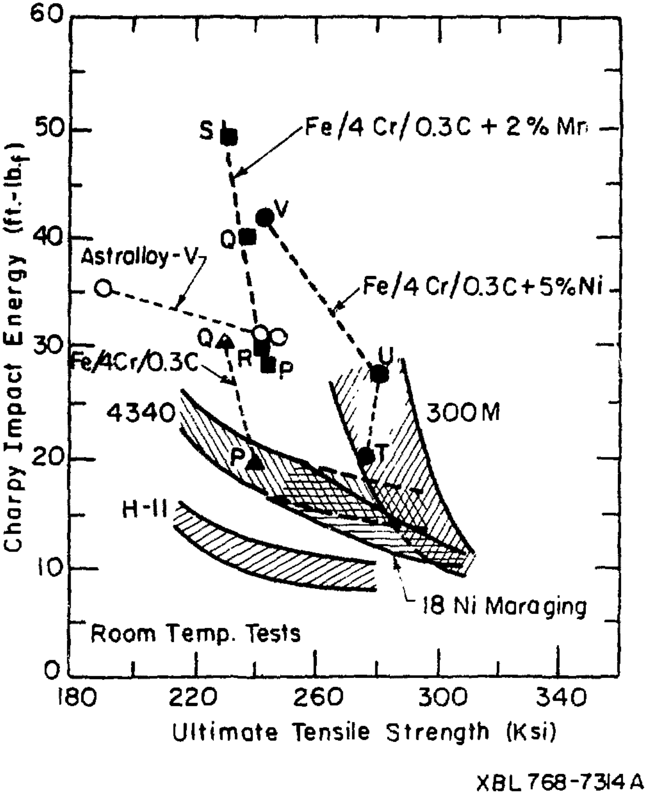
Charpy Impact Energy (ft.-lb.f)
Ultimate Tensile Strength (Ksi)
60
50
40
30
20
10
0
180
220
260
300
340
Fe/4 Cr/0.3C + 2% Mn
Fe/4 Cr/0.3C+5%Ni
Astralloy-V
Fe/4Cr/0.3C
4340
300M
H-11
18 Ni Maraging
Room Temp. Tests
S
Q
V
Q
R
P
P
U
T
XBL 768-7314 A

Fig. 53 (a)

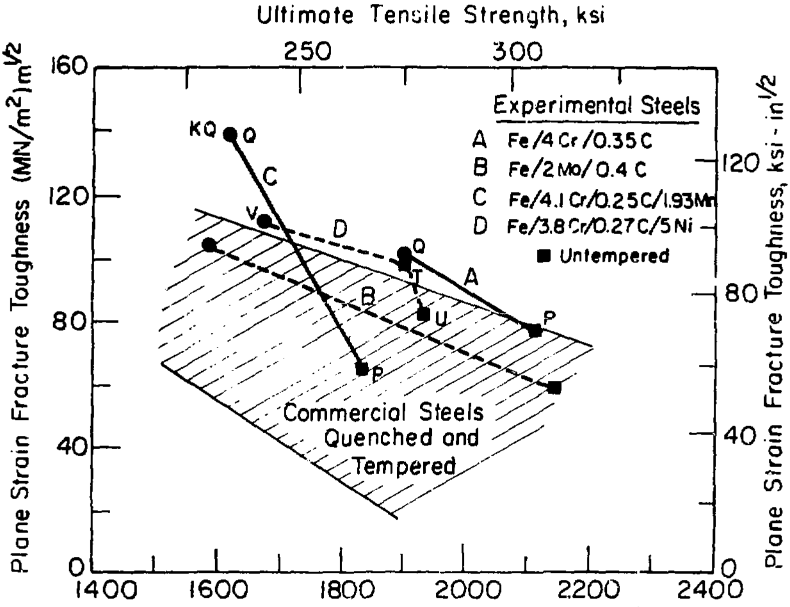

XBL 7710-6803

Fig. 53 (b)

XBB 775-4292

Fig. 54 (a)

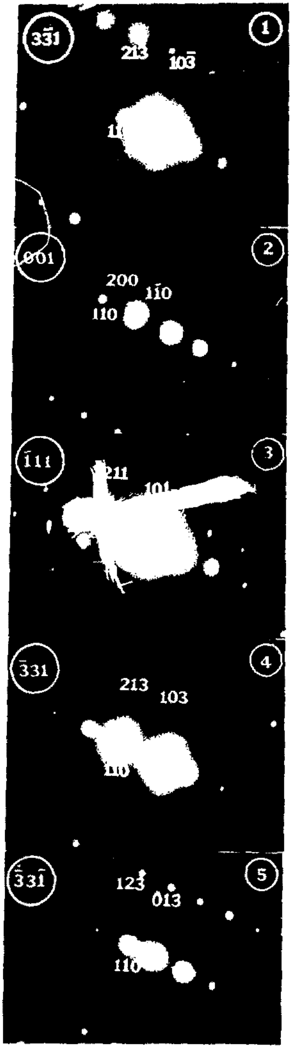

XBB 775-4293

Fig. 54 (b)

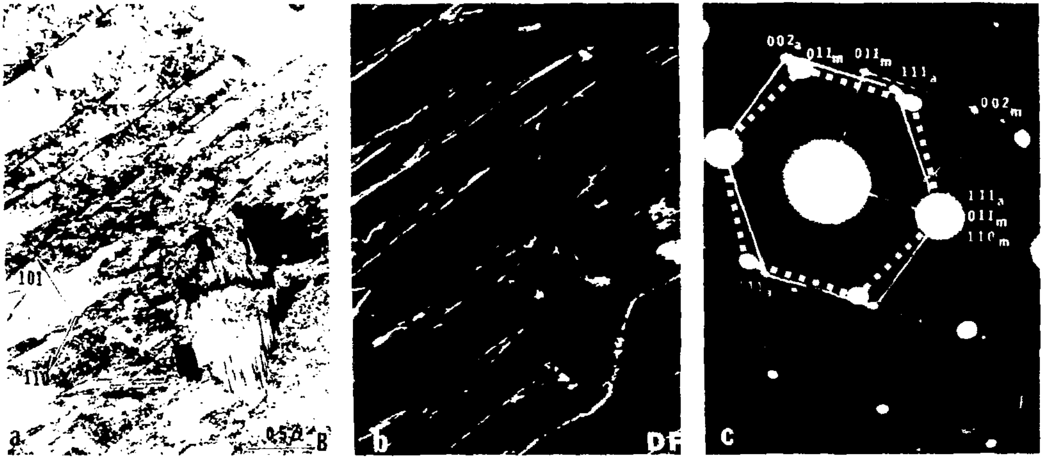

XBB 778-7952

Fig. 55 (a-c)

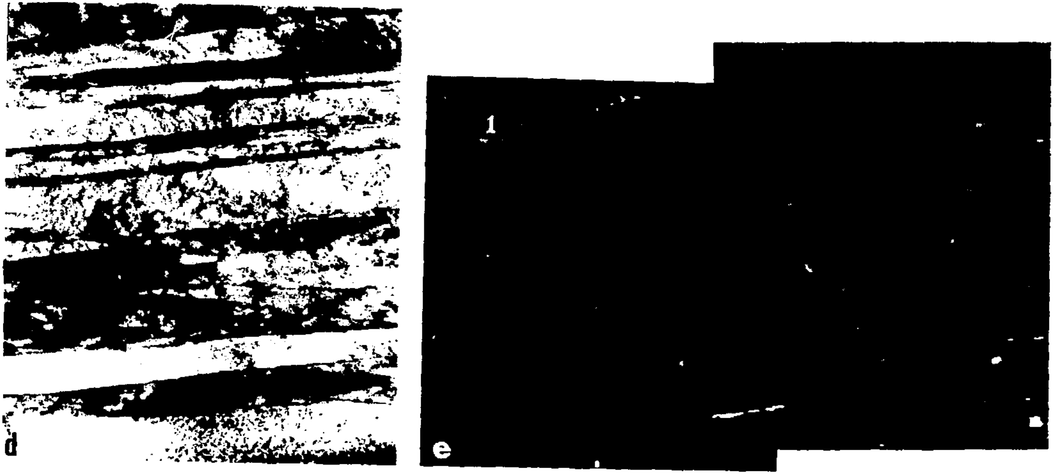

XBB 775-4291

Fig. 55 (d-e)

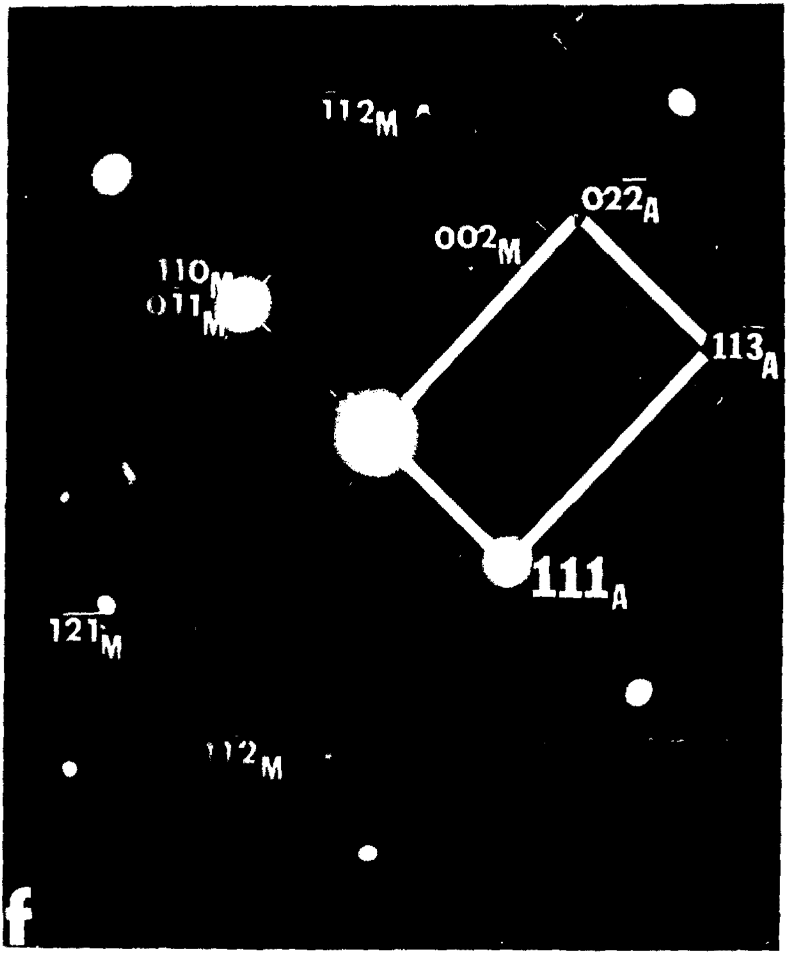

XBB 775-4290

Fig. 55 (f)

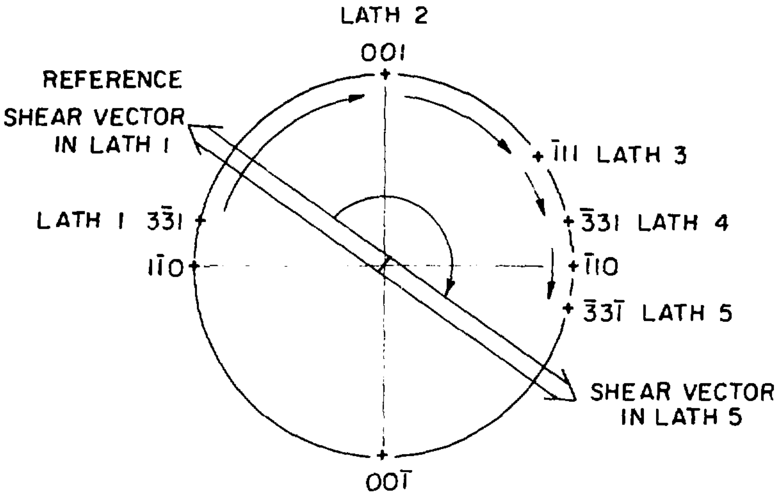

LATH REGION		ROTATION (DEGREES)
FROM	TO	
1	2	76.75
2	3	54.71
3	4	22.01
4	5	26.53
		180 TOTAL

XBL 7710 6265

Fig. 56

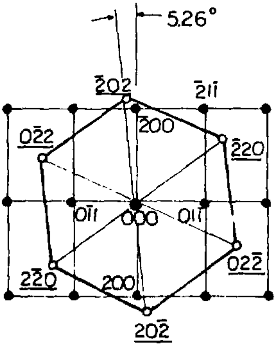

K-S ORIENTATION RELATION:

$(011)_{bcc} \parallel (111)_{fcc}$

$[\bar{1}1\bar{1}]_{bcc} \parallel [\bar{1}10]_{fcc}$

● hkℓ bcc

○ hkℓ fcc

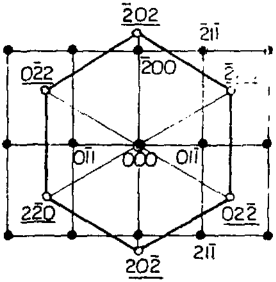

N-W ORIENTATION RELATION

$(011)_{bcc} \parallel (111)_{fcc}$

$[100]_{bcc} \parallel [10\bar{1}]_{fcc}$

XBL 7710-6262

Fig. 57

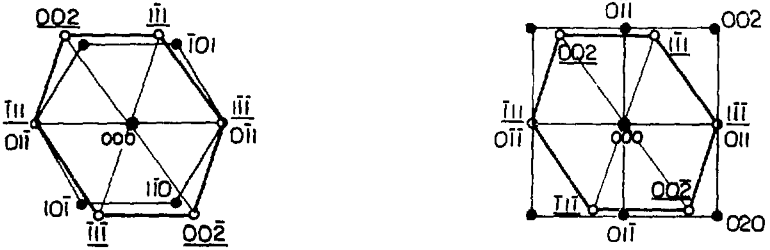

K - S

$(011)_{bcc} // (1\bar{1}\bar{1})_{fcc}$

$[111]_{bcc} // [110]_{fcc}$

N- W

$(011)_{bcc} // (1\bar{1}\bar{1})_{fcc}$

$[100]_{bcc} // [110]_{fcc}$

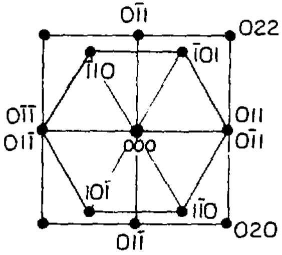

K-S AND N-W

$(011)_{bcc} // (0\bar{1}1)_{bcc}$

$[100]_{bcc} // [111]_{bcc}$

● hkℓ bcc

○ hkℓ fcc

XBL 7710-6263

Fig. 58

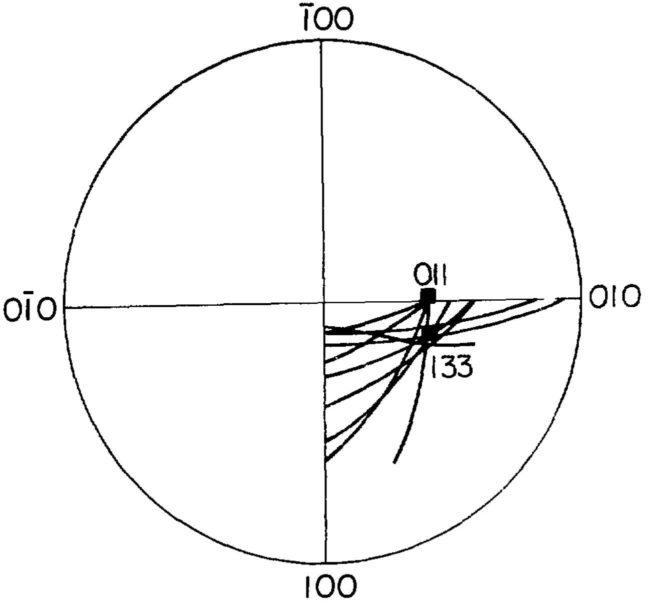

XBL 774-5395

Fig. 59 (a)

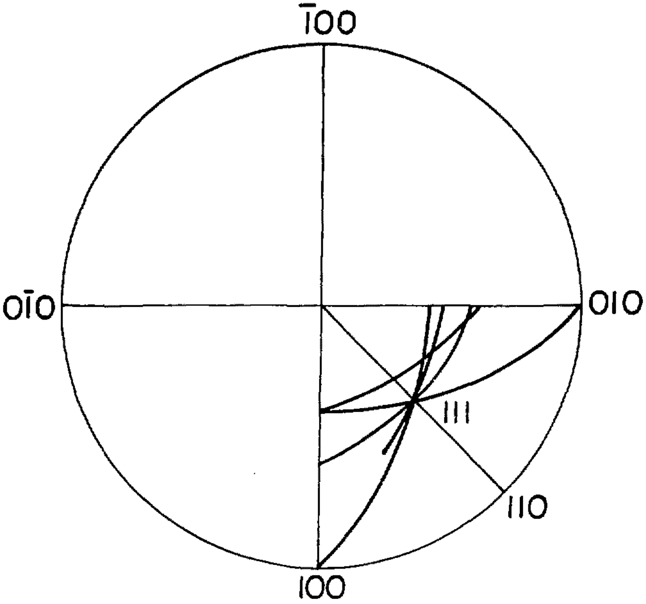

XBL 774-5396

Fig. 59 (b)

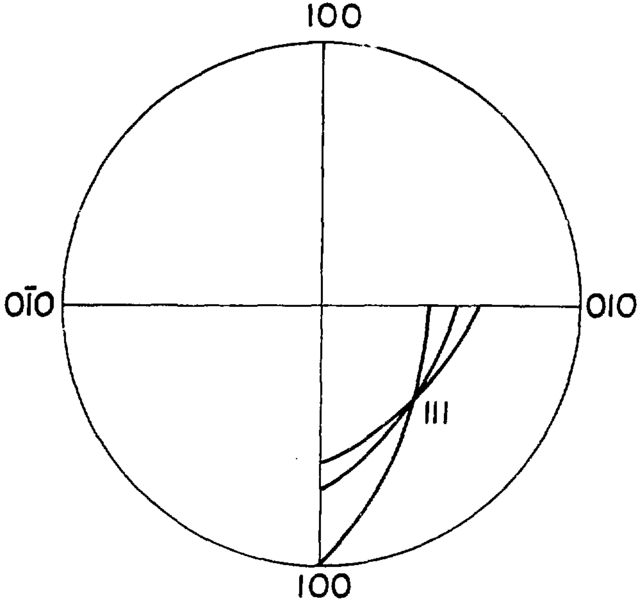

XBL 774-5397

Fig. 59 (c)

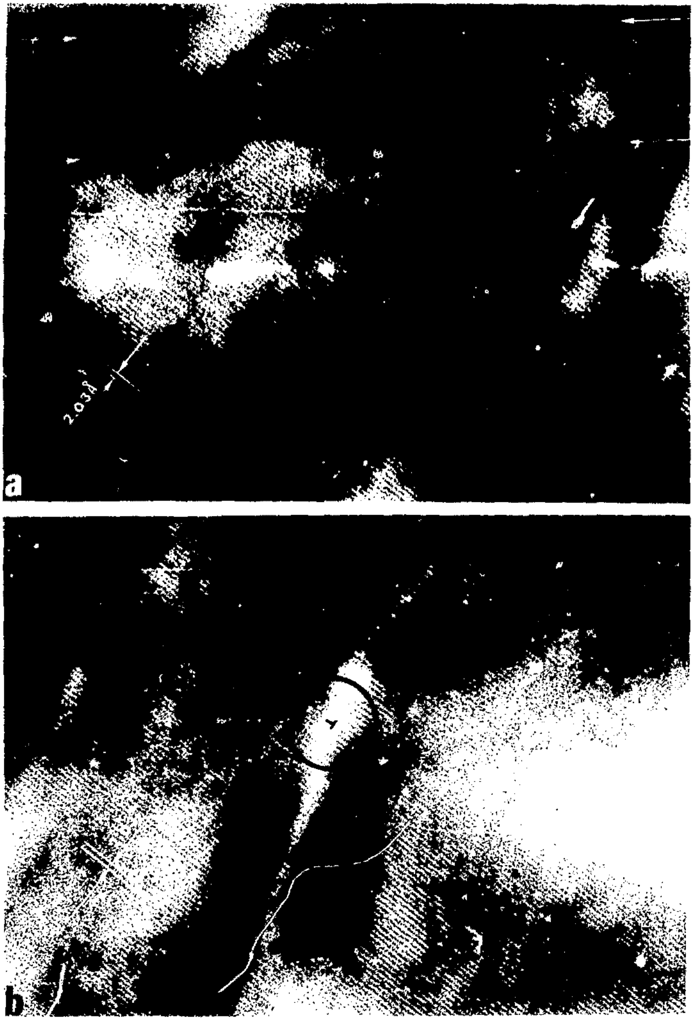

XBB 778-7992

Fig. 60

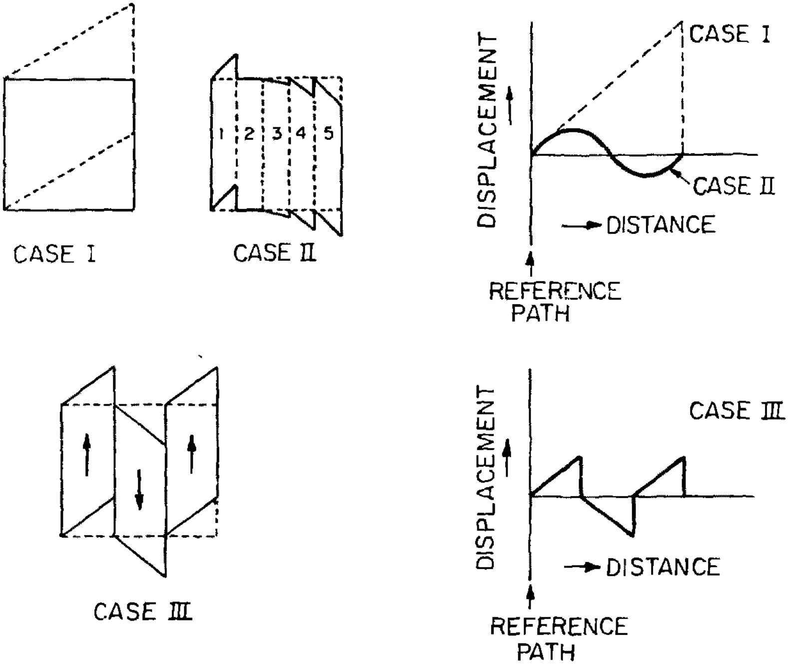

XBL 7710-6264

Fig. 61

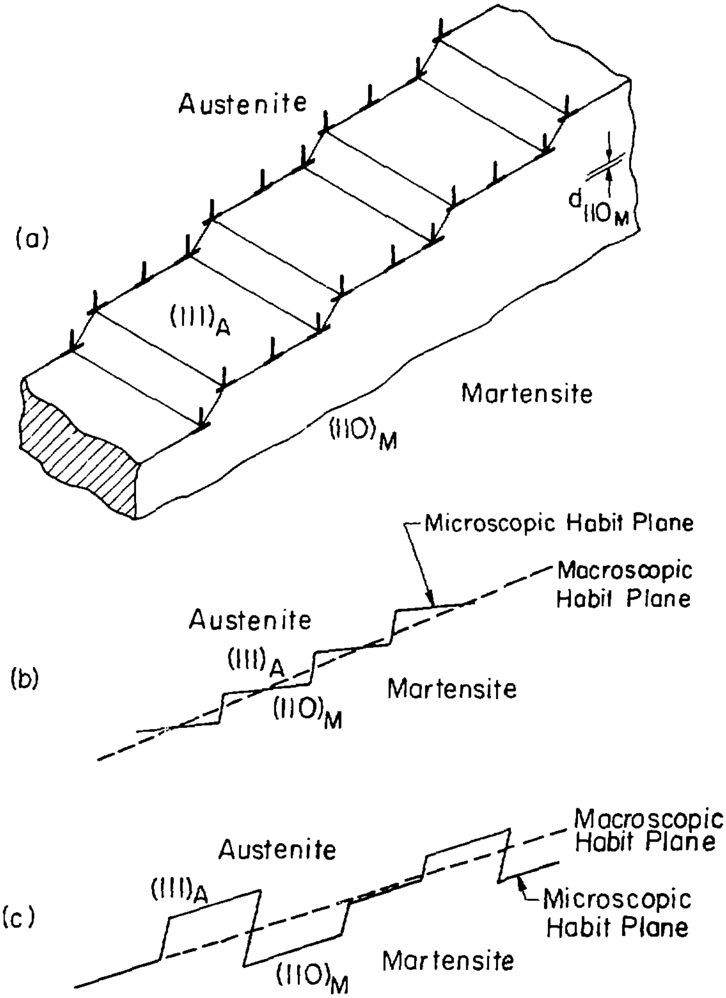

XBL 774-5394

Fig. 62

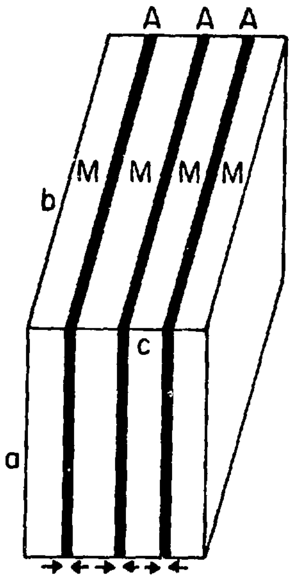

XBL 774-5393

Fig. 63